Important Notice

UNIVERSITY OF CALGARY

Sensitivity of interval Vp/Vs analysis of seismic data

by

Rafael Asuaje

A THESIS

SUBMITTED TO THE FACULTY OF GRADUATE STUDIES

IN PARTIAL FULFILMENT OF THE REQUIREMENTS FOR THE

DEGREE OF MASTERS OF SCIENCE

GRADUATE PROGRAM IN GEOLOGY AND GEOPHYSICS

CALGARY, ALBERTA

OCTOBER, 2016

Abstract

Three studies were conducted to evaluate the behavior of Vp/Vs ratio error in beds with different thickness. In the first study, a synthetic model was created to understand how the interval time would affect the calculation of the interval Vp/Vs and an equation was derived to estimate the percent error in the uncertainty of the ratio calculation.

In a second study, the seismic data at Hussar, Alberta showed that Vp/Vs error increased as the analysis time window interval decreased. In addition, the percent error of the Vp/Vs values due to uncertainty was examined and it is suggested to use isochron intervals greater than 150 ms in PP time for robust results. Interval Vp/Vs analysis for data with intervals greater than this isochron have low uncertainty.

In the third study, at Spring Coulee, Alberta, results showed that horizon pick adjustments can reduce error uncertainty by a small factor. In this and the previous studies, it was confirmed that beds with small thickness can have a significant impact on interval Vp/Vs uncertainties, which could lead to erroneous results. Additionally, all studies indicated that interpreters should work with bed intervals greater than 150 ms in PP times and perform horizon adjustments for more precise results.

Acknowledgements

First and foremost I would like to thank my supervisor, Dr. Don C. Lawton, for his patience, encouragement and the advice that he provided me during my Master's program. It has been an honour to learn under his guidance and I am very grateful to work with him on the projects he suggested for me.

Secondly, I would like to thank all CREWES staff and the consortium for allowing me the opportunity to do research with their excellent group. I would like to thank Helen Issac for performing all the processing of the Hussar and Spring Coulee data and for an excellent discussion about the processing of these datasets. Also, thanks to Malcolm Bertram for great explanations on data acquisition. Thanks to Kevin Hall for help with technical issues and answering question about the acquisition of projects. Also, I would like to thank Laura Baird for always making sure we meet deadlines and send information about talks, seminar, and events that could be very beneficial for the students. I would like to thank Dr. Larry Lines for being part of my committee for my thesis defense and for being a great geophysics teacher.

Thanks to all CREWES friends, especially and in no particular order to Tianci Cui, Babatunde Arenrin, Shahin Moradi, Shahin Jabbari, Michelle Montano, Raul Cova, Adriana Gordon, Eric Rops, Bobby Gunning, Scott Keating, Marcelo Guarido, Sina Esmaeili, Penny Pan, Davood Nowroozi and Saul Guevara for their friendship and collaborations during my stay at the university of Calgary.

Thanks to Laura Haitel for helping in correcting this document and for always encouraging me to try my best during my studies. Also, I want to thank my family for their unconditional support in all the decisions in my life and for their advice, especially my parents

Ramon Asuaje and Zaida de Asuaje and brother and sisters Ramon Asuaje, Carolina Asuaje and Gricel Asuaje for their love and support.

Dedication

To all my family for their love and support, Ramon Asuaje (dad), Zaida de Asuaje (mom), Carolina Asuaje (sister), Gricel Asuaje (sister), Ramon Asuaje (brother). And all my new friends from Canada.

Table of Contents

List of Tables

List of Figures and Illustrations

List of Symbols, Abbreviations and Nomenclature

Symbol	Definition
%	Percentage
2D	Two-Dimensional
3C	Three-Component
3D	Three-Dimensional
APC	Asymptotic Conversion Point
API	American Petroleum Institute (Gamma Ray Units)
ARAM	Aries Remote Acquisition Module
AVO	Amplitude Variation with Offset
c	Sensitivity Coefficient
CDP	Common Depth Point
CMP	Common Mid-Point
CP	Conversion Point
CREWES	Consortium of Research in Elastic Waves Exploration Seismologist
dB	Decibel
F_d	Dominant Frequency
GR	Gamma Ray
Hz	Hertz
K	Thousand
K	Bulk Modulus
kg/m3	Kilograms per Cubic Meter
km	Kilometer
m	Meter
m/s	Meters per Seconds
ms	Milliseconds
LS	Limestone
PP	Wave that propagates and reflects as a P-wave.
PS	Wave that propagates as a P-wave and reflects as an S-wave.
P-wave	Compressional Wave
Q	Quality Factor
R	Receiver
RHOB	Bulk Density
S	Source

SS	Sandstone
SH	Shale
S-wave	Shear Wave
t	Time
t_o	Initial Time
T	Wavelength Period
TWT	Two-Way-Travel time
TVD	True Vertical Depth
T_P	Travel Time of P-Wave
T_S	Travel Time of S-Wave
T_{PP}	Travel Time of PP-Wave
T_{SS}	Travel Time of PS-Wave
u	Uncertainty Error
V	Velocity
υ	Poisson's Ratio
V_P	P-wave Velocity
V_P/V_S	Ratio between P-wave and S-wave Velocities
V_S	S-wave Velocity
x, X	Offset
z, Z	Depth
Z	Minimum Thickness
λ	Wavelength
ρ	Density
α	P-wave Velocity
β	S-wave Velocity
ΔPP	Interval PP Time
ΔPS	Interval PS Time
ΔT	Interval Time
<	Less Than
>	Greater Than
μ	Shear Modulus
θ	Angle of Incidence
ø	Angle of Reflection
δ	Partial Derivative
Δ	Uncorrected Horizons
□	Corrected Horizons

Chapter One: Introduction

Compressional waves (P-waves) have dominated seismic exploration in the oil industry for the past sixty years because they have generally provided better resolution than shear waves (S-waves). P-waves can travel through fluids and the particle motion is parallel to the direction of propagation. On the other hand, S-waves travel at approximately half the speed of the compressional wave and have transverse particle propagation. S-waves do not propagate through liquids due to shear modulus being zero in this medium, so they do not propagate in a marine environment (Yilmaz, 2001).

Through the analysis of multicomponent seismic data, important rock properties such as Vp/Vs can be extracted. This thesis uses the analysis of both P-waves and PS-waves to calculate Vp/Vs throughout an entire seismic section. In addition, synthetic models are used to compare results from ideal conditions to those from a real data set. The ratio of compressional and shear wave velocities is key to the determination of lithology as well as to the identification of pore fluids using along with, for example, amplitude variation with offset (AVO) analysis (Yilmaz, 2001).

1.1 Seismic Waves

Converted waves, specifically downgoing P-waves that convert on reflection to upcoming S-waves, are increasingly being used to explore and better understand exploration targets. P-waves are body waves in which the particles move elastically, parallel to the direction in which the wave is moving; these are usually called primary waves since they are commonly the first waves to arrive at the seismic recorders (Kearey, 2002). The velocity, Vp, of a P-wave is given by Equation 1.1:

$$Vp = \sqrt{\frac{K + {}^{4}/_{3}\,\mu}{\rho}}$$

(1.1)

The variable K represents the bulk modulus or the modulus of incompressibility, μ is the shear modulus or the modulus of rigidity and ρ is the density of the medium in which the wave is propagating. P-waves can travel through solids, liquids, and gases.

An S-wave, also known as a shear or transverse wave, is a type of body wave in which the particle motion is perpendicular to the direction of wave propagation. The S-wave velocity, Sv, is given by Equation 1.2, where μ is the shear modulus or modulus of rigidity and ρ is the density of the medium of propagation.

$$Vs = \sqrt{\frac{\mu}{p}}$$

(1.2)

S-waves need a medium rigid enough to sustain wave propagation. Hence, S-waves do not propagate through liquids, and travel at velocities much slower than P-waves, typically between 40 % and 60 % of the P-wave velocity (Kearey, 2002).

1.2 Converted Waves

When a P-wave strikes an interface with a non-zero incident angle, several different wave modes are produced. These are an upgoing P-wave, a transmitted downgoing P-wave, a converted S-wave reflection, or a converted S-wave transmission. The relative strength of these wave modes is a function of incident angle, and contrast in rock properties across the interface.

A single downgoing P-wave will create multiple mode conversions simultaneously upon contact with a boundary. The mode conversions could be for both the reflected and transmitted

waves, as shown in Figure 1.1. This thesis, however, only focuses on PS converted-wave reflections (downgoing P- and reflected upgoing S-waves).

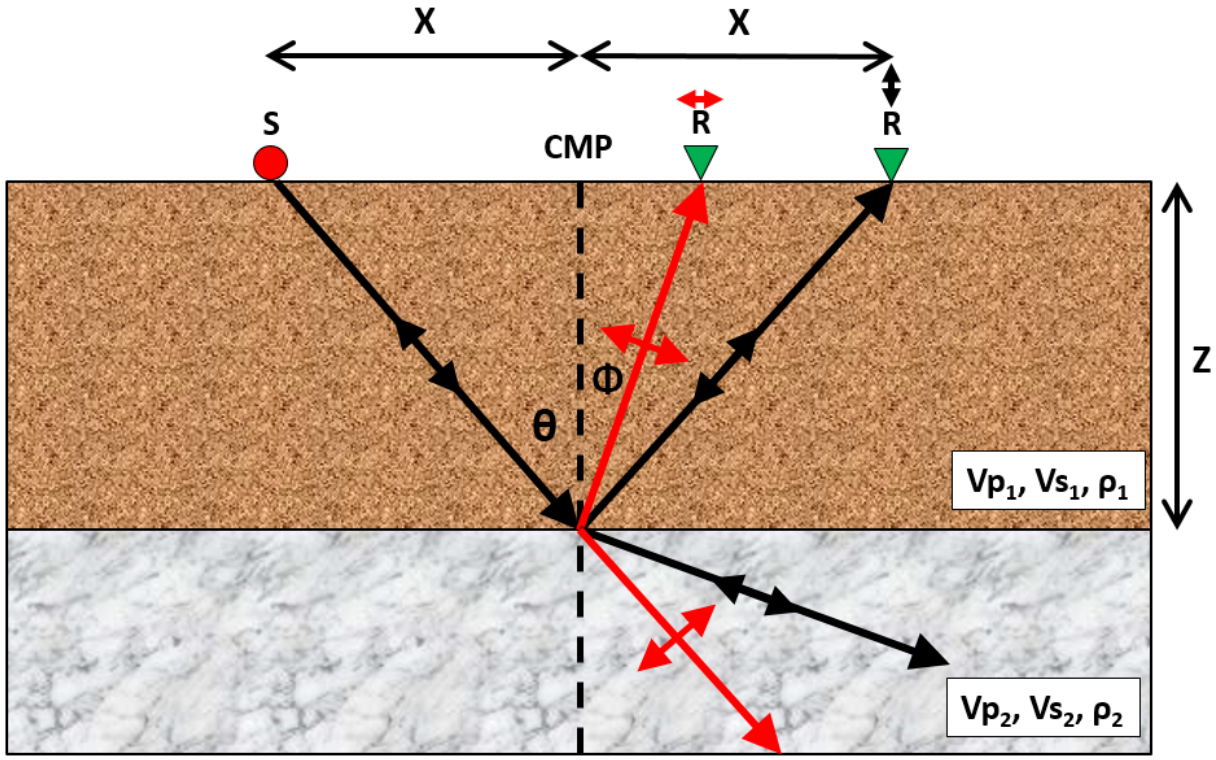

Figure 1-1: Mode conversions through an isotropic media with a boundary with no dip. Black lines represent P-waves and red lines represent S-waves.

Figure 1.2 shows a P-wave propagating downward away from a source (S), then reflected as an upgoing P-wave back to the receiver (R). In this particular case, reflection point is midway between the source and the receiver. This point is commonly called common mid-point (CMP). The one-way travel time of a vertically reflected ray is given by Equation 1.3:

$$t_o = \frac{2z}{V} \tag{1.3}$$

The term z represents the depth of the layer and V is the velocity of the medium. The equation for the travel time t of the reflected ray from the shot point to a detector at a horizontal offset x is given by the ratio of the travel path length to the velocity (Equation 1.4):

$$t = \frac{(x^2 + 4z^2)^{1/2}}{V} \rightarrow t^2 = \frac{4z^2}{V^2} + \frac{x^2}{V^2} \tag{1.4}$$

Substituting Equation 1.3 into 1.4, time can be written as Equation 1.5:

$$t = {t_o}^2 + \frac{x^2}{V^2} \tag{1.5}$$

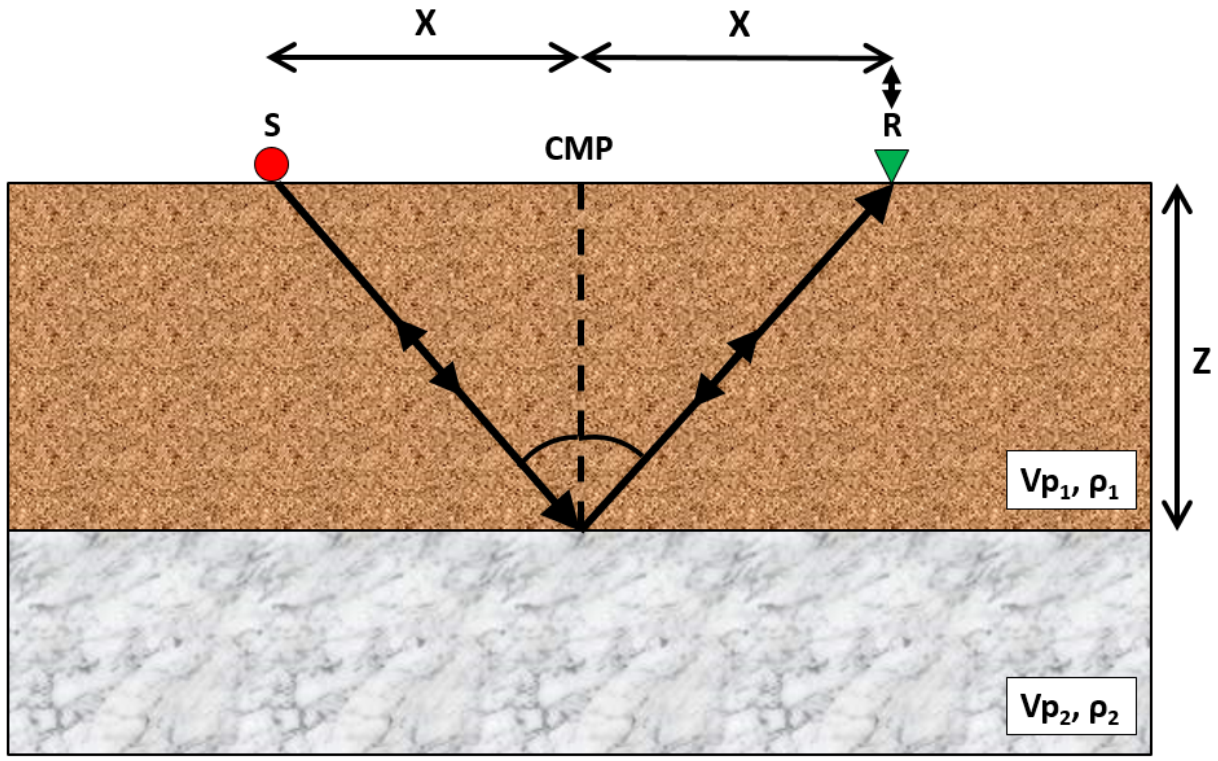

Figure 1-2: PP-wave propagation through an isotropic medium with a boundary with no dip. S represents the source, R represent the receiver, H is the depth of the interface and CMP is the common mid-point.

Upon reflection, a P-wave can have a mode conversion from a P- to S-wave, as shown in Figure 1.3. In this particular example, particles in the downward wave propagate in the same direction as the wave motion, but after the reflection, the particle motion is perpendicular to the wave motion. The point of reflection for this PS-converted wave is not midway between the source and receiver, due to the different velocities of the P and S-waves. The point of reflection in this example is called the conversion point (CP) and is closer to the receiver than to the source. To calculate the two-way travel time for PS-waves (t_{PS}), the time of propagation downward and upward are calculated separately, then added. Equation 1.6 shows the travel time for the PS-waves from the source to the conversion point to the receiver is given as:

$$t_{PS} = t_P(downward) + t_S(upward)$$

$$t_{PS} = \frac{\sqrt{{x_1}^2 + z^2}}{Vp_1} + \frac{\sqrt{{x_2}^2 + z^2}}{Vs_1} = \frac{\sqrt{{x_1}^2 + z^2}}{\alpha} + \frac{\sqrt{{x_2}^2 + z^2}}{\beta} \tag{1.6}$$

The variable t_P represents the time for the downgoing ray trace as a P-wave, t_S represents the time for the upgoing ray trace as a S-wave, x_1 is the offset distance from the source point to the conversion point, x_2 is the offset distance from the conversion point to the receiver, z represents the depth of the layer, and α and β represent the medium velocities for P-wave and S-wave, respectively.

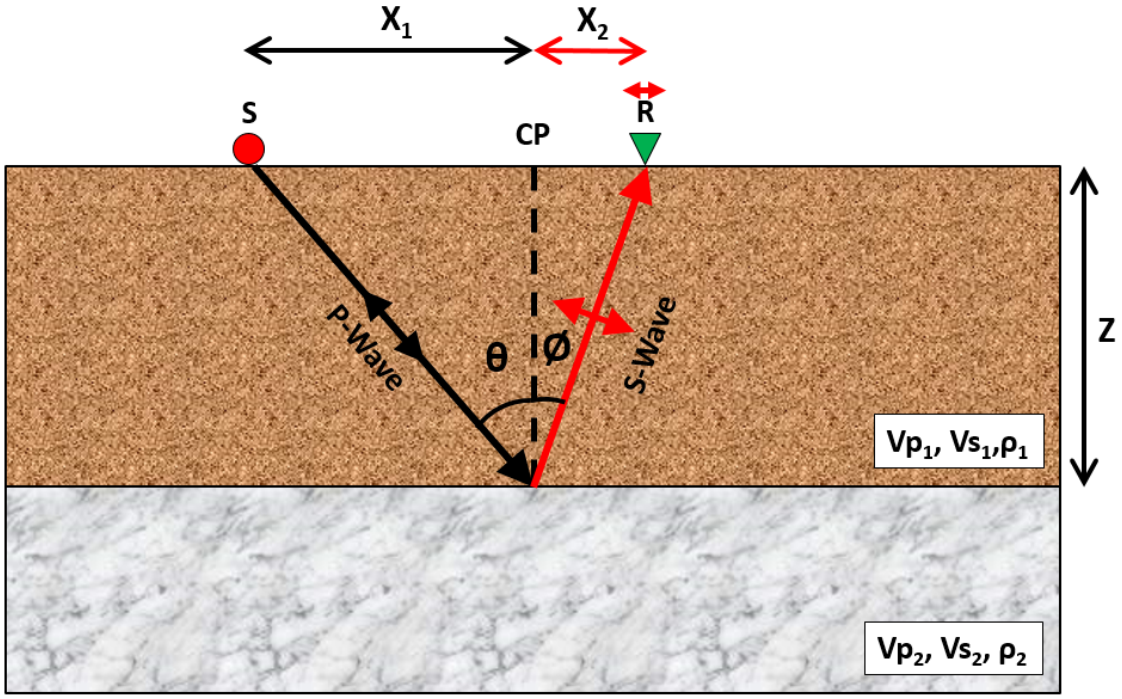

Figure 1-3: PS-wave propagation through an isotropic medium with a boundary with no dip. S represents the source, R represent the receiver, H is the depth of the interface and CP is the conversion point.

It is important to note that the conversion point (CP) moves closer to the common midpoint (CMP) between the source and receiver as the depth of the reflector increases (Figure 1.4). At infinite depth, the CP reaches an asymptotic conversion point (ACP) (Yilmaz, 2001).

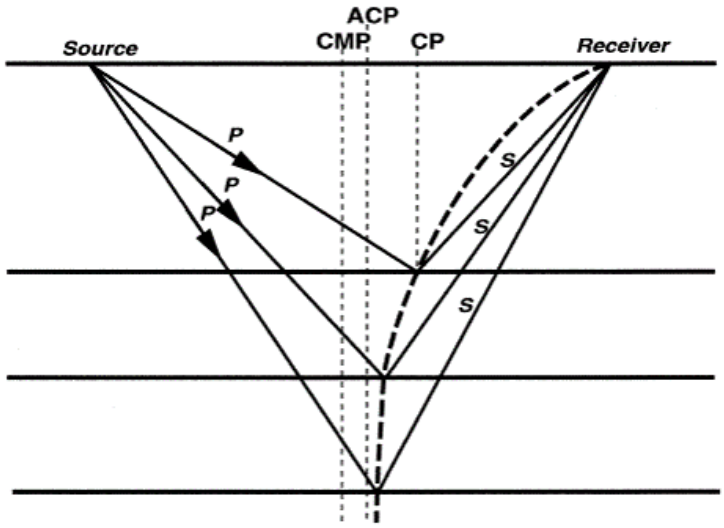

Figure 1-4: Geometry of conversion-point (CP) and ray paths. As depth increases, the CP location reaches an asymptotic conversion point (APC) (modified from Yilmaz, 2001).

1.3 Vp/Vs Garotta Equation

The Garotta equation approach is based on post stack data which is the projection to zero offset of all the offsets. Figure 1.5 shows a representation of the PP wave and PS wave at zero offset. This graph provides the foundation that Garotta used to derive the equation to estimate the Vp/Vs ratio.

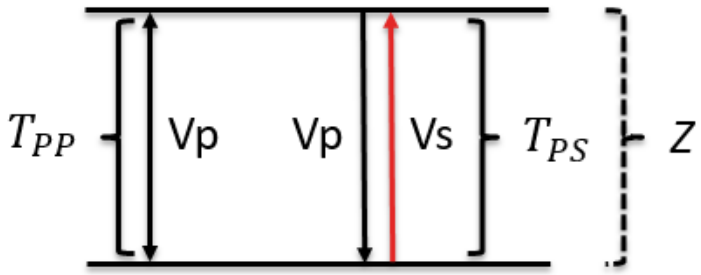

Figure 1-5: Representation of a zero offset PP wave and a zero offset PS wave. T_{pp} represents the total travel time for the PP wave, T_{ps} represents the total travel time for the PS wave, Z represent the depth, and V_p and V_s represent the P-wave and S-wave velocity, respectively.

The ratio of the P-wave velocity to the S-wave velocity, also known as the Vp/Vs ratio, can be determined as follows. Section 1.2 introduced how to determine the two-way travel times (TWT) for different waves, as found derived by Garotta (1987). In the case of converted waves, the two-wave travel time is given by Equation 1.7.

$$T_{PS} = T_P + T_S \tag{1.7}$$

Using the equation for speed for each wave, Equation 1.7 can be expanded to Equation 1.8.

$$T_{PS} = \frac{z}{V_p} + \frac{z}{Vs} \tag{1.8}$$

Where d, represents the depth of the boundary where the seismic wave reflects back to the surface. Vp represents the downgoing P-wave and Vs represents the upgoing reflected S-wave. During acquisition, PP- and PS-waves are acquired simultaneously. The calculation of the TWT for PP-waves is given by Equation 1.9.

$$T_{PP} = \frac{2z}{V_p} \Longrightarrow \frac{z}{V_p} = \frac{T_{PP}}{2} \tag{1.9}$$

Substituting Equation 1.9 into Equation 1.8 yields Equation 1.10.

$$T_{PS} = \frac{T_{PP}\cancel{V_p}}{2\cancel{V_p}} + \frac{T_{PP}V_p}{2Vs}$$

$$T_{PS} = \frac{T_{PP}\cancel{V_p}}{2\cancel{V_p}} + \frac{T_{PP}V_p}{2Vs}$$

(1.10)

Solving Equation 1.10 for Vp/Vs gives the final equation, Equation 1.11.

$$\frac{V_P}{V_S} = \frac{2T_{PS} - T_{PP}}{T_{PP}}$$

(1.11)

Equation 1.11 (Garotta, 1987) is used to calculate the Vp/Vs ratio based on the interval times of PP- and PS-waves and only applies to post stack analysis. One of the advantages of using this equation for the ratio calculation is that, unlike a well log, the ratio can be calculated at any point along a seismic line.

Another method that can be used to estimate Vp/Vs is from amplitude inversion, as shown by Pengelly (2005), in which the travel times and the inversion methods were compared. Although both approaches gave similar results, it was found out that the travel times method could suffer from uncertainty error in the picked horizons, especially when the data is noisy.

1.4 Relation of Vp/Vs and Lithology

Vp/Vs is an important rock diagnostic parameter that can be directly determined by multicomponent seismic analysis. Historically, most seismic surveys used only P-waves and therefore required vertical-component receivers in order to detect only near-vertical P-waves at the ground surface. The recording of S-waves provides greater information about the subsurface, but at a greater acquisition cost due to the three-component recording (vertical, and two horizontal components for the S-wave) and additional time for the dataset processing. With the advancement of technology, multicomponent surveys are becoming more common.

While the information from P-waves is very useful, as seen in Section 1.1, it is only a function of three separate properties of the rock and by itself, it is a general indicator of rock lithology (Kearey, 2002). The Vp/Vs ratio, on the other hand, is independent of density and can be used to derive Poisson's ratio, υ, (Equation 1.12), which is also a diagnostic lithological indicator. This relationship is given as follows. (Refer to section A1 in the appendix for a complete derivation.)

$$\upsilon = \frac{1}{2}\frac{(V_p/V_s)^2-2}{(V_p/V_s)^2-1} \tag{1.12}$$

The basis of much of the lithology work in PS-wave exploration relates to irregular changes in Vs with respect to Vp. A changing Vp/Vs value is often closely tied to a changing lithology (Rider, 2011). Examining laboratory data and field data from different formations (Pickett, 1960) revealed that measurements corresponding to limestone and dolomites were found to be Vp/Vs ≈ 1.9 for limestone and ≈ 1.8 for dolomite. For sandstone, it was determined that there was a range of velocity ratios from about 1.6 to 1.75, with an upper limit corresponding to high-porosity sands under low effective stress. With the availability of routine shear and compressional velocities, this technique became useful for lithology determination and the identification of gas. Using Pickett's data (Domenico, 1984), the Poisson's ratio for all of the samples was determined. Figure 1.6 plots the value of Poisson's ratio (ν) as a function of the ratio of Vp/Vs. It shows a clear separation between sandstone and limestone.

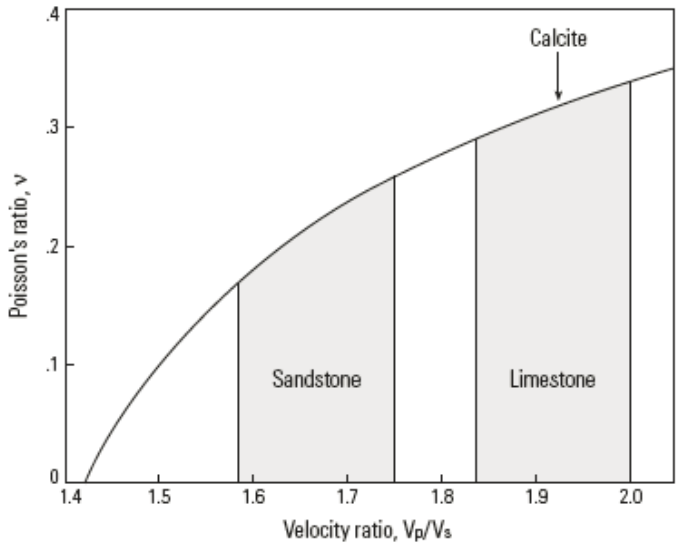

Figure 1-6: Analysis of Pickett's data on rock samples of Poisson's ratio (v) as a function of the velocity ratio, Vp/Vs. This forms the basis for distinguishing among the three major rock types (from Domenico, 1984).

By taking the ratio of the two velocities, Vp and Vs, the density is eliminated. Thus, the ratio of velocities depends on the ratio of bulk modulus to shear modulus of the rock. As mentioned earlier, it is known that the bulk modulus depends strongly on the fluid bulk modulus, whereas the shear modulus doesn't depend on it. If a compressible gas replaces relatively incompressible fluids in a porous rock, the ratio Vp/Vs will reflect the bulk modulus change and can therefore be used as an indicator for the presence of gas. One promising technique to extract a more quantitative analysis of the gas saturation is based on a cross-plot of the velocity ratio Vp/Vs versus the compressional velocity Vp. Miller and Stewart (1990) used this technique to differentiate lithologies in studies conducted in Alberta, Canada and their results are shown in Figure 1.7.

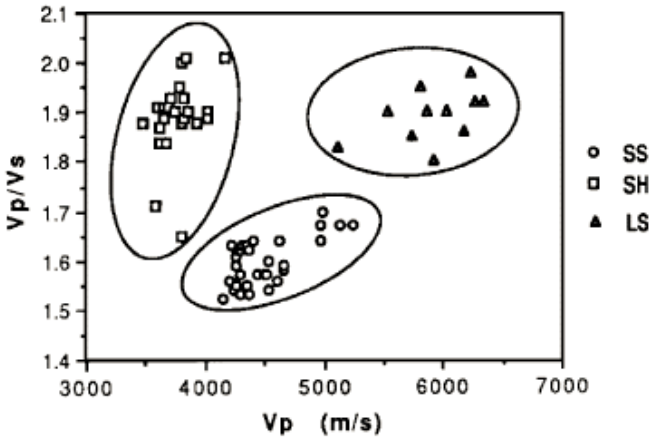

Figure 1-7: Analysis of velocity ratio, Vp/Vs on rock samples as a function of compressional velocity (Vp). Three major rock types are distinguishable in this analysis SS=sandstone, SH=shale, and LS=limestone (from Miller and Stewart, 1990).

1.5 Thesis Objectives

This thesis has contributed to setting guidelines for the interpretation and calculation of a reliable interval velocity ratio, Vp/Vs, that could be used to discriminate lithologies. Reliable velocity ratios are highly dependent on the vertical separation of reflectors, and thus their time separation (isochron). The main objective of this thesis is to evaluate the influence of using variable isochrons lengths and to calculate an uncertainty error associated with each length to determine the smallest isochrons that will provide reliable velocity ratios.

This study was conducted by analyzing two datasets from different areas within the province of Alberta, Canada. Additionally, a geological model was built with the objective of estimating velocity ratio error for very thin beds under ideal conditions. To complete the main goal specific objectives were defined for each dataset:

- For the synthetic study, a geological model and sonic and density logs were built. The objective of this test was to obtain velocity ratio errors for thin isochrons.

- For the first dataset, the Hussar experiment, the objective was to evaluate multiple isochrons in PP time obtained from the three wells available in the area. The evaluation was carried out by calculating the error of Vp/Vs for each time interval. This was accomplished by deriving an equation that took into consideration uncertainties encountered during the interpretation process. An assumption of ±2ms uncertainty was used for the horizon interpretation.
- For the second dataset, the Spring Coulee experiment, the objective was to reduce the uncertainty for the horizon interpretation, calculate the error for the different isochrons in PP time and perform a comparison with the error obtained before and after the horizon pick uncertainties were reduced, in order to understand how the horizon picks uncertainty can influence the calculated velocity ratio.

The results from all the studies were compared for consistency. The results were used to determine the ideal range for isochrons length for velocity ratio interpretation. The errors obtained in all the cases were consistent with the relative isochron length. Thus, a reliable minimum bed thickness was suggested for velocity ratio analysis.

1.6 Thesis Outline

The thesis contains a total of five chapters which undertakes the goals set for this research.

Chapter 1 includes the background information about converted waves, the relation between Vp/Vs and lithology, and the Garotta Method. Additional information includes objectives and the software used.

Chapter 2 presents a synthetic geological model with different velocity ratios on each layer. Some of the layers used in the model are purposely very thin. This was done to understand

how the velocity ratio error behaves in the interval Vp/Vs analysis for these layers. At the end, the results obtained are compared with the analysis from the second and third chapters.

Chapter 3 uses a dataset from Hussar, Alberta. It starts with a geological description of the area, and then describes the data inputs and interpretation work, to determine the isochrons that will be used in the analysis. The interpretation work includes horizon picking and well ties work. The velocity ratio error calculation is explained in detail, and the results are compared to time interval lengths.

Chapter 4 describes the work done on the Spring Coulee dataset. A general overview of the geology of the area is given. After this, the focus is to go over the conditioning of the data, which is done to obtain the isochrons that will be used to perform the velocity ratio analysis.

Chapter 5 provides the conclusion and the recommendations from the results of this thesis.

1.7 Software Used

The following software was used for this thesis research:

- Microsoft Office (Word, Excel, PowerPoint, Picture Manager)
- Hampson-Russell(Suite, ProMc,E-Log)
- Vista 2D-3D Seismic Processing.
- Hampson & Russell (Suite, ProMc, E-Log)
- Matlab – Syngram Module (Log Edit)

Chapter Two: Synthetic Model

2.1 Overview

A synthetic geological model was created to assess the interval Vp/Vs analysis method using results from this model. The model analysis provided ideal conditions in which well synthetic seismograms would achieve a high correlation to the synthetic seismic model and reduce uncertainty in the analysis. The first step in this analysis was to create a layered model; this model had horizontal interfaces with different thicknesses for each layer (Figure 2.1). The next step was to create the synthetic P and S sonic logs from the model. A density log was also created using a Gardner relationship (Gardner, 1974).

The wells were correlated to the PP and PS seismic data and interval Vp/Vs ratios were calculated. The model assumed an isotropic medium for each layer. Well synthetic seismograms were created to tie the wells to the synthetic seismic volume. Ricker wavelets were used to create synthetic seismograms. The dominant frequencies were 40 Hz and 25 Hz for PP and PS traces respectively.

2.2 Objective

The main objective of this chapter is to understand how the interval Vp/Vs analysis error can be evaluated under ideal conditions. These ideal conditions refer to beds that are completely horizontal with no dip and have a completely isotropic medium. Additionally, in this model, an accurate velocity profile and bed thicknesses are known and the seismic data are noise free. The findings from this chapter will be compared to findings from the subsequent case studies to check for consistencies in the results. Moreover, having a model provides the opportunity for testing beds so thin that may not be distinguishable in real seismic surveys due to the limitations in vertical resolution.

2.3 Model Criteria

As shown in Figure 2.1, the model consists of 6 layers of different thickness, denoted with the names Layers 1 to 6. The thickness of each layer was input into the CREWES Syngram program. For this particular model, the thickness of both the shallowest and deepest layers is 500 m. The thinnest bed is 10 m, denoted as layer 5. Logs for dipole sonic and density were also created using Syngram; this information was used to create synthetic seismograms for both the PP and PS data. Velocities for Vp and Vs were input based on common velocities in the Alberta Basin at each specific depth.

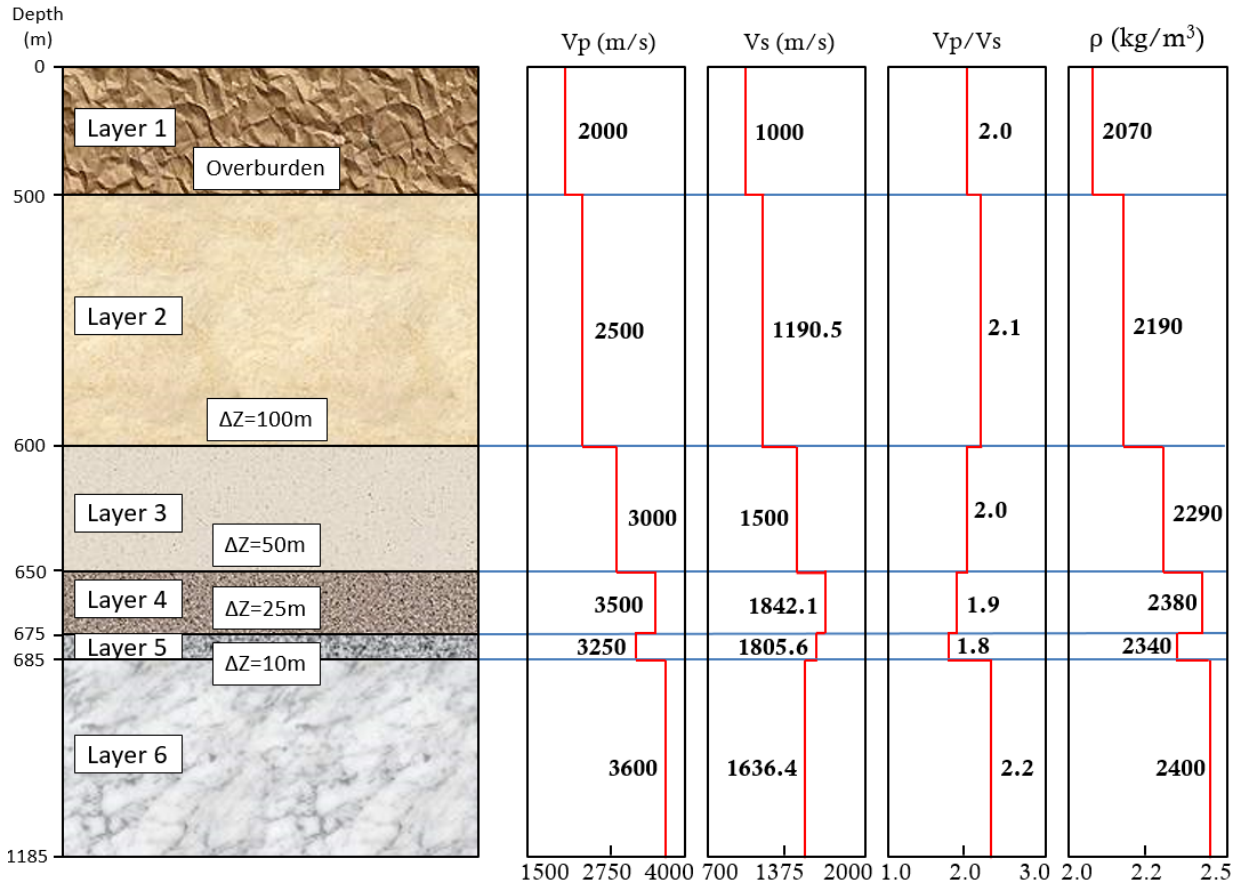

Figure 2-1: Layered model with P-wave, S-wave, Vp/Vs and density log information.

2.4 Synthetic Seismograms

In order to obtain a good correlation between the seismic data and the log, synthetic seismograms were created. The velocity and density logs were convolved with a 40 Hz dominant frequency Ricker wavelet (Figure 2.2) to create the synthetic trace. This wavelet was chosen because it had a frequency response and a bandwidth similar to the seismic data used in the later field studies. This same procedure was applied when creating the synthetic seismogram for the PS correlation; in this case, the impedance from the logs was convolved with a 25 Hz Ricker wavelet. The wavelets and their amplitude spectra are shown in Figures 2.2 and 2.3 respectively. Figures 2.4 and 2.5 show the synthetic seismograms for PP and PS data, respectively. The PS section is shown in Figure 2.6 with its interpreted horizons and Vp/Vs ratio information.

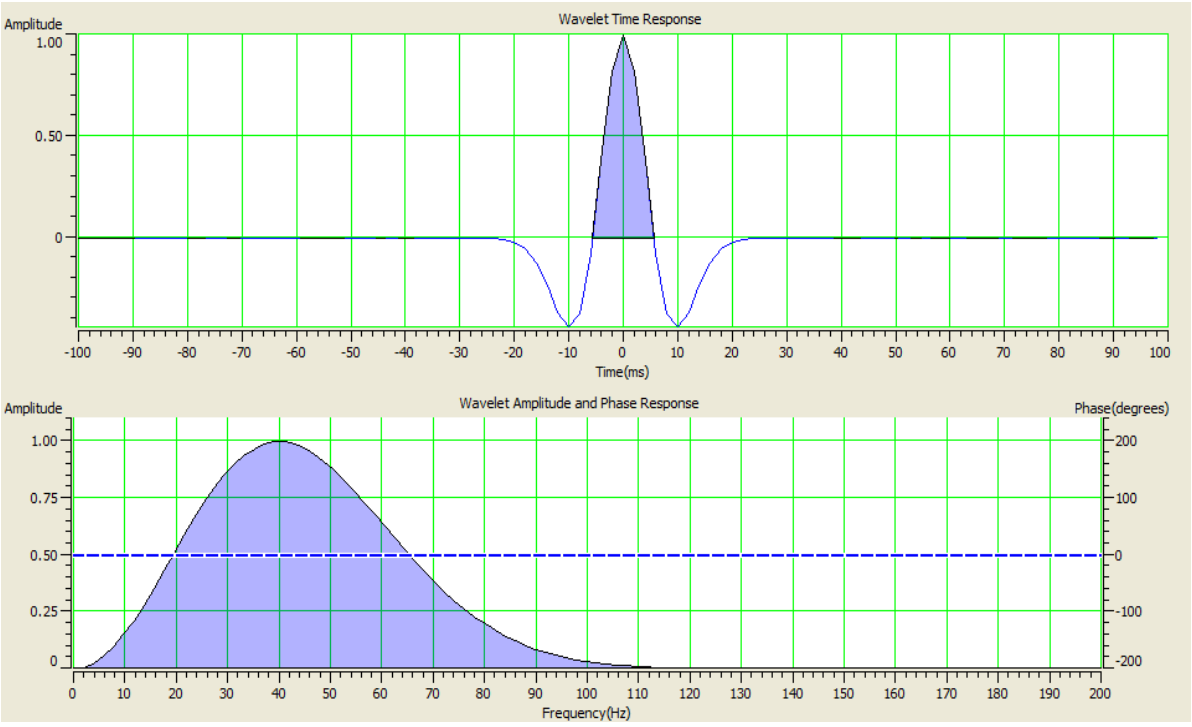

Figure 2-2: 40Hz dominant frequency Ricker wavelet for PP well ties with its amplitude spectrum; the dotted blue line indicates the wavelet zero phase.

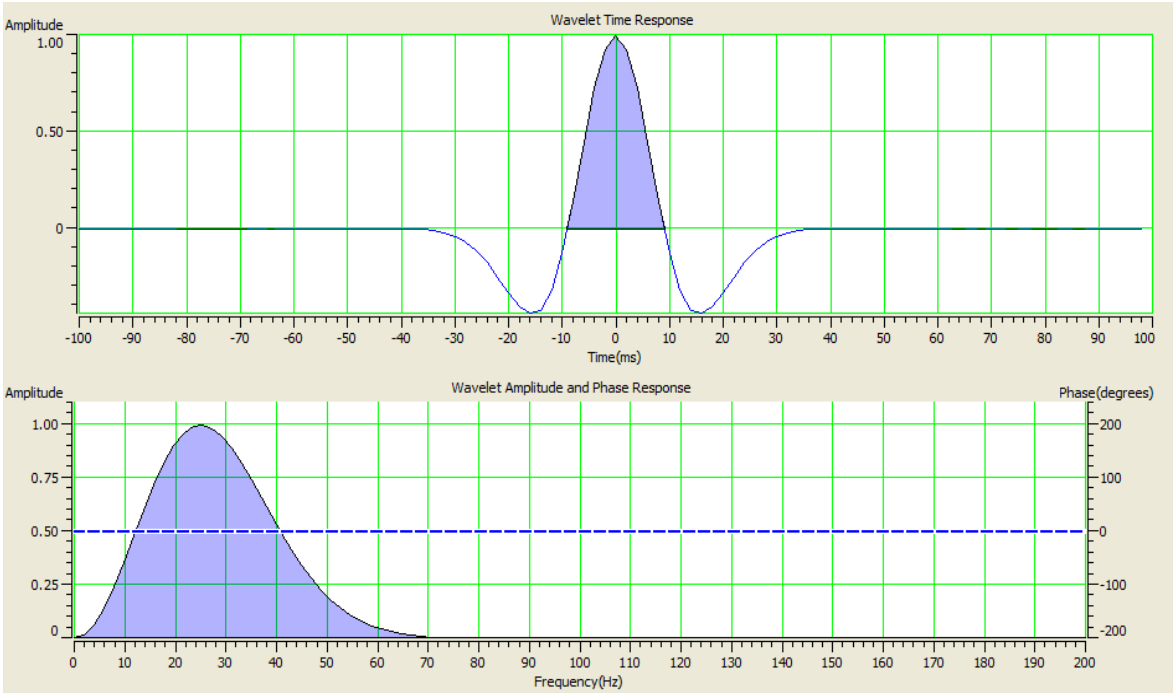

Figure 2-3: 25Hz dominant frequency Ricker wavelet for PS well ties with its amplitude spectrum; the dotted blue line indicates the wavelet is zero phase.

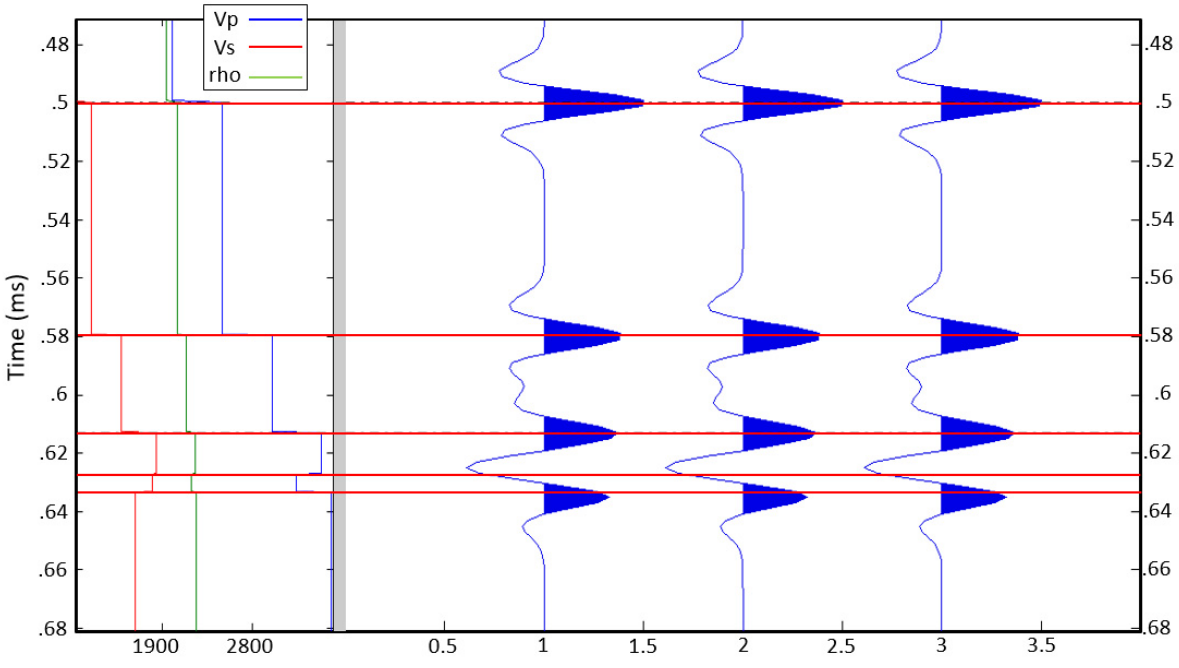

Figure 2-4: Synthetic seismogram for the PP section.

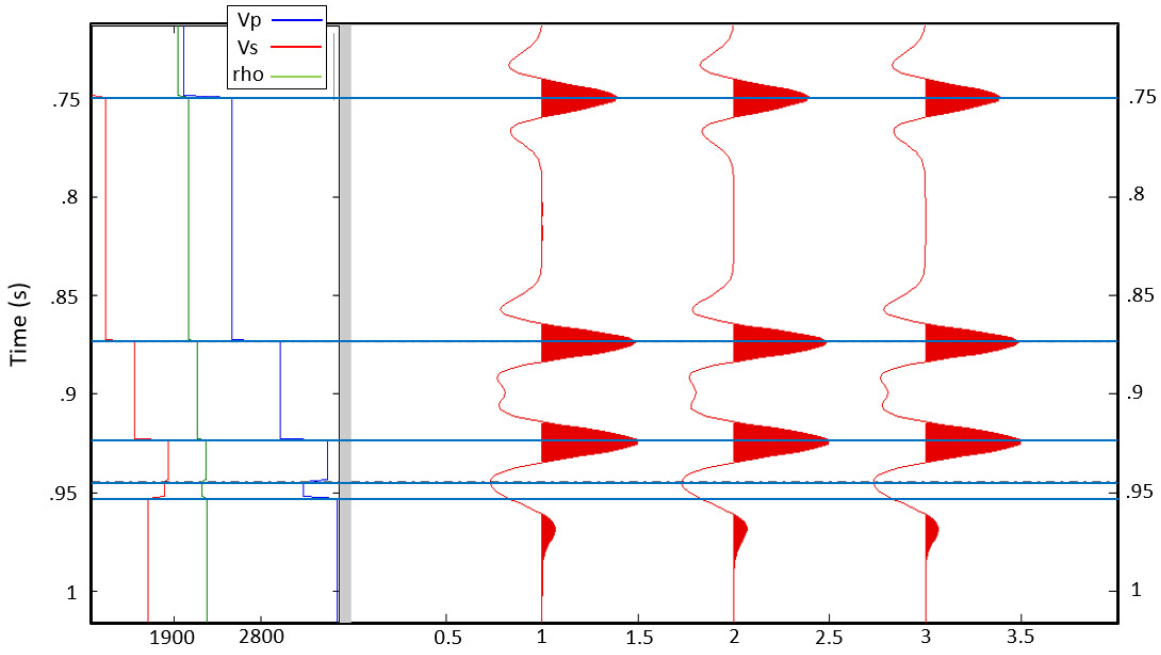

Figure 2-5: Synthetic seismogram for the PS section.

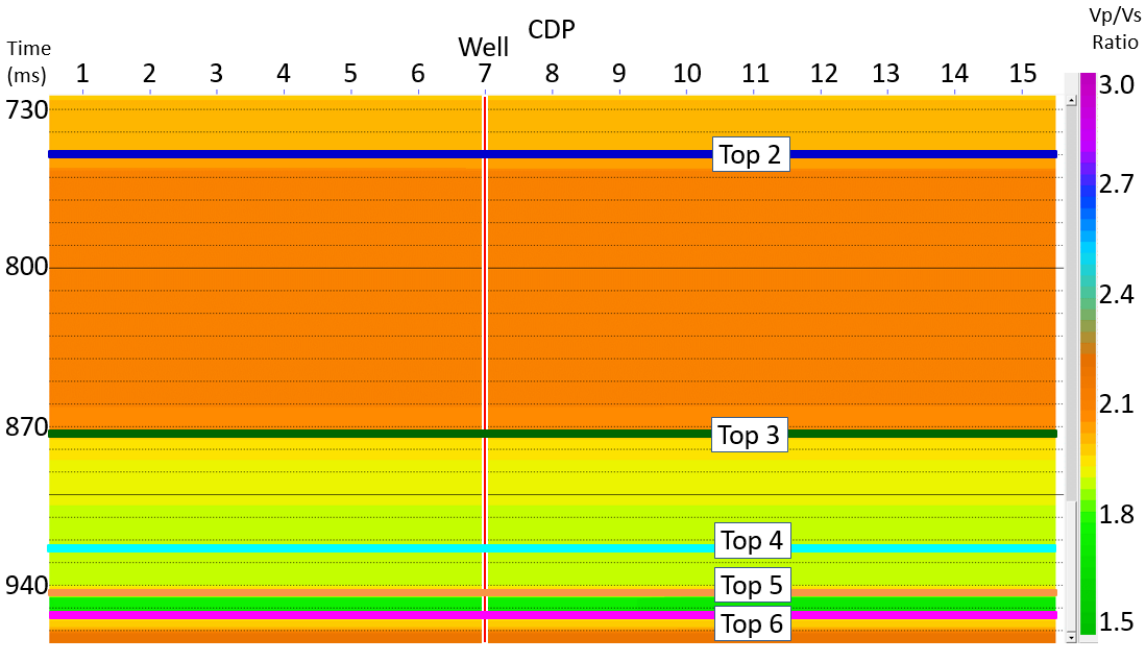

Figure 2-6: Velocity Model (in PS time) section with Vp/Vs ratio information and interpreted horizons.

2.5 Model synthetic ties

In this study, the tie between the seismic data and the well is a good match as expected. The tops of the well aligned perfectly with the events of the seismic data. Figures 2.7 and 2.8 shows the well tie of the model, in which the blue lines represents the calculated synthetics; these lines aligned perfectly to match the red lines, which represents the seismic data. A total of 5 tops were estimated in this analysis. Figure 2.9 shows both PP and PS sections with their respective horizons picks.

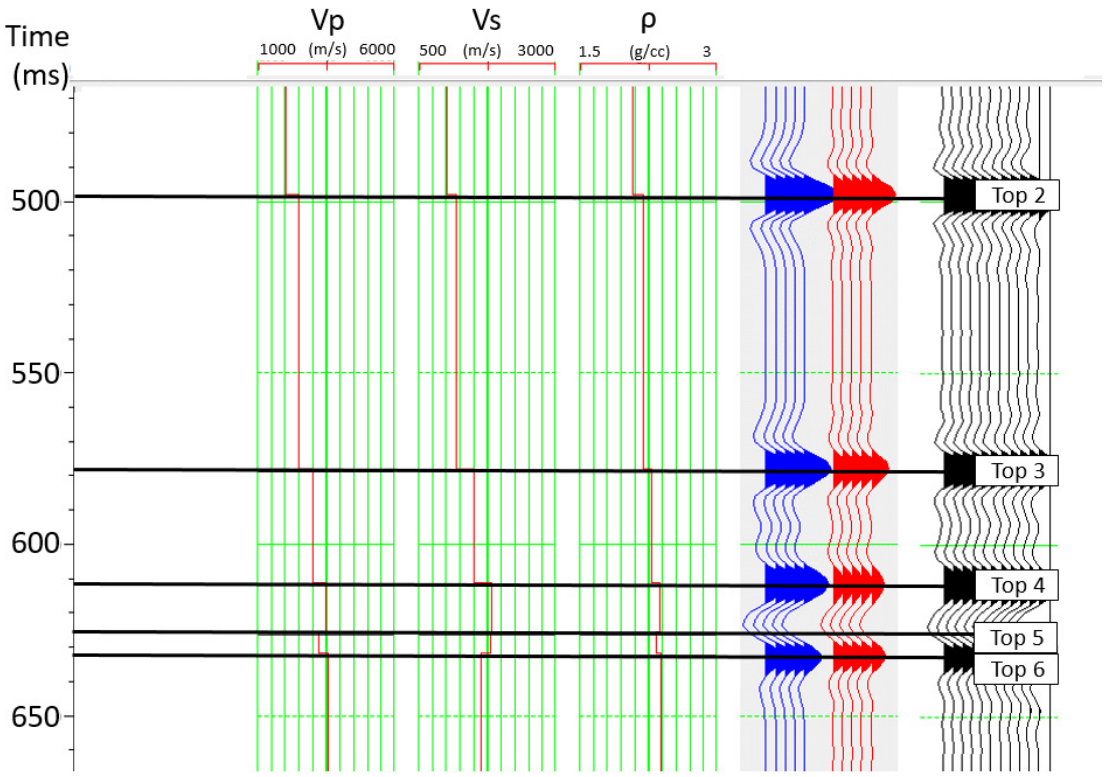

Figure 2-7: Final tie of the synthetic seismogram to the PP times. The blue traces represent the synthetic seismogram and the red traces are the extracted trace from the seismic data near the well location.

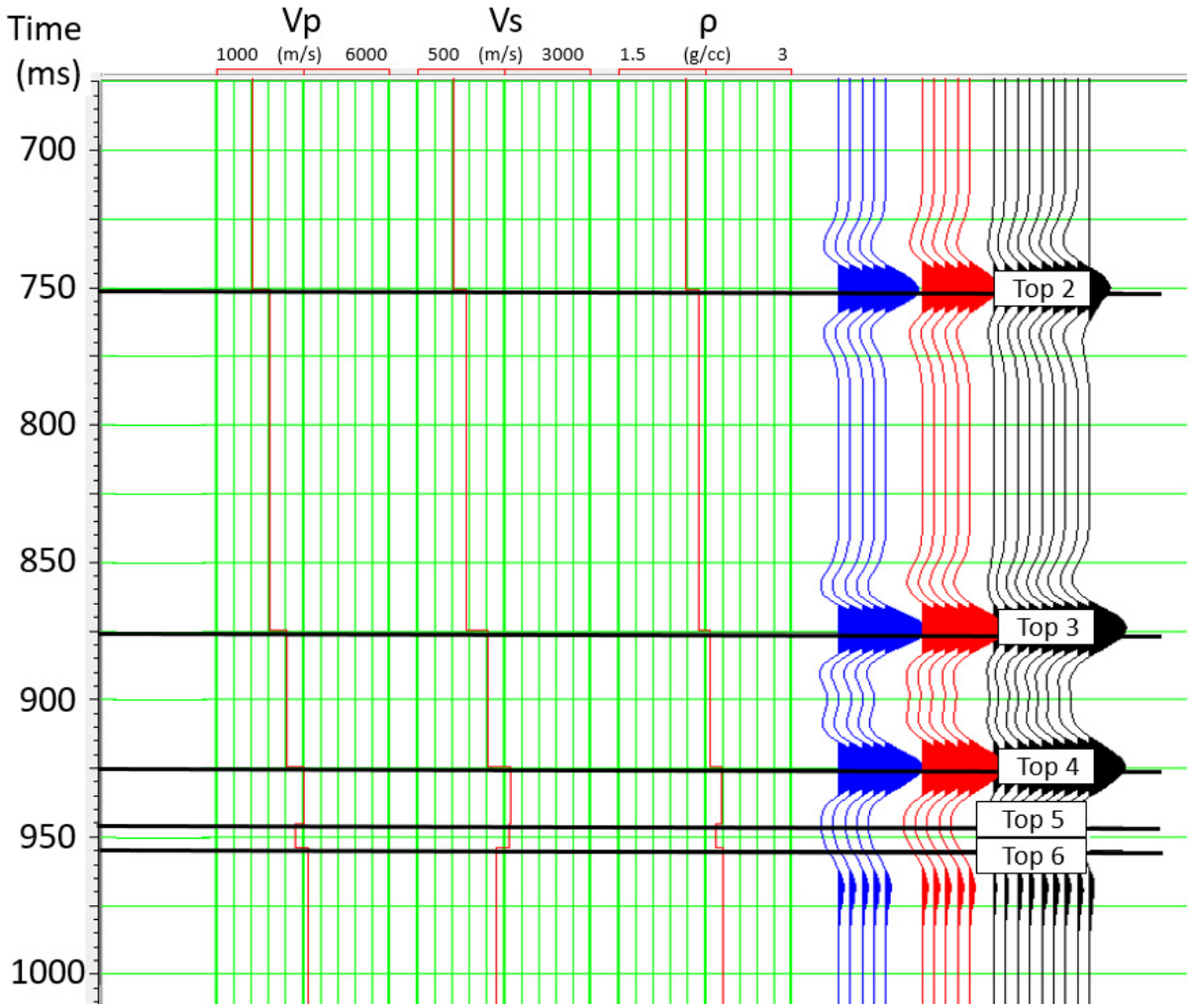

Figure 2-8: Final tie of the synthetic seismogram to the PS times. The blue traces represent the synthetic seismogram and the red traces are the extracted trace from the seismic data near the well location.

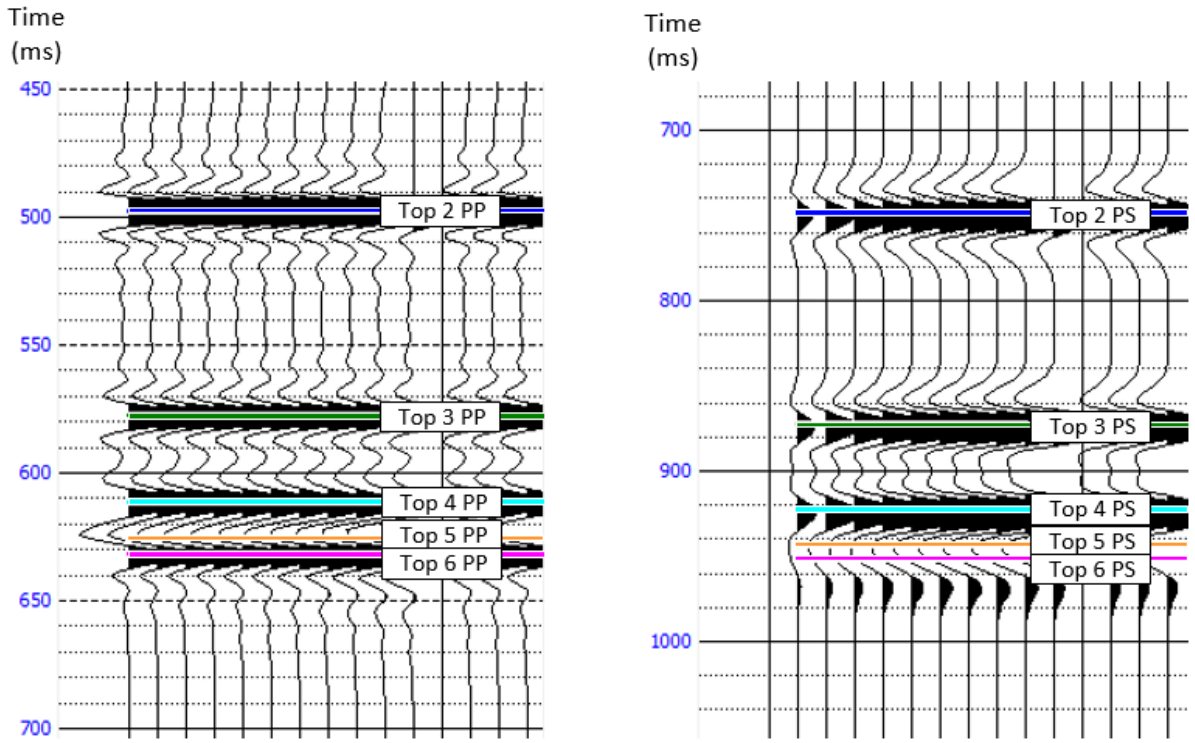

Figure 2-9: Interpretation of (left) the PP section and (right) the PS section; the PS section is plotted at 2/3 the scale of the PP section.

2.6 Horizon Picking

In reality, well top locations do not exactly match the same locations as the geological interfaces. Interpreters commonly pick the peak, trough, or zero crossings to mark horizons and often a time shift is required to reduce this mismatch error. In this synthetic model, interfaces perfectly match the top locations but as the layer's thickness becomes 25m or less, a time shift was required from the picked event. Figures 2.10 and 2.11 shows the time shift corrections that were made for the synthetic model.

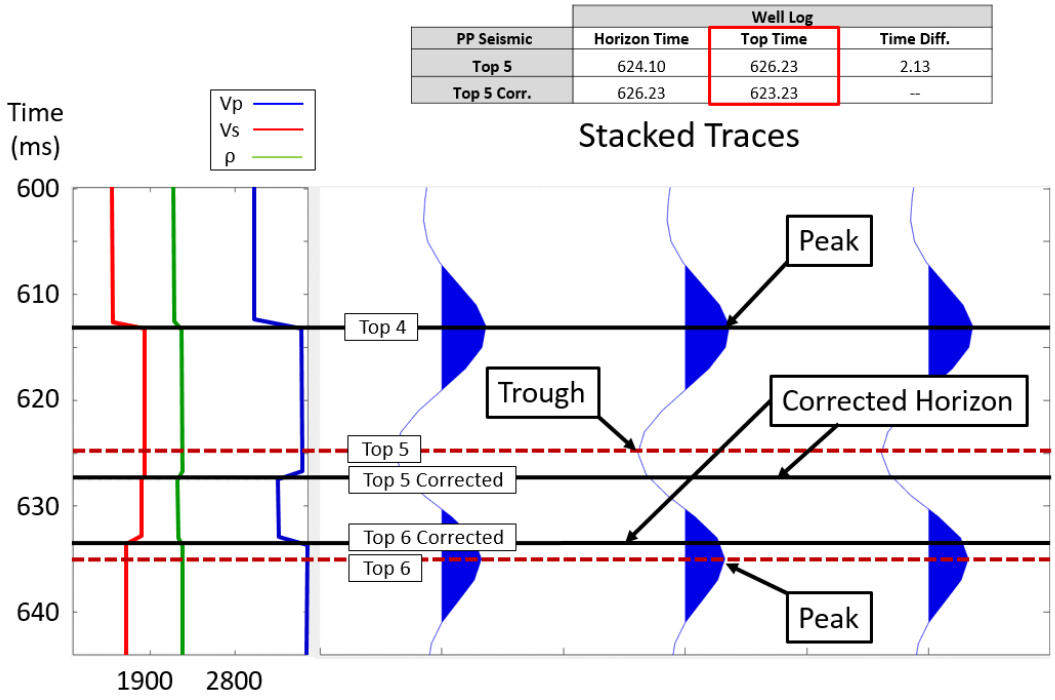

Figure 2-10: The table shows the time improvement applied on the PP section for top 5 and 6. The corrected horizons time for top 5 is noted in the red box.

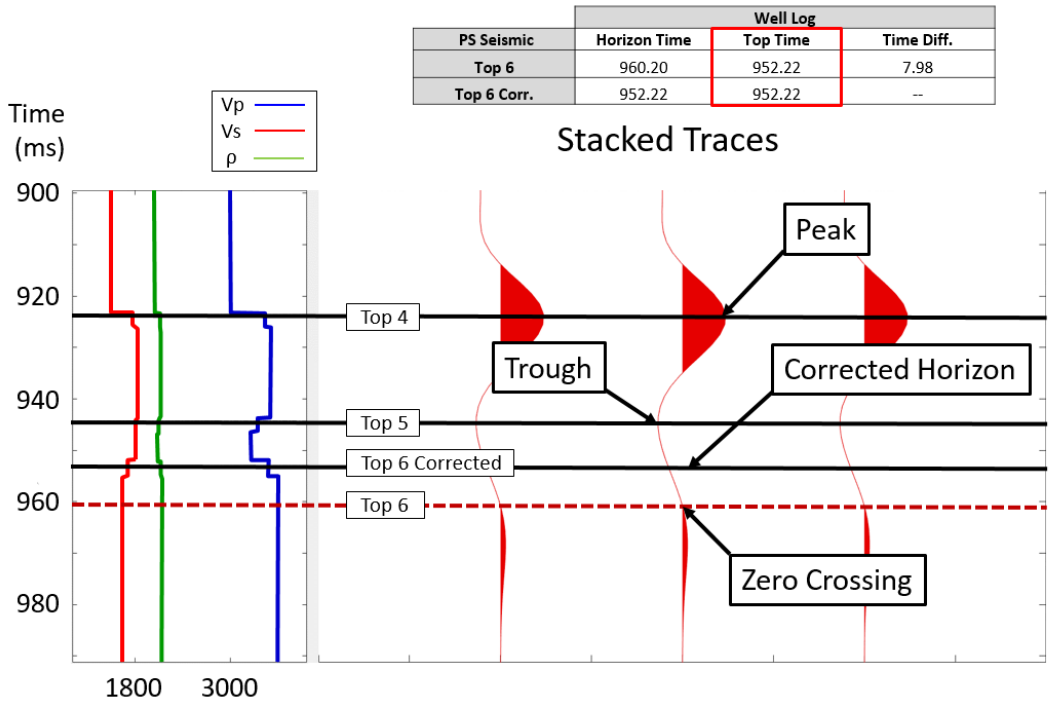

Figure 2-11: The table shows the time improvement applied on the PP section for top 6. The corrected horizons time for top 6 is noted in the red box.

2.7 Vp/Vs Error Estimation

To estimate the error for the Vp/Vs analysis, propagation error method was used. This method calculates the error in the values of a function based on the effects of the uncertainty of the variables on the function (Louro, 2014). An uncertainty of ±2 ms was used for the horizon picks in order to find the uncertainty in Vp/Vs. This value of ±2 ms was chosen based on the results obtained from all the studies in this project. In the case of the PP section, the uncertainty number was slightly higher than ±1 ms and for the PS section it was slightly higher than ±2 ms, both of these values were obtained after the picks were time corrected and our final number was an average of both of these uncertainties.

In this case, the function used to calculate Vp/Vs (equation 1.8) has two variables: ΔTpp and ΔTps. According to the propagation of error equation, if a function y depends on the variables x1, x2,…., xn, where xi is measured with uncertainties $u(x_i)$, the uncertainty in the calculated value y is given by:

$$u(y) = \sqrt{{c_1}^2 u(x_1)^2 + {c_2}^2 u(x_2)^2 + \cdots {c_n}^2 u(x_n)^2} \tag{2.1}$$

where c_i are called sensitivity coefficients because they provide information about how sensitive y is to uncertainties in each of the variables. Each sensitivity coefficient is the partial derivatives of y with respect to each x_i:

$$c_i = \frac{\partial y}{\partial x_i}$$

To simplify the expression, the variables ΔTpp and ΔTps were substituted by z and x, respectively and Vp/Vs was substituted by the variable y. The sensitivity coefficients can then be written as

$$y = \frac{(2\Delta Tps - \Delta Tpp)}{\Delta Tpp} = \frac{2x - z}{z}$$

$$c_1 = \frac{\partial y}{\partial x} = \frac{\partial}{\partial x}\left(\frac{2x - z}{z}\right) = \frac{(2)(z) - (0)}{z^2} = \frac{2}{z};$$

$$c_1{}^2 = \frac{4}{z^2} \tag{2.2}$$

$$c_2 = \frac{\partial y}{\partial z} = \frac{\partial}{\partial z}\frac{(2x - z)}{z} = \frac{(-1)(z) - (1)(2x - z)}{z^2} = \frac{-z - 2x + z}{z^2} = \frac{-2x}{z^2};$$

$$c_2{}^2 = \frac{4x^2}{z^4} \tag{2.3}$$

Then substituting equations 2.2 and 2.3 into 2.1, and with the uncertainties u (x) and u (z) equal to ±2 ms, the final absolute error equation for Vp/Vs will be given by

$$Vp/_{Vs}\,(error) = \left(\sqrt{\frac{4}{z^2}u(2)^2 + \frac{4x^2}{z^4}u(2)^2}\right) \times \frac{100}{Isochron\ Length};$$

$$^{Vp}/_{Vs}\,(error) = \left(4\sqrt{\frac{1}{\Delta Tpp^2} + \frac{\Delta Tps^2}{\Delta Tpp^4}}\right) \times \frac{100}{Isochron\ Length} \tag{2.4}$$

Vp/Vs uncertainty error was calculated using Equation 2.4. Figure 2.13 shows that the relative error in Vp/Vs for each isochron is small for large isochrons on both corrected and uncorrected horizons. The percent error increases by a power relation and moves asymptotically as the time interval decreases. The percent error of the thinnest interval was approximately 62 % when horizons were time corrected, indicating that obtaining an accurate estimation of the Vp/Vs ratio is very unlikely.

As mentioned earlier for this particular model, geological interfaces and well tops have a perfect match for large isochrons, which is not always the case in reality. On the other hand, for the small isochrons, a mismatch was noticed. In this model, the smallest isochron for uncorrected horizons has an error of 32.5 %, due to this isochron being picked to be 11.1 ms when in reality it should be 6.1 ms.

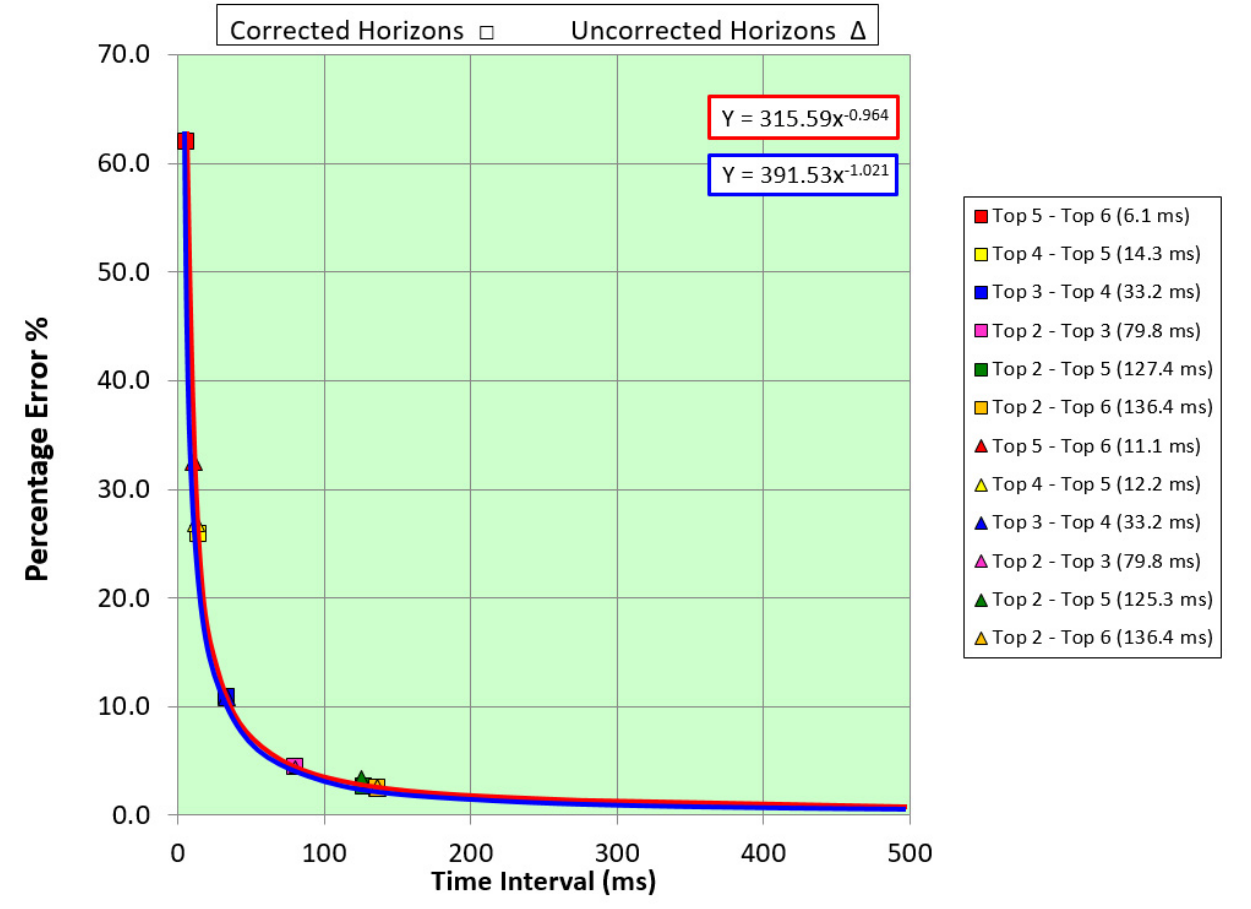

Figure 2-12: Cross-plot of percent relative error in Vp/Vs versus ΔTpp time interval; the error tends to increase as the time interval becomes smaller. The red trendline represents horizons with time corrections and is represented by the power function in the red box. The blue line represents the uncorrected horizons and is represented by the power function in the blue box.

2.8 Summary

Uncertainty plays a factor in the estimation of Vp/Vs ratio error, especially when the beds were as thin as the ones built in the synthetic model. Although the model presented isotropic properties, it did follow the trend line of the power function. In addition, the time correction performed on the horizons provided small improvements to the accuracy of the interval Vp/Vs calculations for isochrons greater than approximately 12 ms.

Chapter Three: The Hussar Experiment

3.1 Hussar Experiment Overview

3.1.1 Introduction

The objective of the Hussar experiment was the use of existing seismic and log data to make precise estimates of interval Vp/Vs values. Part of this objective was to analyze how bed thickness and interpretation (picking) errors could affect the estimation of these values. In addition, this study provided a suggestion for the minimum time intervals that should be used by interpreters in order to estimate robust interval Vp/Vs values.

3.1.2 Geology Overview

The data location is in central Alberta and is characterized by plains where the underlying surface formations are Cretaceous and Tertiary moderately indurated sediments that dip gently to the southwest (Allan and Rutherford, 1934). A stratigraphic chart from this area is shown in Figure 3.1.

The specific target of interest for the horizon interpretation is the Manville Group, which belongs to the oldest Cretaceous rocks and represents a major episode of subsidence and sedimentation following a long period of uplift, exposure and erosion of older strata (Mossop and Shetsen, 1994). The Mannville Group (Figure 3.1) is less than 40 m thick in some areas, but in the Rocky Mountain foothills, it is more than 700 m thick. Gas and oil are trapped in fluvial reservoir sandstones in the south and in shoreline sandstone units throughout northern and central regions (Smith et al., 1994). The Mannville Group is disconformably overlain by the Joli Fou Formation shale of the Colorado Group and it is underlain by older Paleozoic carbonates (Mossop and Shetsen, 1994).

This group also consists of interbedded continental sand and shale at the base (Detrital and Ellerslie Member), followed by a Calcareous Sandstone Member, marine shale (Ostracod beds) and Glauconitic Sandstones. The Glauconitic/Bluesky strata record the maximum transgression and subsequent early regressive stages of the lower Cretaceous Sea in the southern and central parts of the Basin. Marine evidence prevails in the Glauconitic Sandstone in Central Alberta and in the Bluesky Formation in northern Alberta (Gavotti and Lawton, 2014).

The Glauconitic Sandstone consists of very fine to medium quartz-rich sandstone in eastern Alberta and quartz sandstone intermixed with coarser sandstone in the western part of the province. Commonly, the glauconite content decreases and clay content increases in southern Alberta, where the unit becomes less marine.

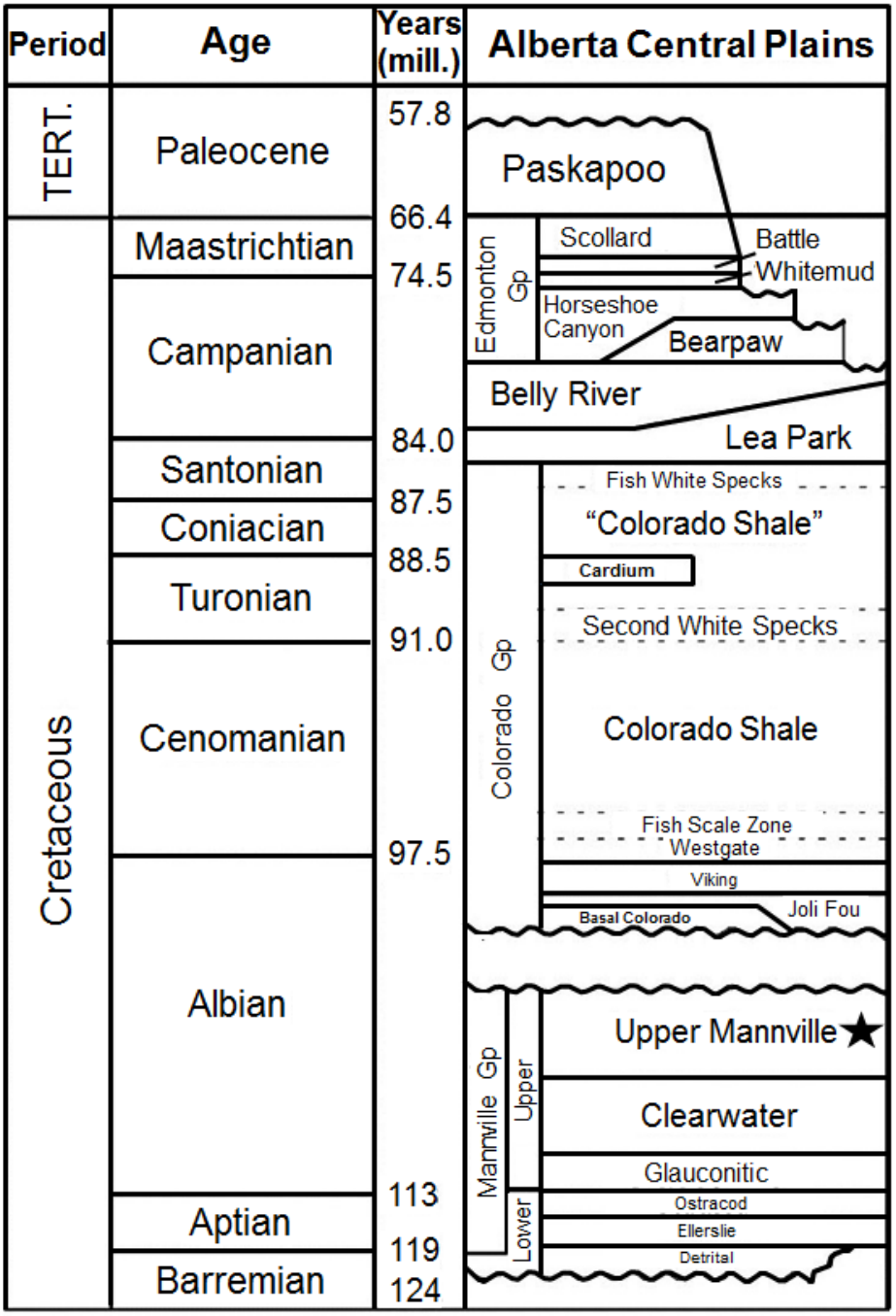

Figure 3-1: Stratigraphic chart of the Mesozoid and Cenozoid strata in central Alberta. The star indicates the target formation (modified from Pemberton and MacEachen, 1995).

3.2 Hussar Data

The Hussar experiment was performed in 2011 in association with CREWES and the sponsors INOVA, Geokinetics, and Husky Energy (Margrave et al. 2011). The location for this particular experiment was near Hussar, Alberta, about 100 km east of the city of Calgary. This site was chosen because of its proximity to Calgary and excellent well data.

The seismic line extended for 4.5 km from northeast to southwest and was acquired with 10 Hz 3C geophones (Figure 3.2). A total of 484 geophones were laid out on this line in intervals of 10 m. Dynamite was used as a source for the seismic data recorded on this line and in this analysis, the three wells closest to the seismic line were included in the study (Figure 3.2).

Well 12-27 had a dipole sonic tool that recorded P-wave and S-wave sonic velocities. In addition, it had density and gamma-ray logs. Both wells 14-27 and 14-35 had a monopole sonic tool that allowed only P-wave velocities to be recorded. Density and gamma-ray logs were also available in these wells (Figure 3.3). A cross-plot of P-wave and S-wave sonic velocities from the target of investigation was created for well 12-17. A best fit linear relationship line was obtained and this information from this line was input into Castagna's equation to derive the S-wave sonic for wells 14-27 and 14-35. It is assumed that the linear relationship is a perfect representation of all the values but in reality these values are somewhat scattered, the linear result is just an approximation, and an uncertainty error might be introduced.

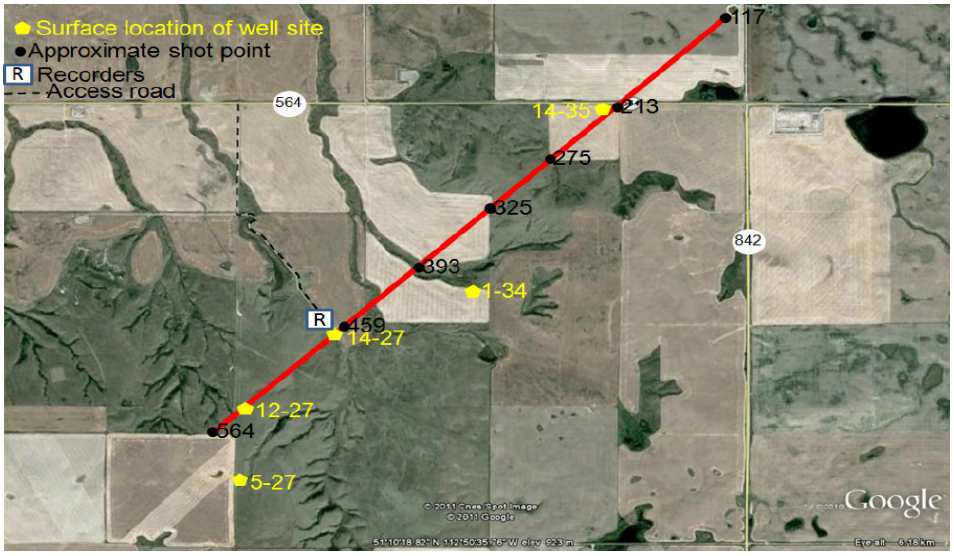

Figure 3-2: Location of the Hussar seismic line with nearby wells, and shot locations. Well 12-27 provided dipole sonic logs; wells 14-27 and 14-35 only provided P-wave logs. (Margrave et al., 2011).

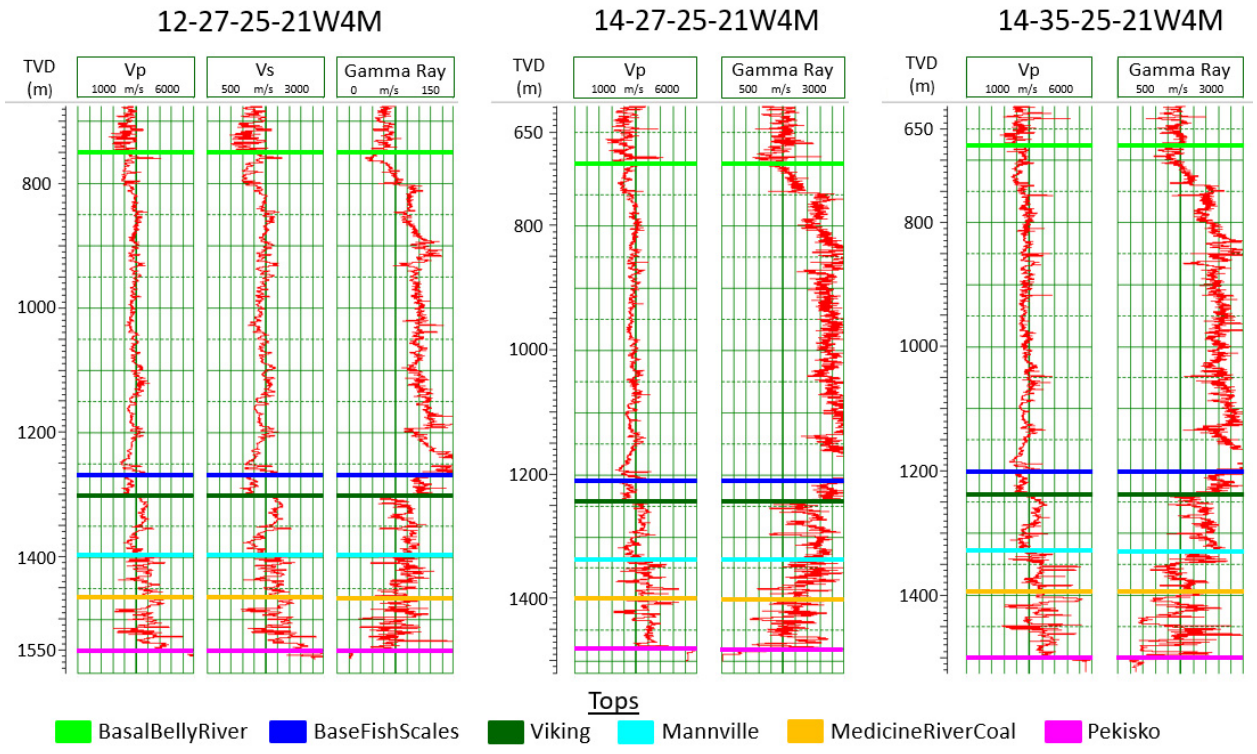

Figure 3-3: Hussar experiment wells. Well 12-27 provided dipole sonic data.

The seismic section was processed (Isaac and Margrave, 2011) in order to attenuate the surface waves and undesirable wavetrains while attending to keep the broadband frequency content of the reflection data. Their processing included radial trace filter and Gabor deconvolution applied for noise attenuation. Static corrections were also applied and the data was post-stack Kirchhoff time migrated. During processing, care was taken to preserve the maximum frequency bandwidth of the signal. (Isaac and Margrave, 2011). As part of my study, FX filtering and band-pass filters were applied to both PP and PS seismic sections to improve the signal (Figures 3.4 and 3.5).

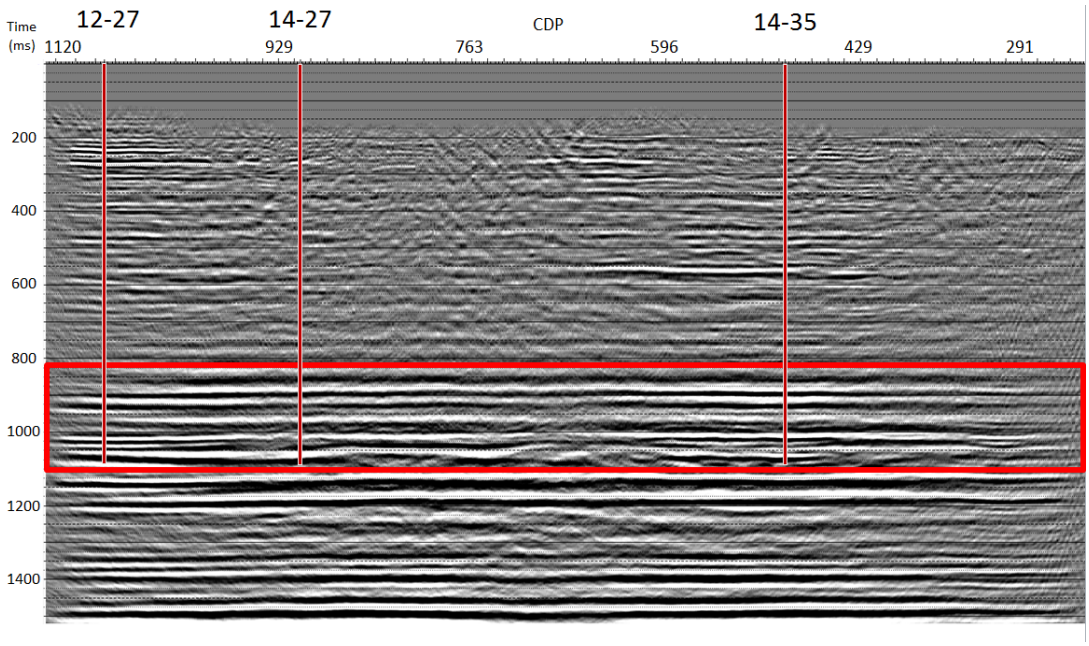

Figure 3-4: Hussar PP seismic section; the red rectangle indicates the main zone of investigation; well locations are indicated by the vertical red lines.

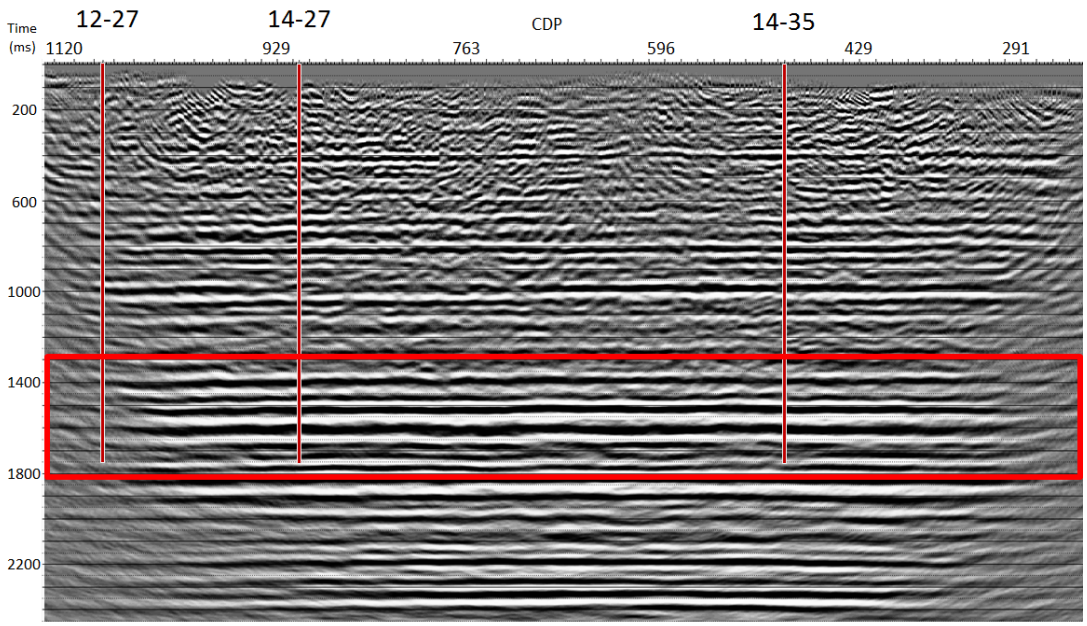

Figure 3-5: Hussar PS seismic section; the red rectangle indicates the main zone of investigation; the uncorrelated well locations are indicated by the vertical red lines.

3.2.1 Wavelet and Resolution

On both PP and PS sections, the statistical wavelets were extracted at the well locations. Figure 3.6 and 3.7 show the final multi-well wavelets extracted from the wells 14-27 and 14-35 with their amplitude spectra for both the PP and PS sections.

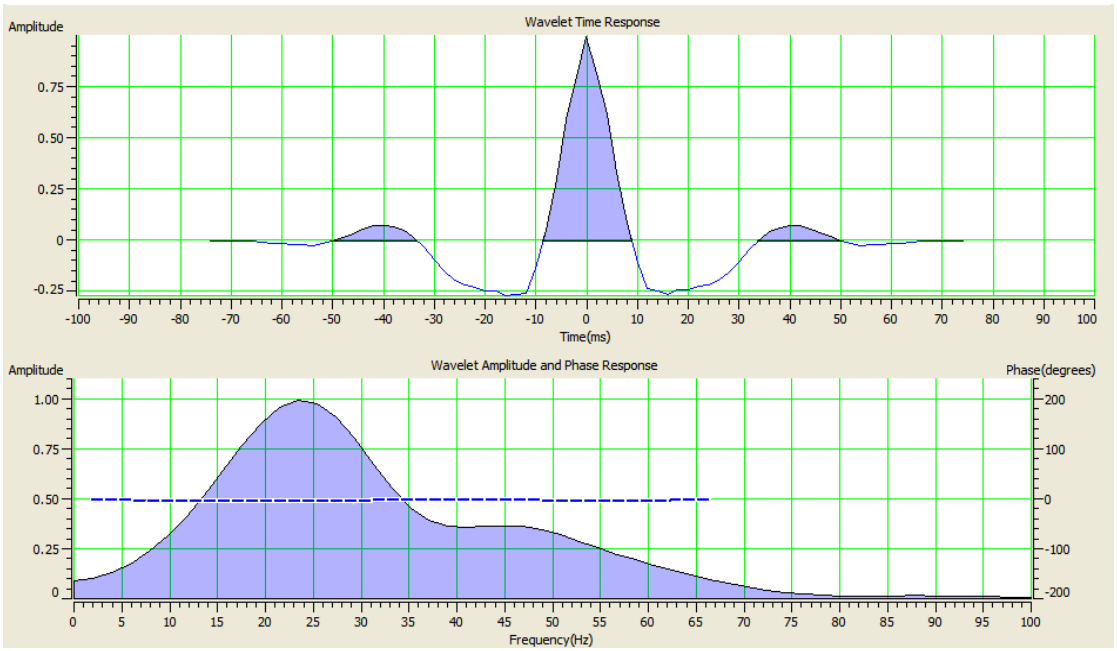

Figure 3-6: PP section multi-well wavelet extracted from the wells 14-27 and 14-35 with its amplitude spectrum; the dotted blue line indicates the wavelet's average phase.

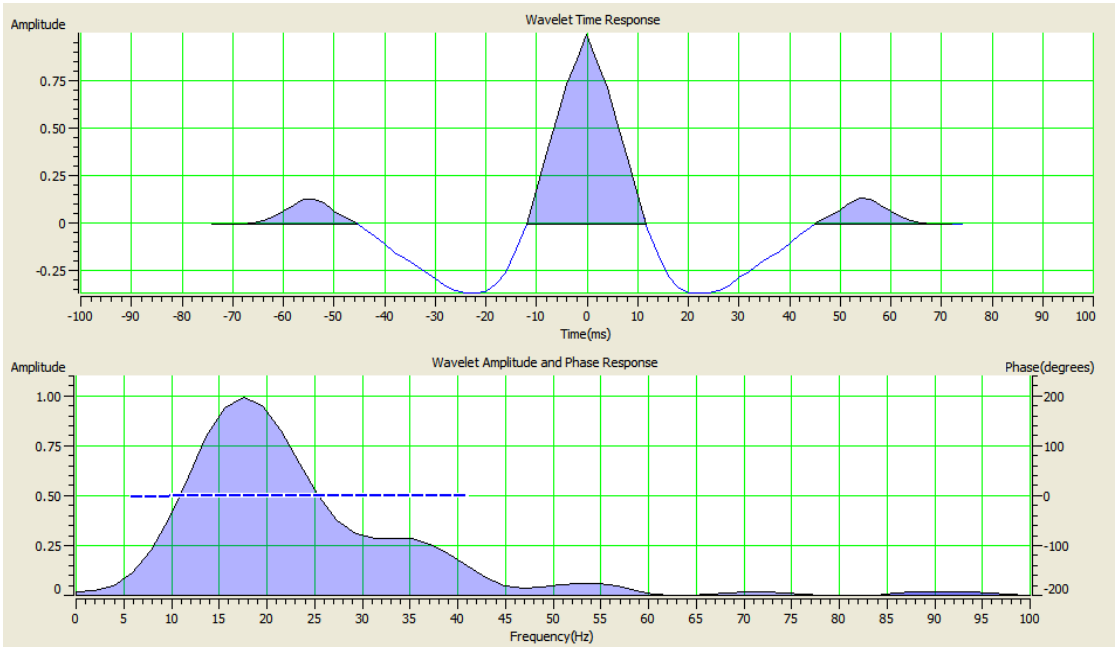

Figure 3-7: PS section multi-well wavelet extracted from the wells 14-27 and 14-35 with its amplitude spectrum; the dotted blue line indicates the wavelet's average phase.

For practical purposes, the tuning thickness can be considered as an indicator of the vertical resolution. Widess (1973) claimed that bed thickness would be discernible if the bed had a thickness 1/8 of the wavelength. The Rayleigh criterion is the generally accepted criterion for vertical resolution; it defines the limit of resolution at 1/4 of the dominant wavelength. From the seismic data, our period was approximately 40 ms and our dominant frequency was 25 Hz (Figure 3.8). The average compressional velocity at our area of investigation was 3400 m/s and the vertical thickness at our point of interest was approximately 34 m.

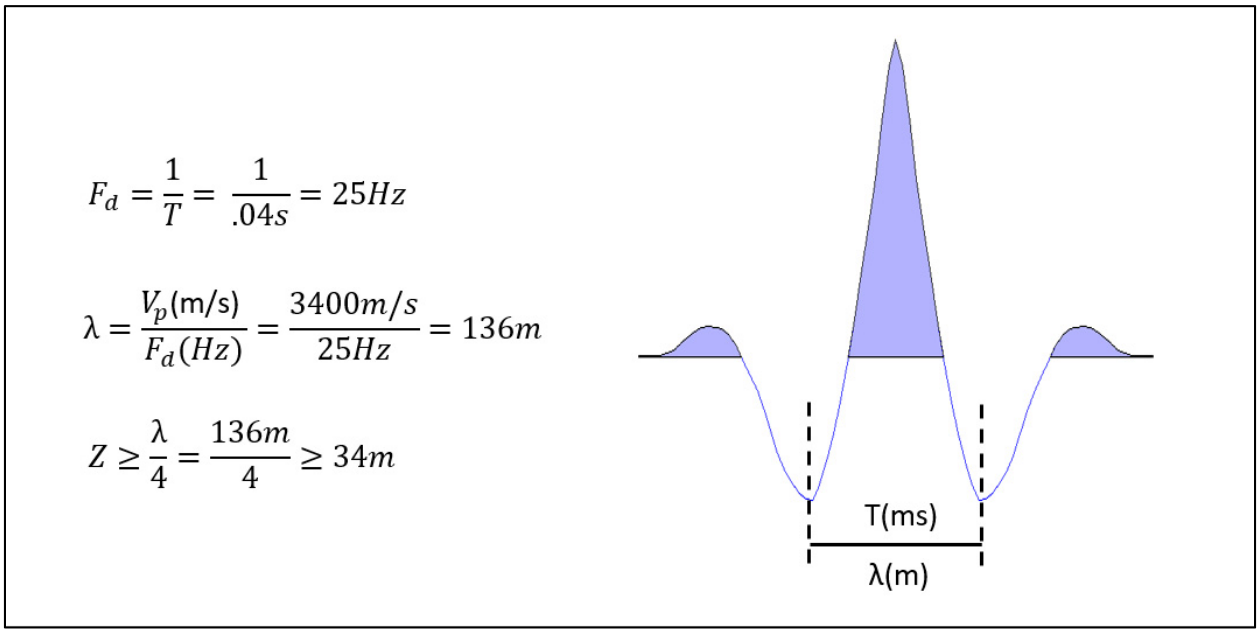

Figure 3-8: The calculation of the minimum bed thickness that can be resolved; Z is the minimum thickness, Fd is the dominant frequency, T is the wavelength period, and λ represents the wavelength.

3.2.2 Lithology Discrimination

Many factors can influence Vp/Vs values, such as the lithology and pore fluids. A lithology investigation was conducted to understand how this could influence the results. The

relationship between Vp and Vs for well 12-27 is shown in Figure 3.9 and is quasi-linear. The relationship between the gradient and the lithology, especially the shale content, is a subject for further investigation. Cross-plots were created from well log curves from well 12-17. Figure 3.10 shows Vp versus Vs cross-plot; the color key shows gamma ray (GR) log where the lower values (GR<50 API) corresponds to cleaner sandstones (Rider, 2011). These cross-plots are from the depth of investigation which covers the Mannville Formation.

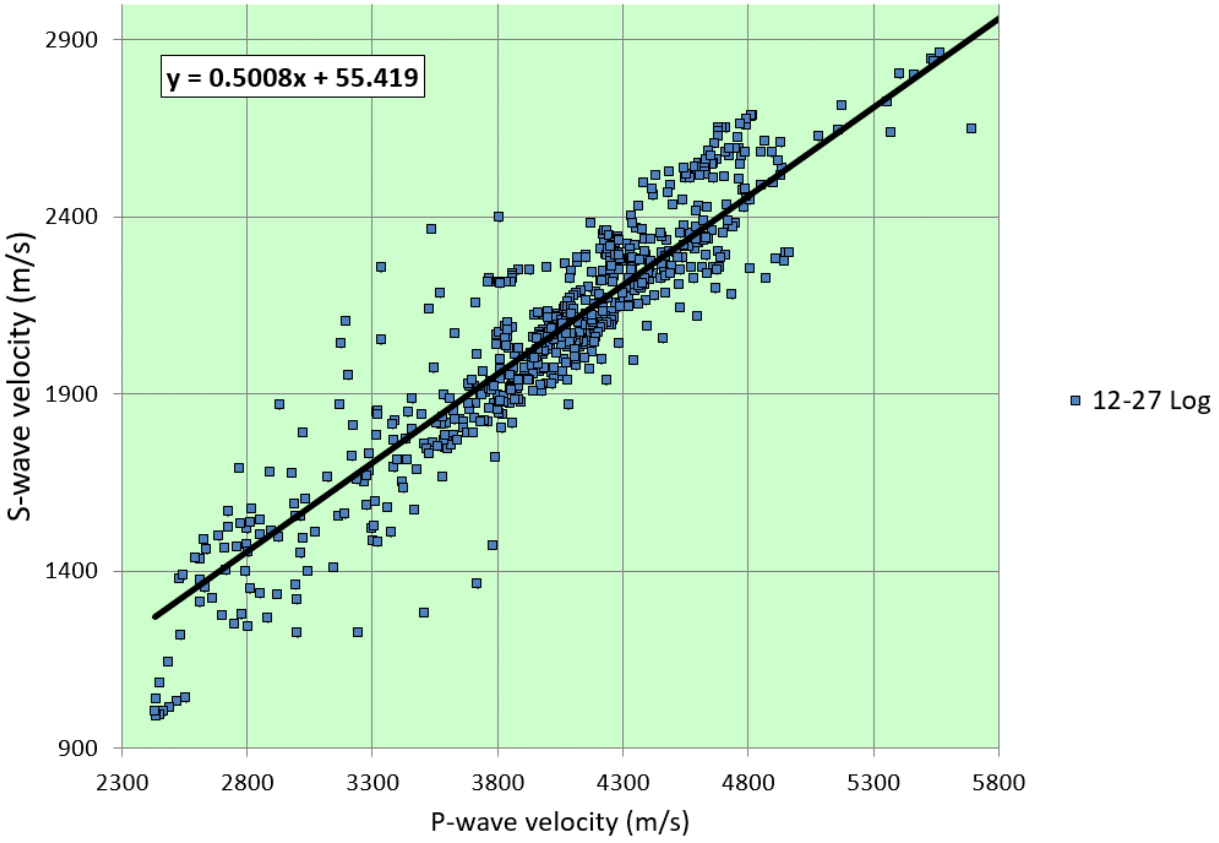

Figure 3-9: Vp against Vs cross-plot with a gradient line of 0.50 for well 12-27 in the Mannville formation.

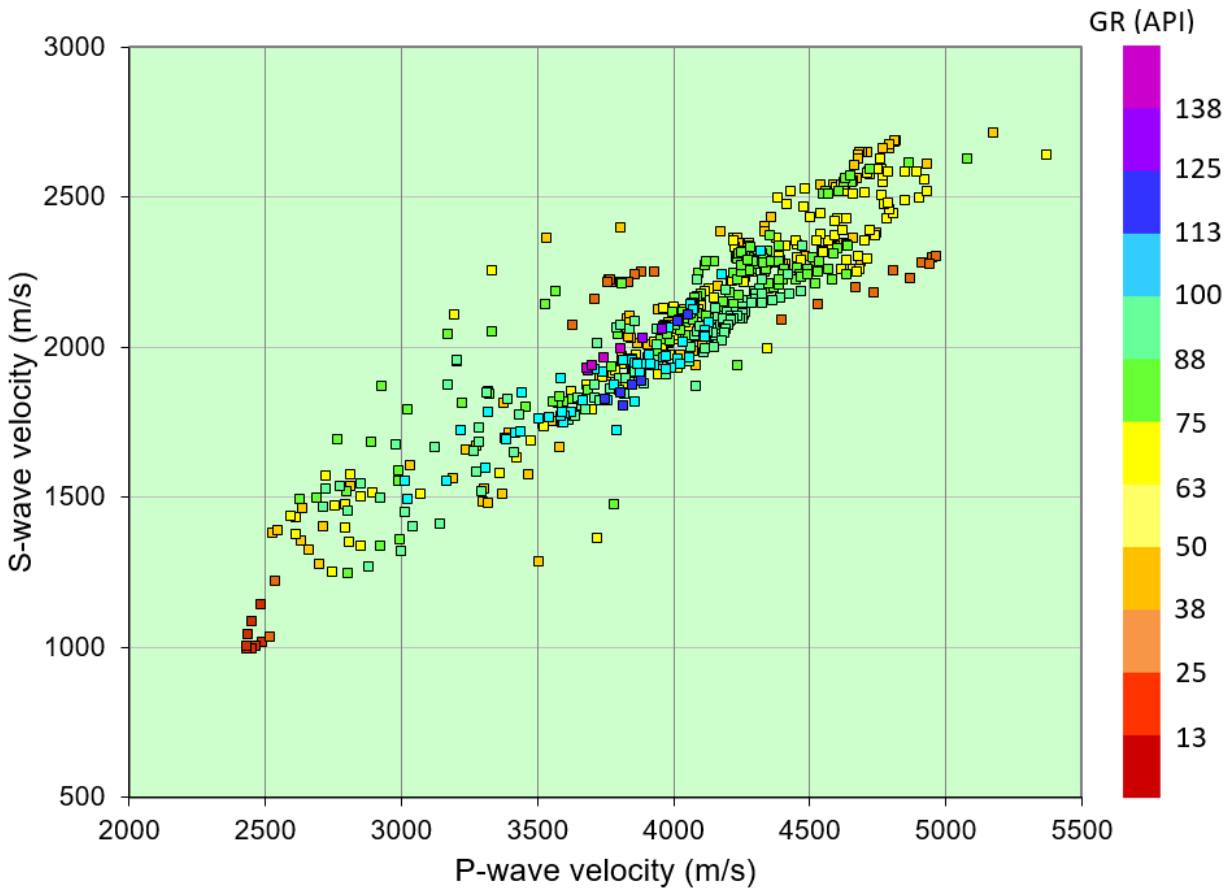

Figure 3-10; Cross-plot Vp against Vs (Color: Gamma-Ray) in well 12-27.

The plot of Vp against Vp/Vs, as shown in Figure 3.11, shows a lot of scatter, but generally Vp/Vs increases as Vp increases. The basis of much of the lithology work in PS exploration relates to anomalous changes in Vs with respect to Vp (Stewart et al., 2002). A changing Vp/Vs value is often closely tied to a changing lithology (Rider, 2011) and perhaps pore geometry and pore fluids. Vp/Vs values cluster between 1.9 and 2.0 at relative high P-wave velocities.

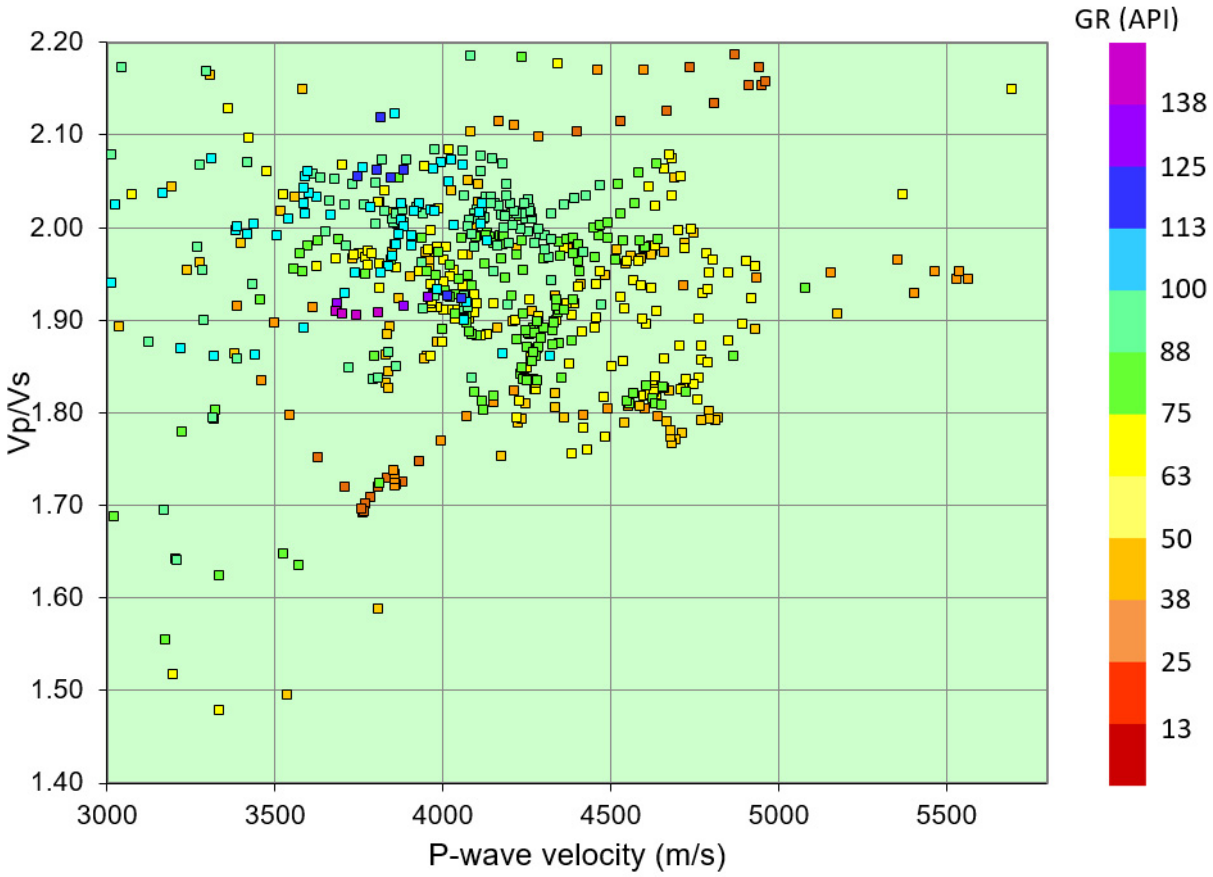

Figure 3-11: Cross-plot Vp versus Vp/Vs for well 12-27.

The plot of the Vp/Vs ratio against gamma log values for well 12-27 is shown in Figure 3.12. The data points are very scattered, although there is a general trend of Vp/Vs increasing with increasing gamma log values, which reflects an increase in shale content. The majority of the data points from well 12-27 have API values less than 100 and there is a dense cluster of points with values of 60 to 95 API. Most points from well 12-27 at the Glauconitic Formation (Mannville Group) have Vp/Vs values ranging from 1.76 to 1.95; by comparing Figures 1.7 and 3.11, it can be seem that these values are dominated more by shaliness than by sand content.

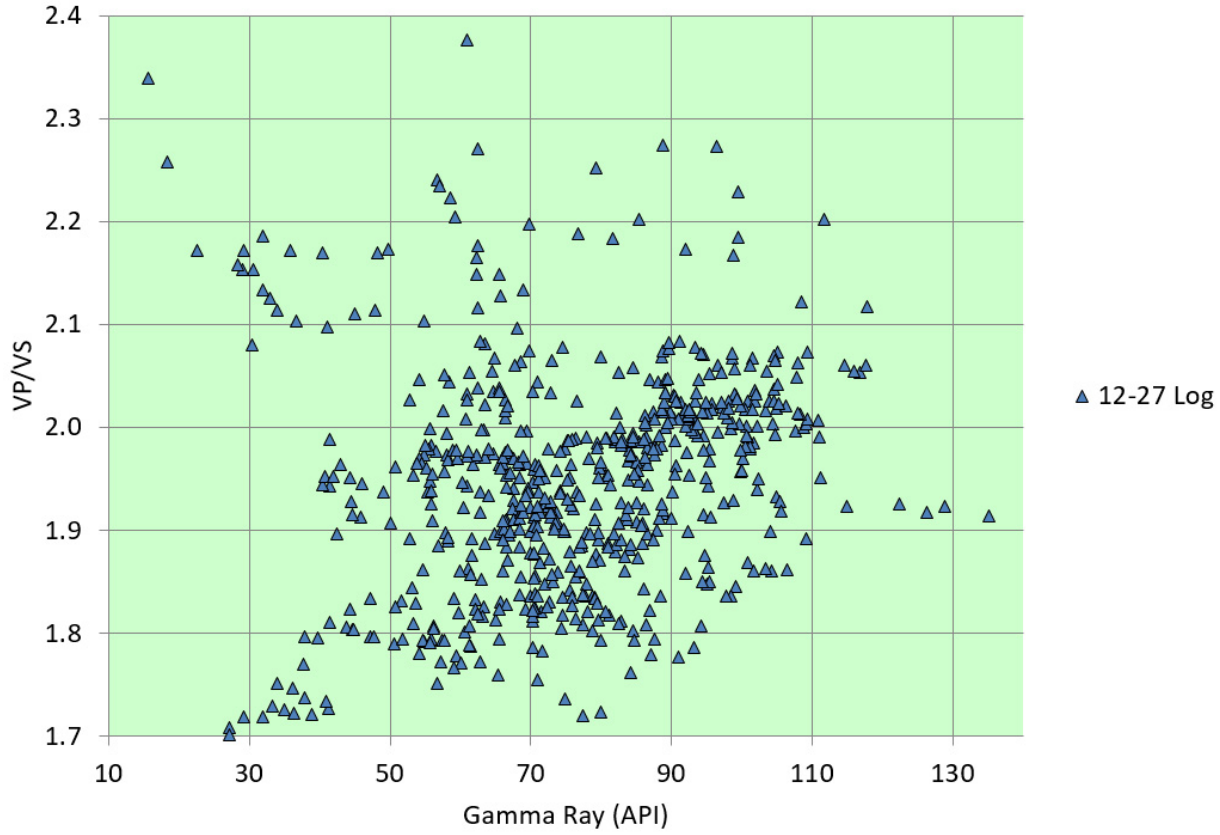

Figure 3-12: Cross-plot of gamma-ray against Vp/Vs for well 12-27.

3.2.3 Well Tie Procedure

As mentioned previously, well 12-27 had dipole sonic logs while 14-27 and 14-35 only had P-wave sonic logs. The linear relationship of Vp versus Vs from well 12-27 (Figure 3.9) was used to derive S-wave velocities for wells 14-27 and 14-35, as shown in figures 3.14 and 3.15 respectively.

Well ties are performed with the objective of relating stratigraphic markers in the wells to events on the seismic section; this helps with the horizon identification interpretation (Simm and Bacon, 2014). After extracting the statistical wavelet from the seismic data, the next step was to extract a wavelet from each well to refine the correlation. A final, multi-wavelet was extracted

from the wells 14-27 and 14-35 due to the similarities in their phases. This final multi-well wavelet, when convolved to the reflectivity from each well, helped with the creation of well synthetic seismograms at each well. Since check shots surveys were not available, the next step was to apply a manual check shot correction by applying the bulk shift to the synthetic seismogram to match known strong events on the seismic section. The bulk shift was required because the software extrapolated the first Vp log value to the surface and it usually overestimates the near surface velocity (Hampson-Russell, 2014). Finally, stretch or squeeze was performed to the logs to modify the time-depth curve to match the measured P-wave seismic times.

The wavelet extraction time window for each well in the PP section ranged from 600 ms to 1200 ms, which covered the depth interval of investigation. A bulk shift was applied to the synthetic seismograms in order to match the well tops to a known interpreted event in the seismic section. Minor stretching was performed to fix mis-ties and to have a better correlation without modifying the sonic logs.

After horizons were picked on the PP and PS sections, the wells ties on the PS section were performed. The wavelet extraction time window for each well ranged from 900 ms to 1800 ms. Correlation value for the PS section is lower in comparison to the PP section due to the lower resolution in the PS seismic section. Figure 3.13 to 3.15 show the results for the well ties for the PP section.

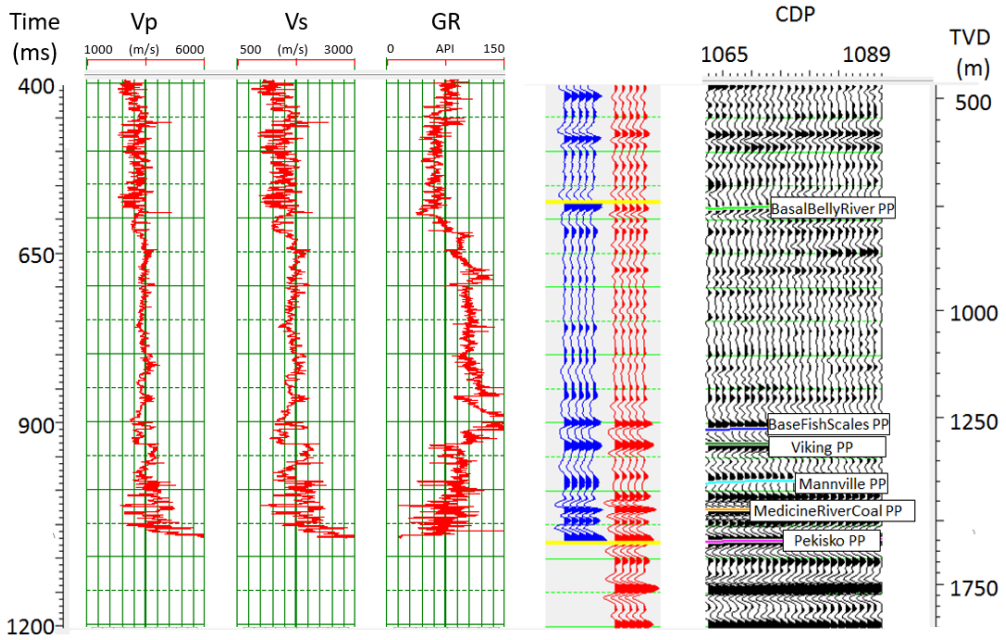

Figure 3-13: The final tie of well 12-27 on the PP section; the blue traces represent the synthetic seismogram and the red traces are the extracted trace from the seismic data near the well location.

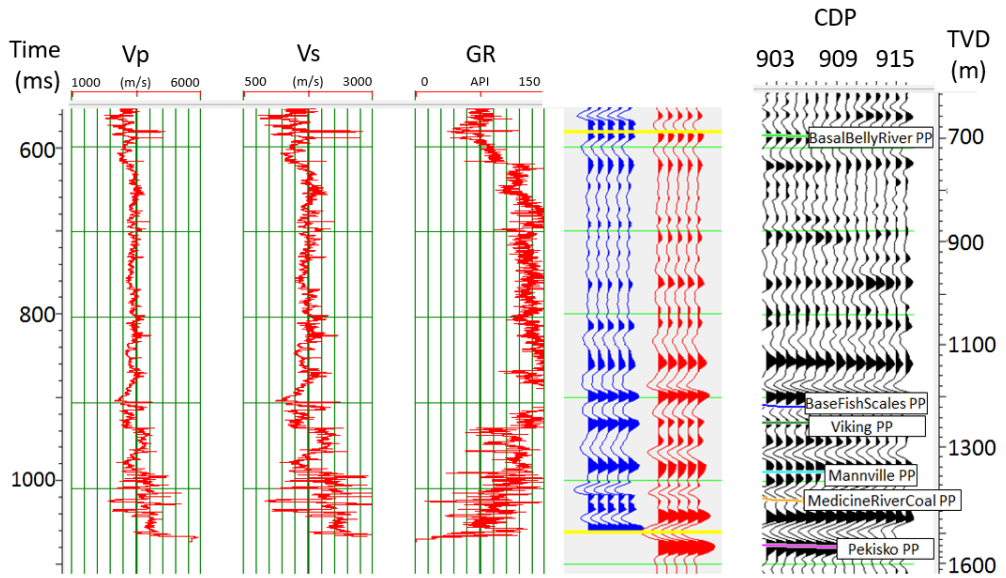

Figure 3-14: The final tie of well 14-27 on the PP section; the blue traces represent the synthetic seismogram and the red traces are the extracted trace from the seismic data near the well location.

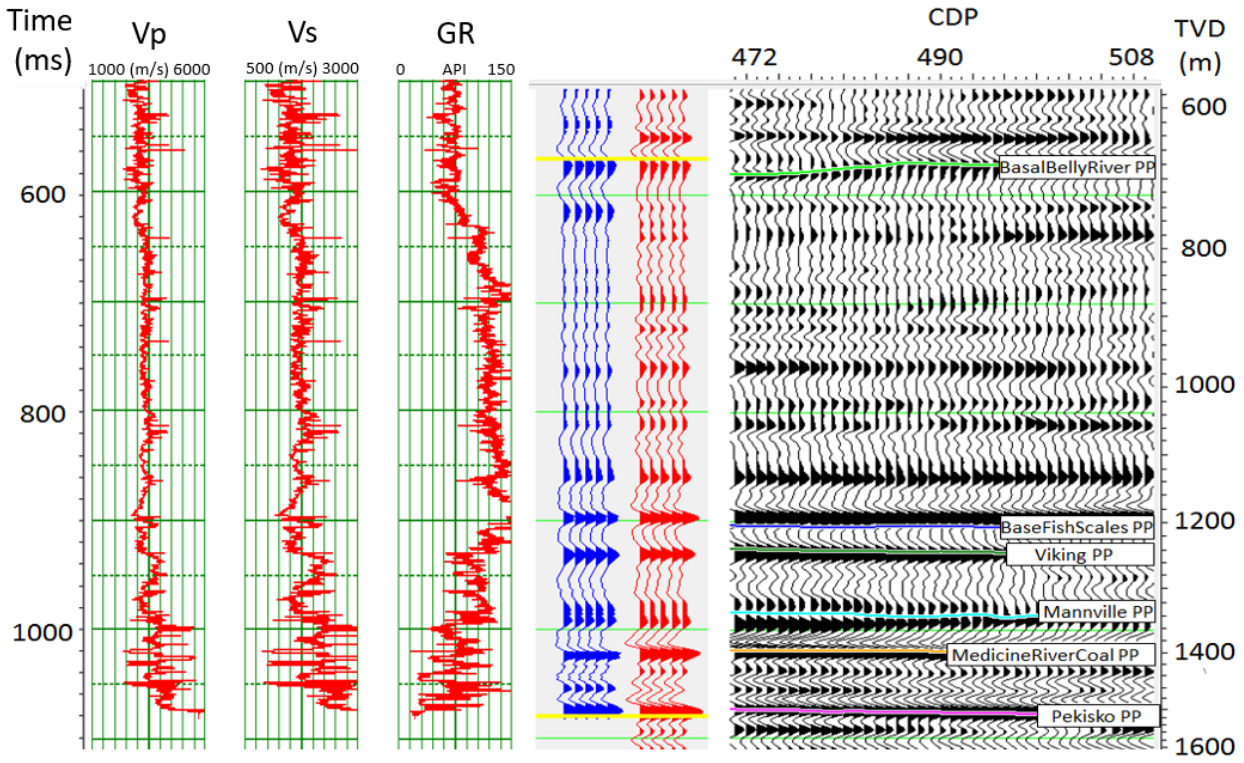

Figure 3-15: The final tie of well 14-35 on the PP section; the blue traces represent the synthetic seismogram and the red traces are the extracted trace from the seismic data near the well location.

Synthetic seismograms are used to assist in the well log calibration process which links seismic events to the corresponding geological markers (Hampson-Russell, 2014). Synthetic traces for PS and PP data were created according to conventional Zoeppritz modeling. Zero offset P-wave synthetics are normally used for correlation with seismic data. PS-waves are not generated at zero offsets; however, small offsets will generate converted wave energy. Figure 3.16 below shows both seismic sections with their PP and PS-wave synthetics.

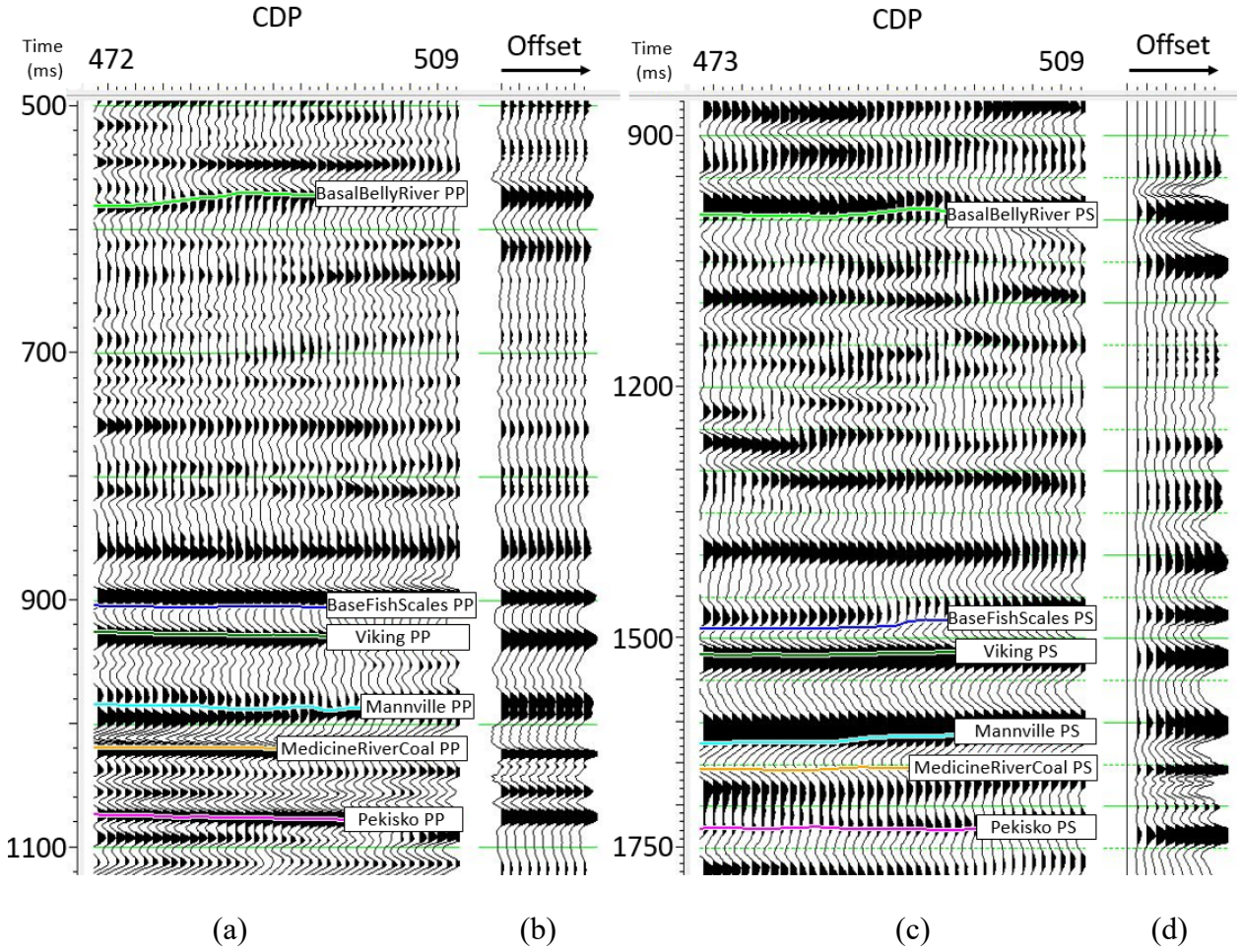

Figure 3-16: (a) PP seismic section with horizon picks and (b) PP synthetic offset gather; (c) PS seismic section with horizons picks and (d) PS synthetic offset gather.

3.2.4 Well Tie Quality Control

Vp/Vs ratio information can also be used to verify the consistency of the PP and PS log correlations. This is done by comparing the ratio provided by the corrected P and S sonic logs to the calculated Vp/Vs value from the corrected depth-time curves. Both ratio lines were plotted on the same track to check for consistency; when major differences occur they can point to inconsistent correlations in the PP or PS time and would require revision to generate agreement

(Hampson-Russell, 2014). Agreement is found when Vp/Vs tends to follow the derived values closely. Figure 3.17 to 3.19 show the consistency of the ratios at each well.

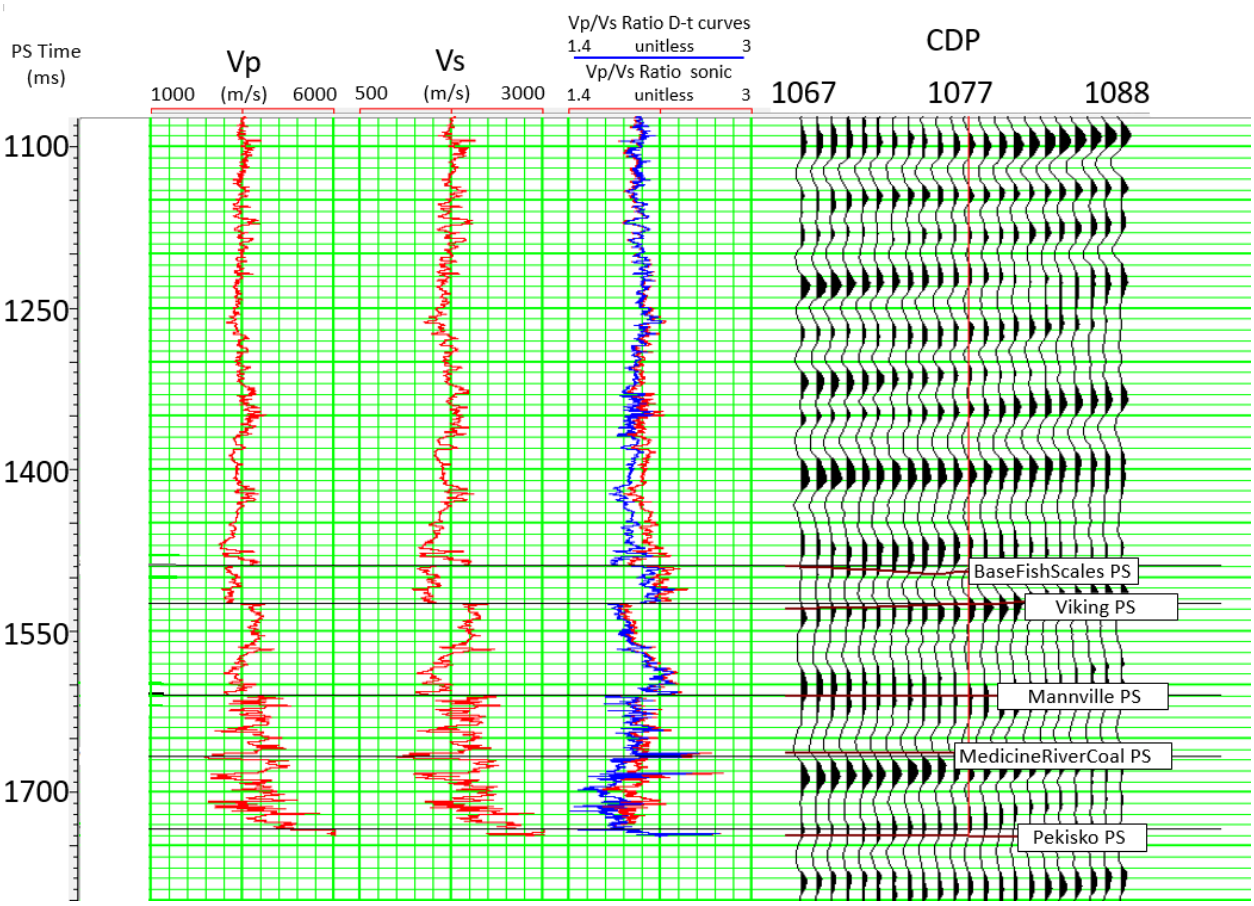

Figure 3-17: Quality control on well 12-27; the blue line represents the calculated Vp/Vs ratio from depth-time curves and the red line on the same track represents the ratio derived from the sonic logs; both lines showed consistency in the area of investigation.

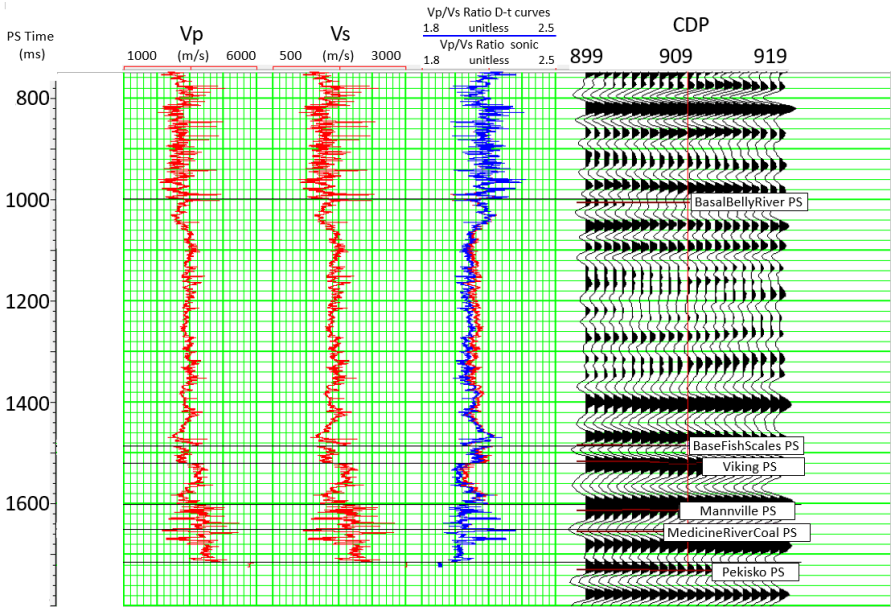

Figure 3-18: Quality control on well 14-27; the blue line represents the calculated Vp/Vs ratio from depth-time curves and the red line on the same track represents the ratio derived from the sonic logs; both lines showed consistency in the area of investigation.

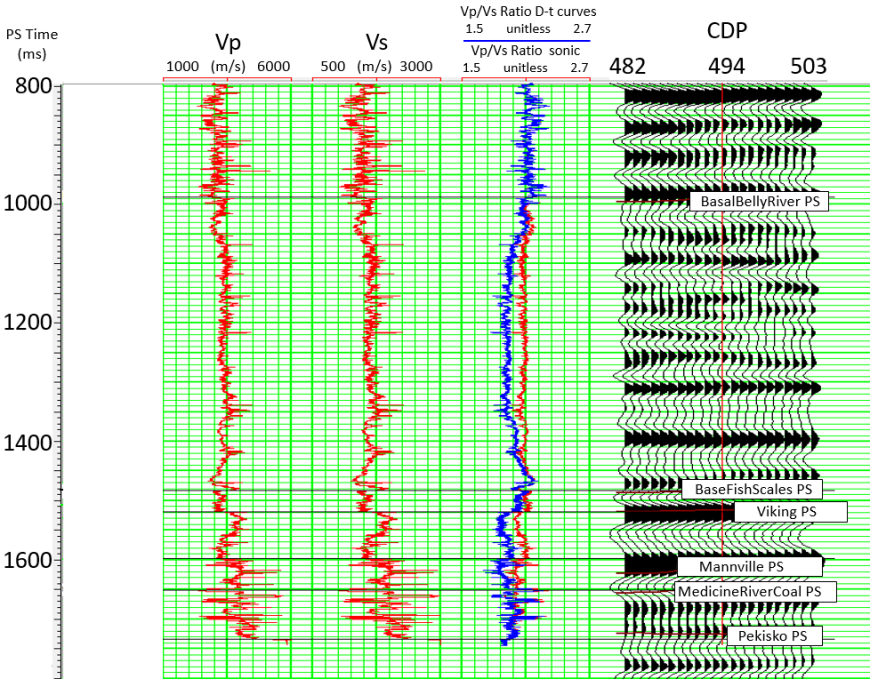

Figure 3-19: Quality control on well 14-35; the blue line represents the calculated Vp/Vs ratio from depth-time curves and the red line on the same track represents the ratio derived from the sonic logs; both lines showed consistency in the area of investigation.

3.3 **Horizon Picking**

Once the events of interest were identified and correlated to both seismic sections, horizons were picked using an automatic picker with manual editing. Intervals of Vp/Vs values between horizons were calculated using the following relationship, derived in Chapter 1:

$$Vp/Vs = \frac{(2\Delta Tps - \Delta Tpp)}{\Delta Tpp}$$

In this equation, ΔTpp and ΔTps represent the isochrons across the same depth intervals for both PP and PS sections. Horizons were carefully picked and corrected when necessary in order to accurately interpret lateral variations in Vp/Vs. The ratio could be affected due to changes in lithology, porosity, pore fluid, and other formation characteristics (Tatham and McCormack, 1991). A total of six horizons were picked for our analysis; this allowed the study of several isochron intervals for the Vp/Vs error study.

The horizons interpreted on the PP section are shown in Figures 3.20 and 3.21, and were picked based on the well top information from all the wells. Using an auto picker, the horizons were picked at the peak, trough, or zero crossings closest to the well tops locations. In Figure 3.22 the PS section is plotted at 2/3 the scale of the PP section; both sections are aligned at the same depth intervals and the difference in times is due to the slowness of the S-wave which contributes to the PS-wave total travel time.

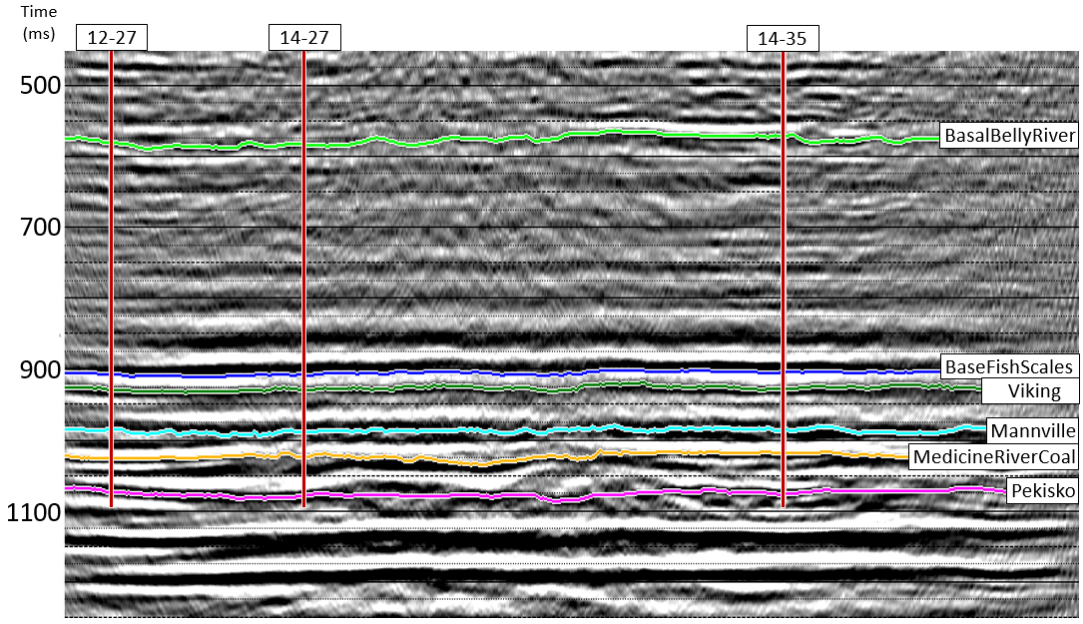

Figure 3-20: PP seismic section with six interpreted horizons and the three well locations; well 12-27 have the dipole sonic logs and the other wells provided only monopole sonic logs.

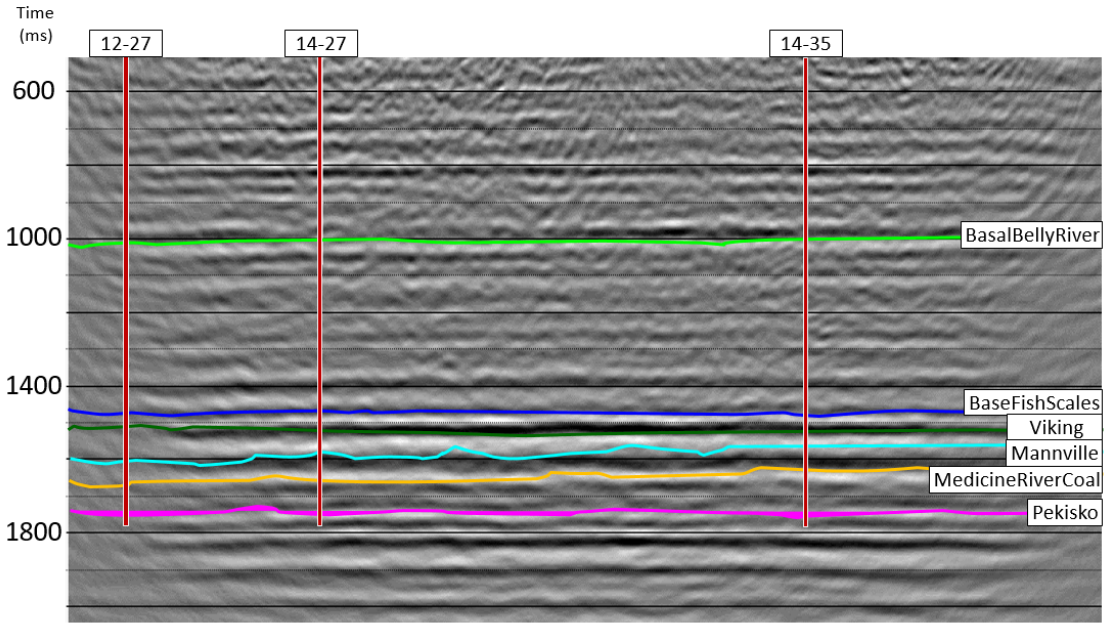

Figure 3-21: PS seismic section with six interpreted horizons and the three well locations; well 12-27 have the dipole sonic logs and the other wells provided only monopole sonic logs.

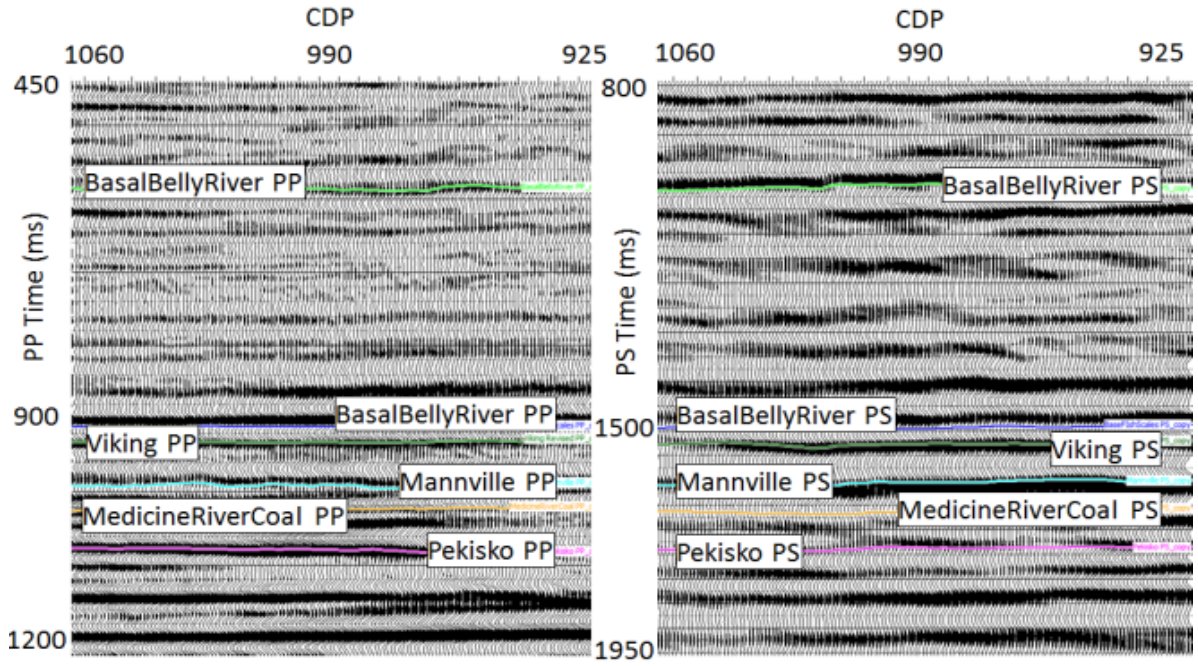

(a) **(b)**

Figure 3-22: Interpretation of (a) the PP section and (b) the PS section; the PS section is plotted at 2/3 the scale of the PP section.

In order to improve the interpreted horizon picks, a time shift was applied to each event in order to tie better at the well locations. When picking horizons, the software would only allow picks to be done at the peak, trough, or zero crossing. After the well ties, the geological tops do not necessarily fall specifically at any of these locations and may differ between PP and PS sections, as mentioned previously. Sometimes a time shift is necessary to precisely locate the horizons at the tops and minimize the uncertainty. The first step to finding the time shift was to average time differences between the geological top and its interpreted horizons at two well locations (12-27 and 14-35). The average was used to shift the horizon; this step was performed for all the horizons on both PP and PS sections. The improvement to the horizon placement reduces the error of interval Vp/Vs computed from the isochrons. Figure 3.23 to 3.26 show the refined time shifted picks applied to both seismic sections.

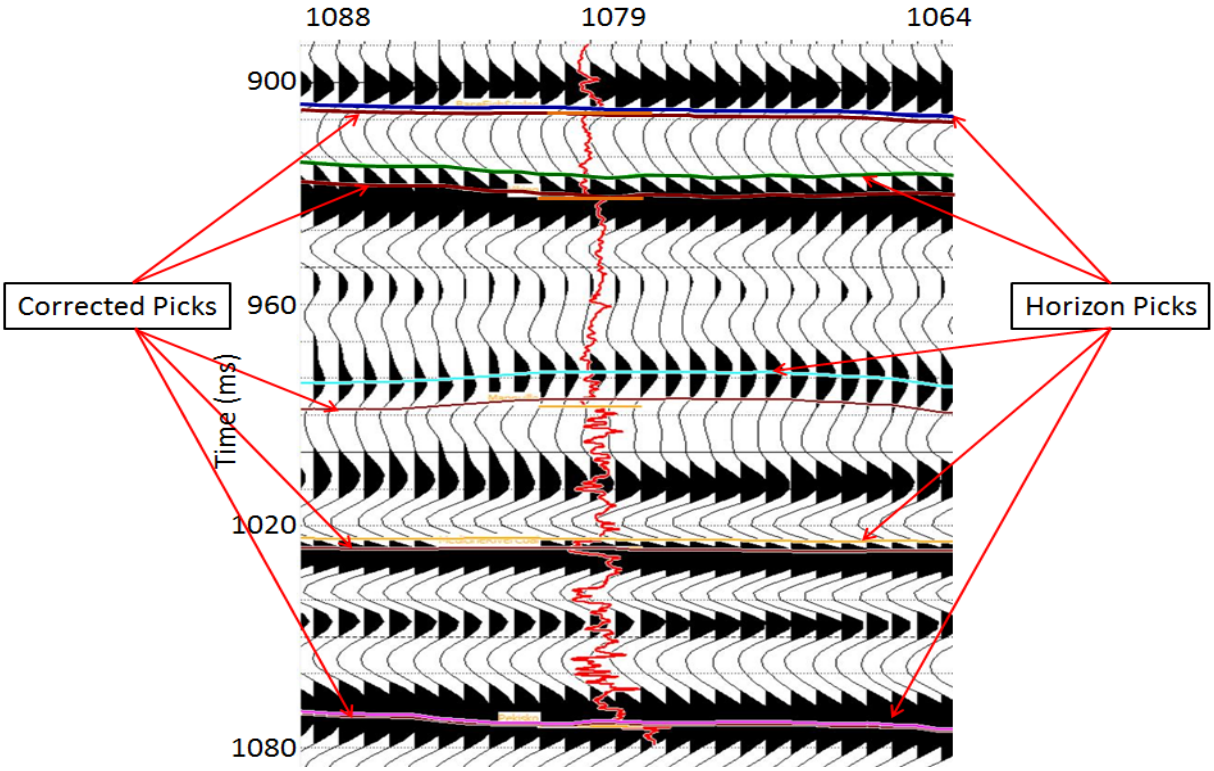

Figure 3-23: PP section with interpreted horizons before and after the time shift correction; yellow bars on the logs represent the geological tops.

	12-27 Log			All Logs
PP Seismic	Horizon Time	Top Time	Time Diff.	Average Corr.
BasalBellyRiver	584.02	582.51	-1.51	-1.35
BasalBellyRiver Corr.	582.67	582.51	-.16	--

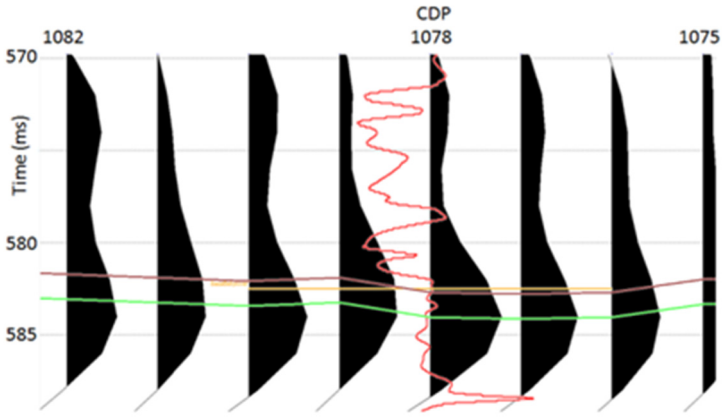

Figure 3-24: The table shows the time improvement in the red box after the corrections were applied on the PP section for the BasalBellyRiver horizon. The corrected horizon time is noted in the red box.

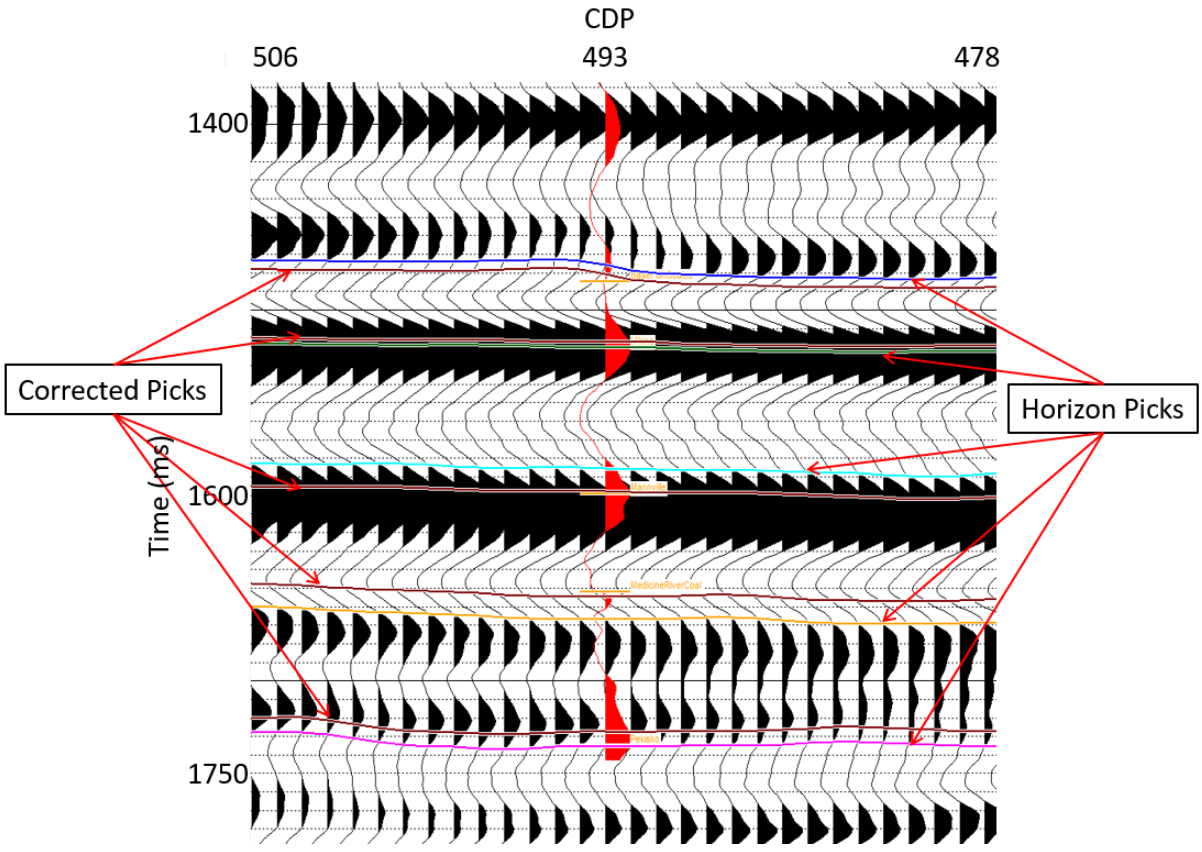

Figure 3-25: PS section with interpreted horizons before and after the time shift correction; yellow bars on the logs represent the geological tops.

	14-35 Log			All Logs
PS Seismic	Horizon Time	Top Time	Time Diff.	Average Corr.
BasalBellyRiver	976.26	989.27	13.01	10.86
BasalBellyRiver Corr.	987.12	989.27	2.15	--

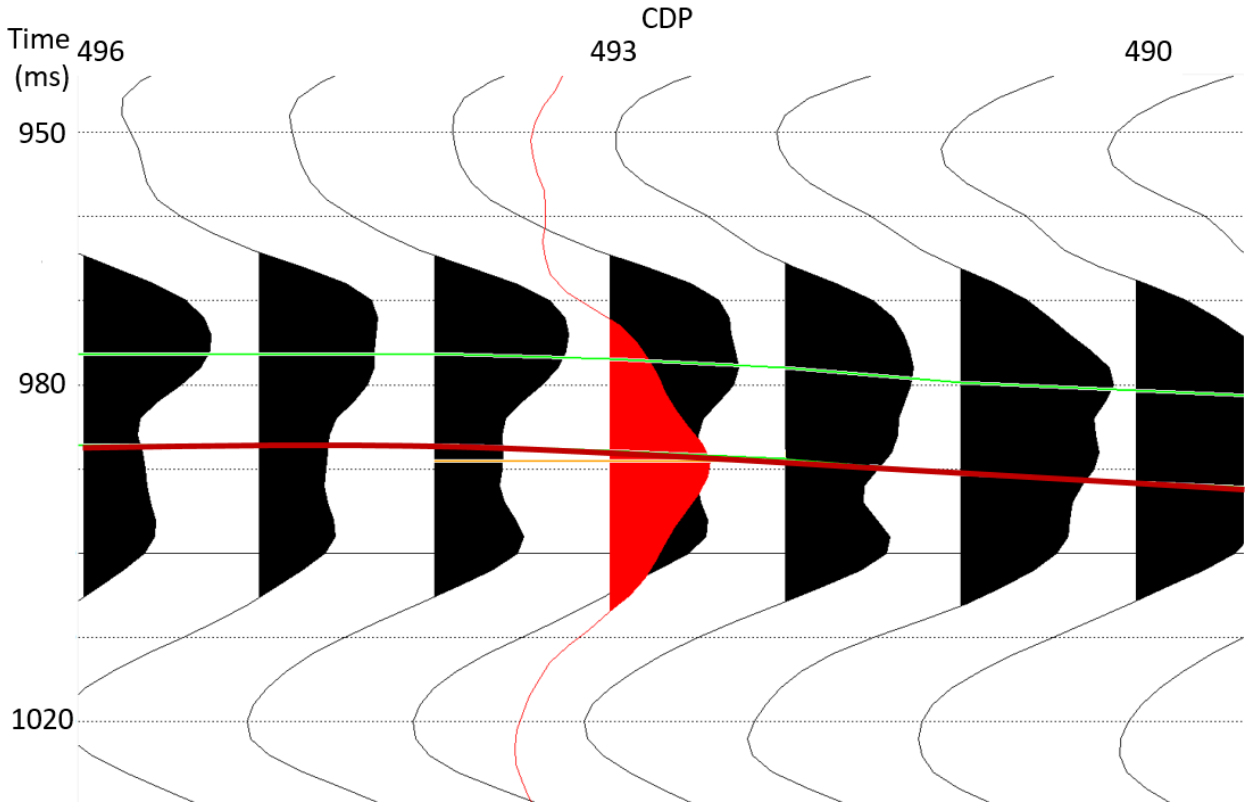

Figure 3-26: The table shows the time improvement in the red box after the corrections were applied on the PS section for the BasalBellyRiver horizon. The corrected horizon time is noted in the red box.

3.4 Vp/Vs Error Analysis

To understand the relationship between the sensitivity of Vp/Vs interval to the time intervals used, we first input the interpreted horizons to create isochrons along the section. A total of eleven isochrons were chosen with intervals ranges from about 22 ms to 500 ms. The table below shows the different intervals in both PP and PS times using the information from all the wells.

Table 3.1: Interval PP time averages from all wells for both corrected and uncorrected horizons.

	PP Time Interval (ms) Corrected Horizons	PP Time Interval (ms) Uncorrected Horizons
BaseFishScales-Viking	22.5	18.7
Mannville-MedicineRiverCoal	38.1	42.6
MedicineRiverCoal-Pekisko	47.4	49.5
Viking-Manville	56.4	79.9
Mannville-Pekisko	89.6	96.2
Viking- Pekisko	146.8	151.7
BasalBellyRiver-BaseFishScales	327.9	487.1
BasalBellyRiver-Mannville	407.0	398.5
BasalBellyRiver-MedicineRiverCoal	443.5	439.5
BasalBellyRiver-Pekisko	496.6	494.7

Vp/Vs calculations for each interval were compared with one another to find patterns and differences (Figures 3.27 and 3.28). The results show that the deviations for smaller isochrons were greater than those for larger isochrons. Based on the results, the Vp/Vs calculations are found in part to be dependent on the time interval chosen. Horizon interpretation mis-picks will result in greater error in the Vp/Vs values for small intervals.

Variations of Vp/Vs in Figure 3.27 are dependent not only on the isochrons lengths but also on the lithology of the area, which has a major influence on the changes of this ratio. As mentioned earlier, the Mannville ground consists of interbedded continental sand and shale at the base, which is followed by calcareous and glauconitic sandstones. As noted in the figure, some areas along the survey line with low ratio values could indicate high sand content, while the areas of higher ratio values could indicate a more shaly sand content.

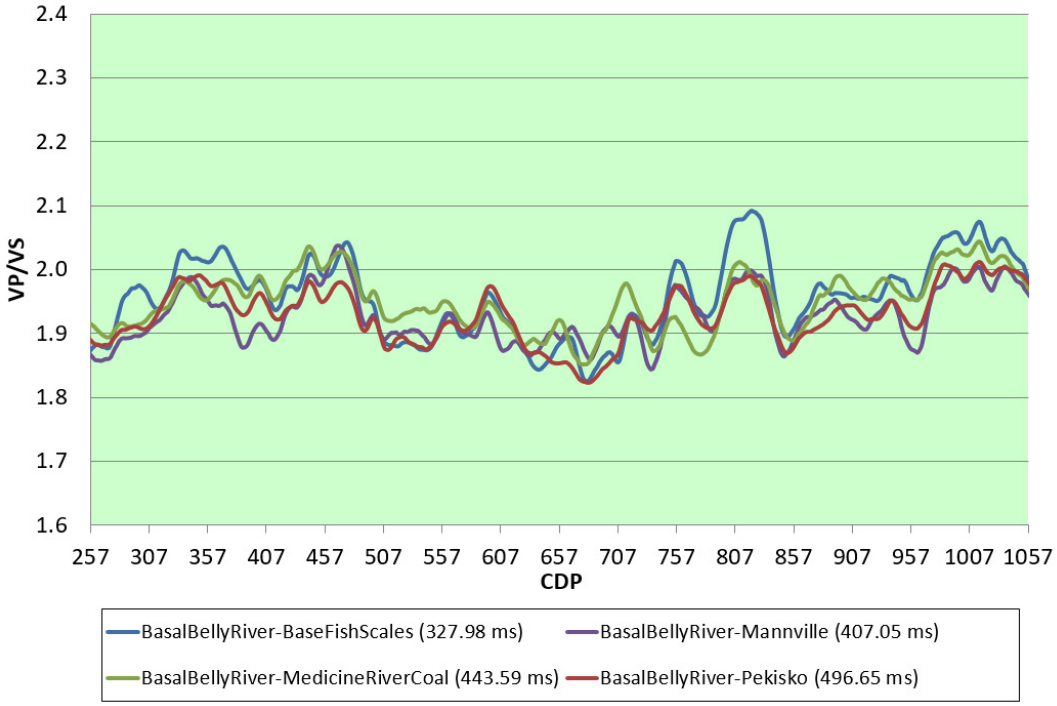

Figure 3-27: Interval Vp/Vs curves for large isochrons in PP times (> 300 ms).

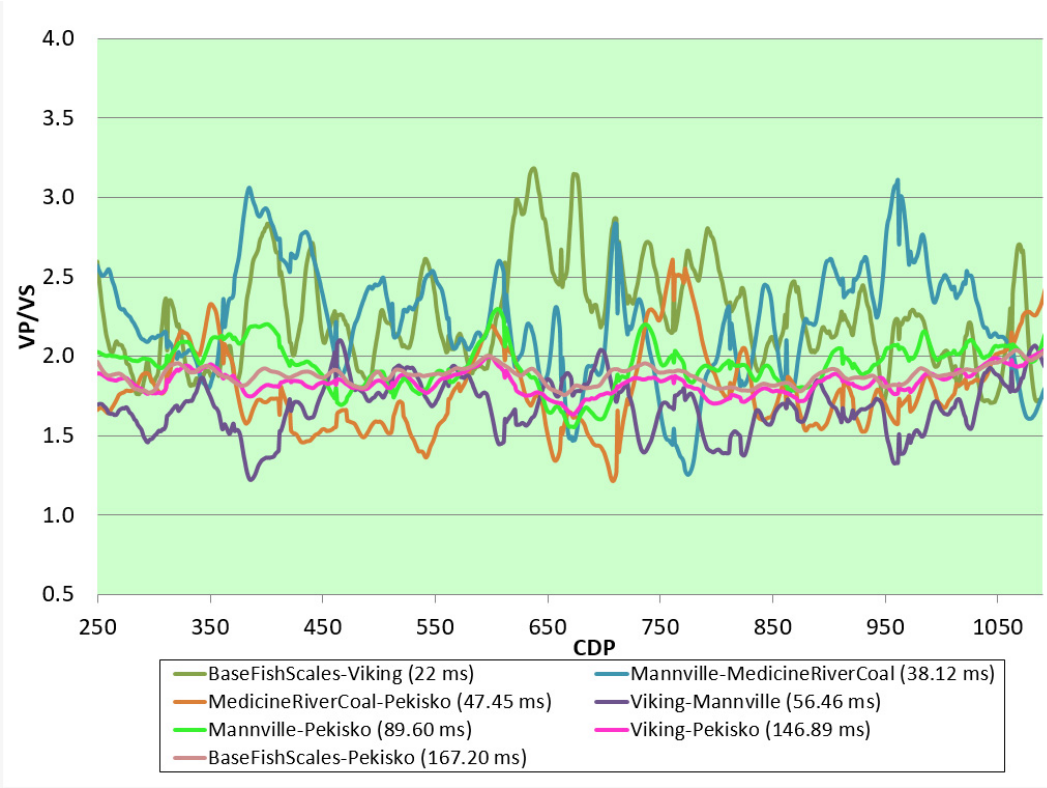

Figure 3-28: Interval Vp/Vs curves for small isochrons in PP times (< 180 ms).

3.4.1 Time Interval Error Analysis

In Figure 3.29 shows all interval Vp/Vs means and standard deviations for large isochrons, which have time intervals greater than 300 ms., the black line with the triangle shows the mean values for all of the curves for every 20 CDP intervals. The vertical bars represent one standard deviation away from the mean at each interval. This graph allows for an analysis of the standard deviation as a function of position on the line, which indicates meaningfulness of the Vp/Vs values. A standard deviation greater than the mean value means that the error overwhelms the geological deviations and the lateral variation of the Vp/Vs is not meaningful. In Figure 3.29, most of the curves at each interval lie within one standard deviation of the interval mean, proving that these values are meaningful. The interval between CDP 422 and 742 is shown to be meaningful Vp/Vs values for geological interpretation.

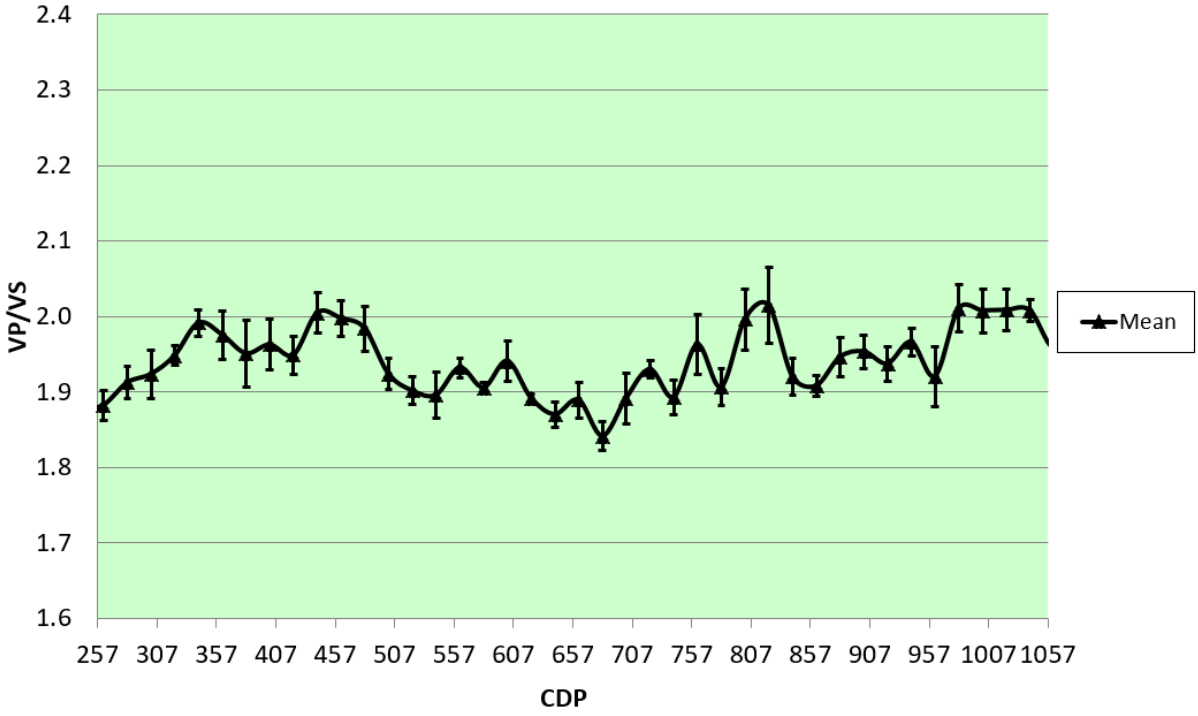

Figure 3-29: Interval Vp/Vs mean and standard deviation for large isochrons in PP times (>300 ms). The black line with the triangle represents the mean Vp/Vs value at a specific

CDP. Vertical bars represents one standard deviation away from the mean at each interval.

Figure 3.30 shows all interval Vp/Vs means and standard deviations for small isochrons, which have time intervals less than 180 ms. In this particular figure, the standard deviation of the interval mean is much greater than that in Figure 3.29 and the curves' values do not land within one standard deviation of the mean. Throughout the entire line, the curve values are very different from each other. This suggests that the Vp/Vs values for these isochrons are not meaningful and should not provide a reliable geological interpretation of the area.

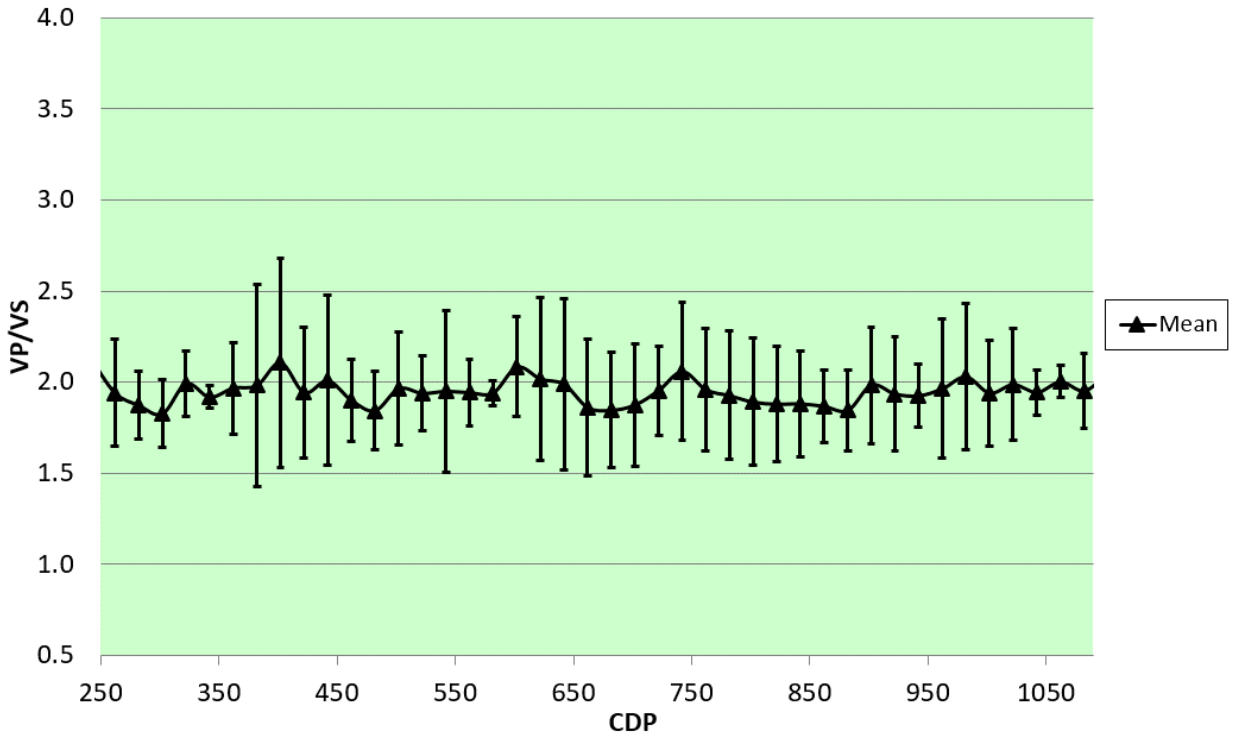

Figure 3-30: Interval Vp/Vs mean and standard deviation for small isochrons in PP times (<180 ms). The black line with the triangle represents the mean Vp/Vs value at a specific CDP. Vertical bars represent one standard deviation away from the mean.

The uncertainty in the Vp/Vs ratio was used to understand how the time interval can affect the percent relative error in the ratio analysis (Figure 3.31). Time intervals greater than

150 ms corresponded to percent error values that were consistently low, ranging from 0.7 to 2.2 percent. For intervals below this threshold, the percent error increased exponentially; the smallest time intervals in our study were approximately 22 and 38 milliseconds and their corresponding percent errors were 16.5 and 9.7 percent respectively. The calculation for the error assumes an uncertainty of ±2 ms in the interpretation from the horizons picks. Data with horizons with no time correction was also added to observe the error differences. For the most part for this particular data, the time correction did not affect the calculated percentage error, especially for large isochrons. However, there were small noticeable changes on the calculated error for the smallest isochron, but it was still relatively small at less than 1% difference.

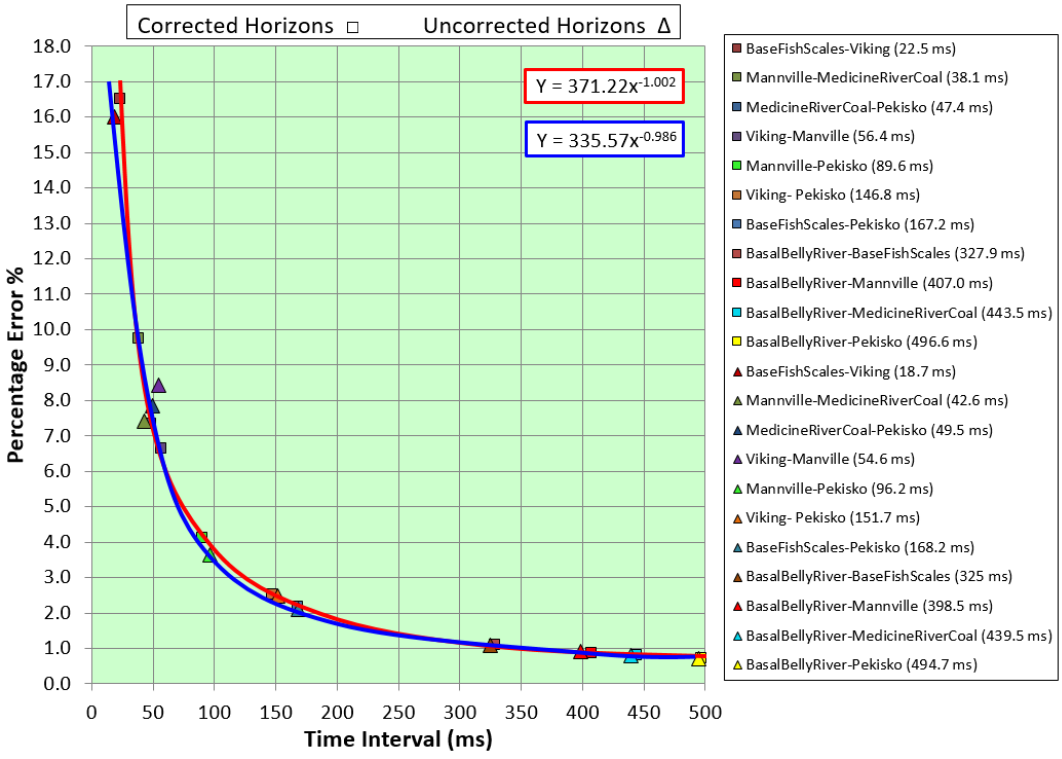

Figure 3-31: Cross-plot of percent relative error in Vp/Vs versus ΔTpp time interval; the error tends to increase as the time interval becomes smaller. The red trendline represents horizons with time corrections and is represented by the power function in the red box. The blue line represents the uncorrected horizons and is represented by the power function in the blue box.

3.5 Summary

Analysis performed on the Hussar data indicates that the uncertainty in Vp/Vs values will increase as time interval becomes smaller. It is important for interpreters to understand this relationship in order to avoid erroneous results in interval Vp/Vs analysis. Based on the increasing behavior of error with respect to decreasing in the time interval, as well as taking into consideration the variability of the Vp/Vs values due to the uncertainty it is suggested to use isochron intervals greater than 150 ms. Interval Vp/Vs analysis for data with intervals greater than this time presented low uncertainty.

Chapter Four: The Spring Coulee Experiment

4.1 Spring Coulee Experiment Overview

4.1.1 Introduction

Similar to the Hussar experiment, the objective of the Spring Coulee experiment was to use the existing seismic and well data to perform a Vp/Vs precision analysis. The seismic data had a high signal to noise ratio, which facilitated the interpretation. However, no wells were located near the seismic line. Instead, a well approximately 10 km from the line was used to help interpret the subsurface geology.

The main objective of this particular experiment was to calculate Vp/Vs for different time thicknesses in the Spring Coulee area and to compare them with the findings from the previous chapter, as well as to determine a minimum time interval that interpreters can use to calculate Vp/Vs over small isochrones (thin beds).

4.1.2 Geology Overview

The seismic data for this survey was acquired in Spring Coulee, Alberta. Nearly the entire area is covered by a mantle of glacial drift, in which most of the exposure occurs in the river channels or in coulees (William and Dyer, 1930).

Figure 4.1 shows a stratigraphic chart from the southern plains region of Alberta. The target zone for horizon picks included the Colorado Group, which consist of several sandstone and conglomerate units, some of which are prolific hydrocarbon producers (Mossop and Shetsen, 1994). Other horizon picks included the Rundle Group, a carbonate unit of Mississippian age which consists of massive limestone interbedded with dark argillaceous limestone. Chert nodules are observed in the shaley beds, and crinoids and brachiopods are observed in the clean

massive beds (Douglas, 1953). Lastly, two more horizons were picked for strata of both Mississippian and Devonian age.

Exploration in the area has traditionally been focused on the generally thin Cretaceous Mannville sandstones which include the Glauconitic and the Basal Quartz channel sands (Geis, 1990). As in the Hussar data, the Mannville Formation serves as a major oil play for companies. Natural gas is also extracted from the Ostracod and Glauconite beds in southern Alberta (Mossop and Shetsen, 1994). Both beds are sub-units of the lower Mannville subdivisions.

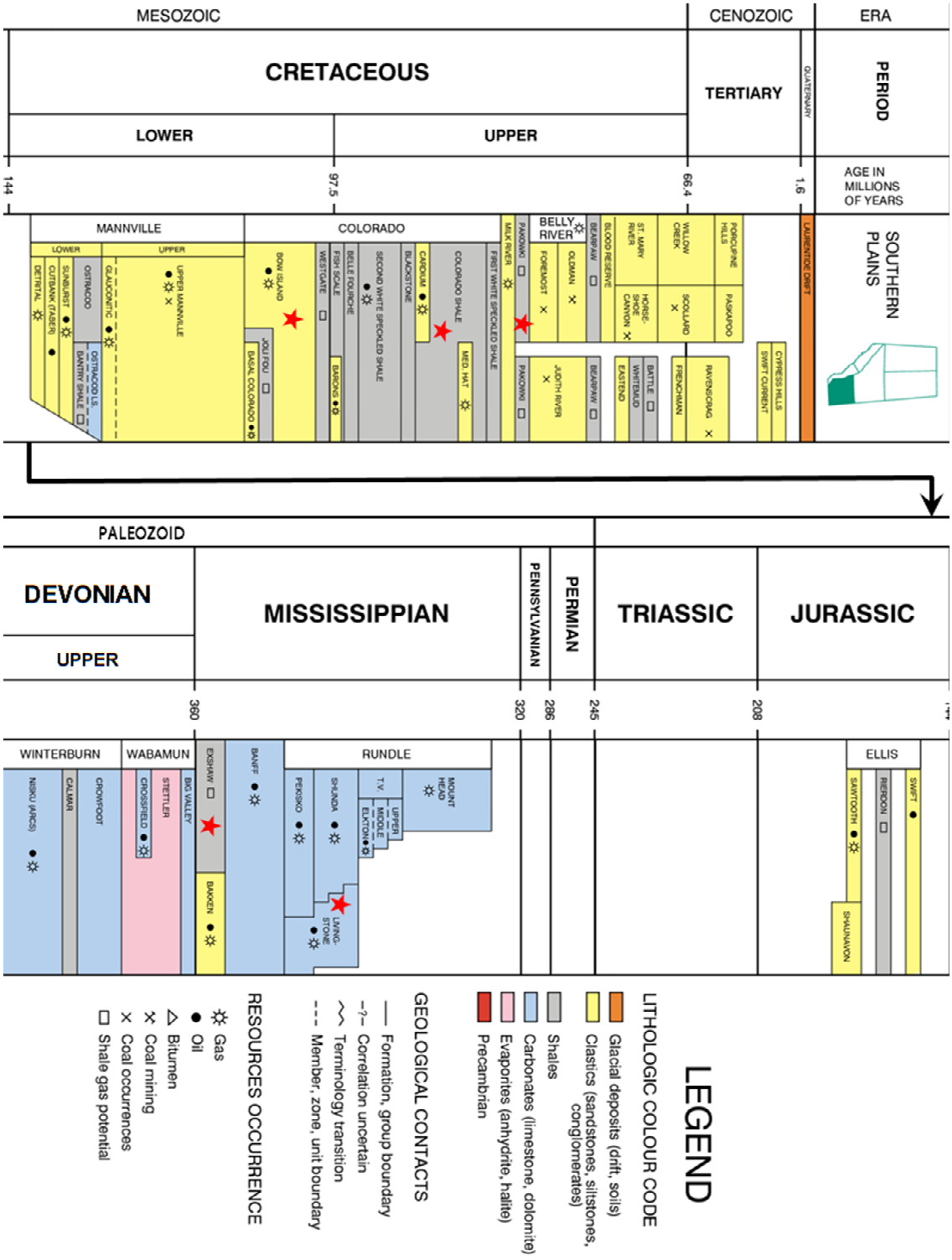

Figure 4-1: Stratigraphy chart of the southern Alberta region. The red star denotes the horizon picks locations. (Modified from Alberta Geological Services, 2009).

4.2 Spring Coulee Data

The Spring Coulee dataset was acquired in 2008 near Spring Coulee, Alberta by CREWES in association with ARAM Systems Ltd. This survey is located approximately 250 km south-east of Calgary in the Southern Alberta plains. This site was chosen following the discovery that the University of Calgary had been endowed with the mineral rights to work in this area (Bertram, 2008). Specifically Sections 14 and 23 T4 R23 W4M (Figure 4.2).

The seismic line extended 6.5 km from the northeast to the southwest and contained 3C Sensor SM7 geophones provided by ARAM system Ltd. Six hundred and fifty geophones were spread 10 m apart. A 48 K pound vibroseis provided by CGG Veritas was used to acquire the data. Only one well was used to help interpret the geology of this area. Well 3-32-4-23, located 10 kilometers away from the seismic line, provided density and P-wave log information only (Figure 4.3). Other wells were available but they were not deep enough to identify the geology in our area of investigation. Only one well did have a dipole sonic logs with registration close to the target of investigation depth, and a linear relationship between the sonic logs for this well was acquired. And this relationship was used to estimate a shear sonic log on well 3-32-4-23.

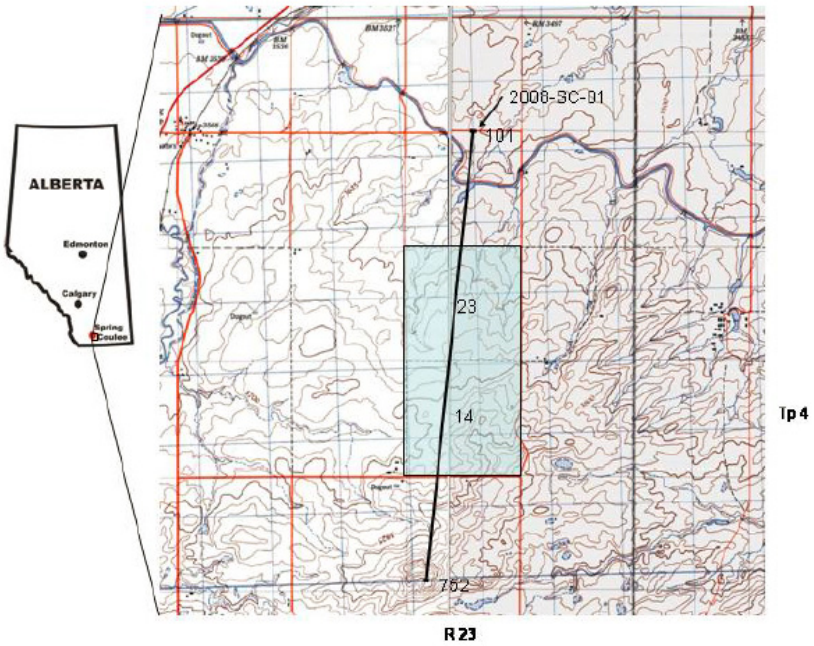

Figure 4-2: Location of the Spring Coulee seismic line and flag locations. (Bertram et al., 2008).

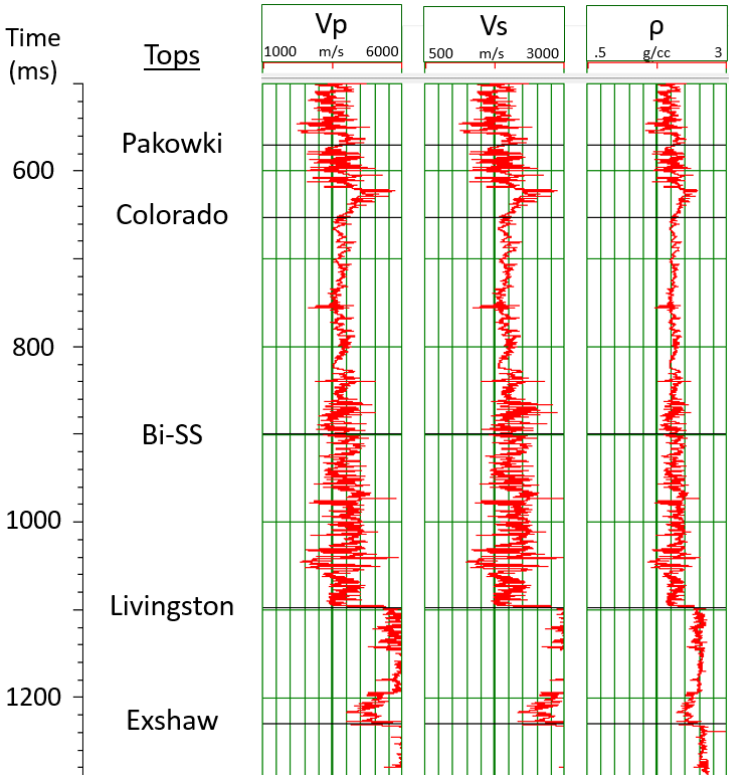

Figure 4-3: P-wave sonic and density logs from well 3-32-4-23.

The seismic data was previously processed by Crewes (Lu, 2008). The weathering layer in this area is characteristically thin; consequently, the dataset was imaged well close to the surface with few artefacts. The dataset was post-stack Kirchhoff time migrated. Figures 4.4 and 4.5 shows the PP and PS sections respectively with their respective target windows denoted by the red rectangle.

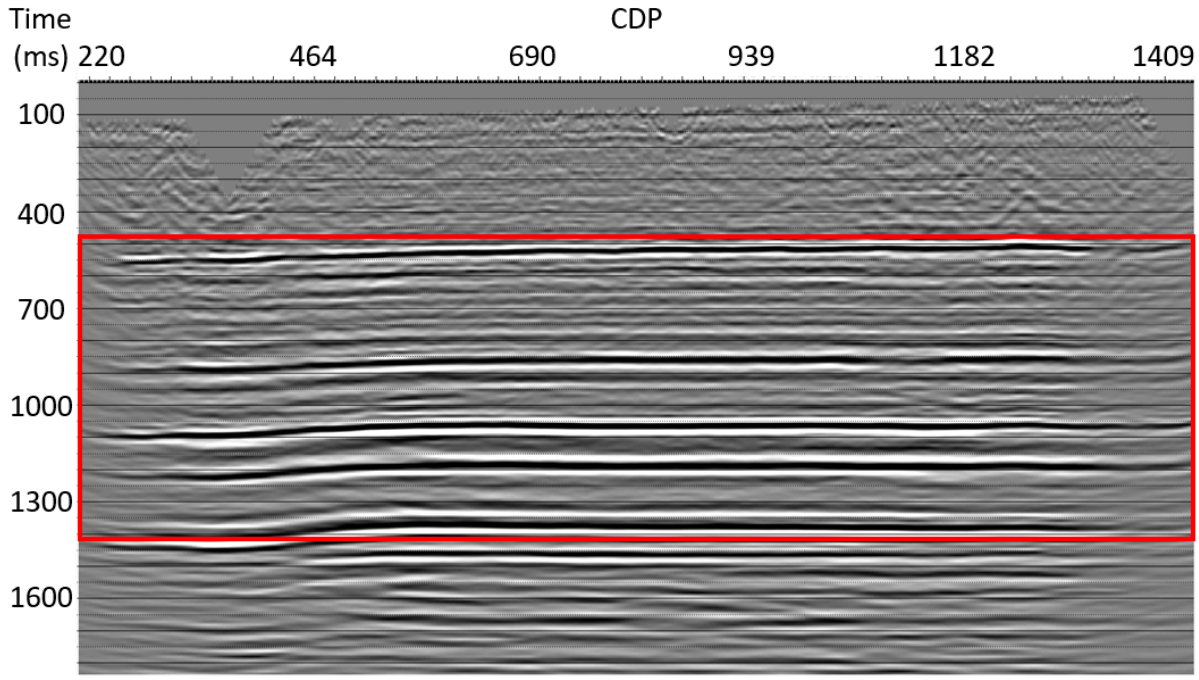

Figure 4-4: Spring Coulee PP seismic section; the red rectangle indicates the area of investigation.

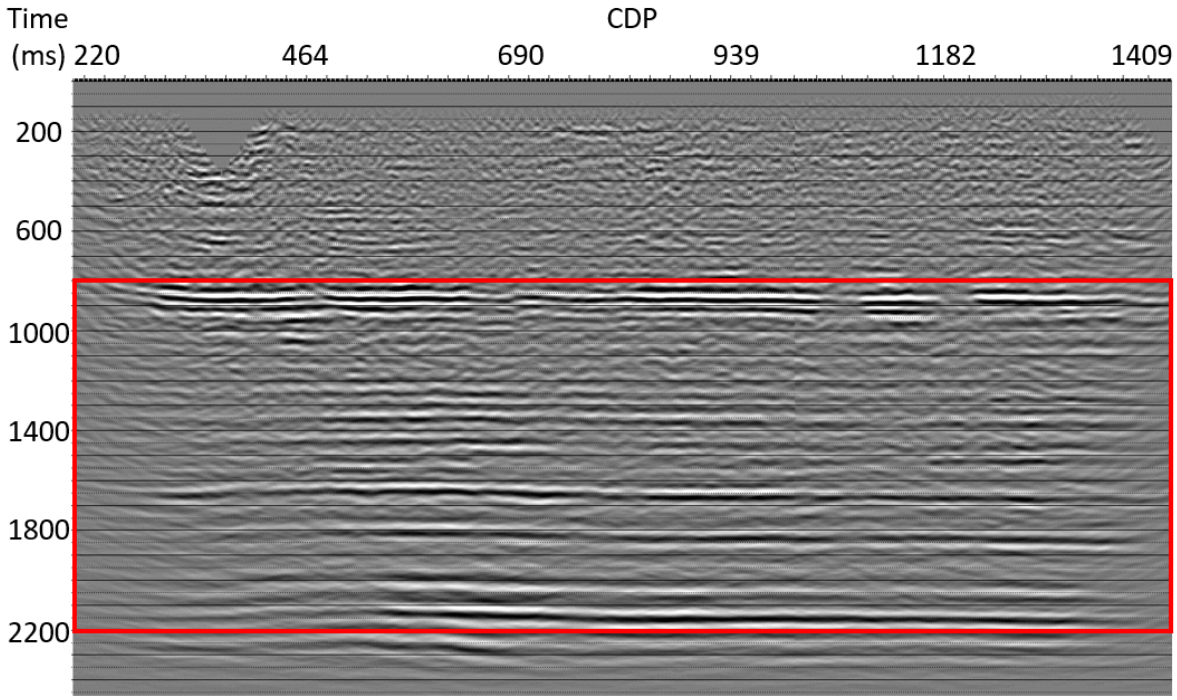

Figure 4-5: Spring Coulee PS seismic section; the red rectangle indicates the interval of investigation.

4.2.1 Wavelet and Resolution

A specific target window for each seismic section was used to first estimate statistical wavelets. The next step was to extract a wavelet for each section, using log data from well 3-32-4-23. This method can give a good estimate of both amplitude and phase spectra of the wavelet (Figures 4.6 and 4.7). As mentioned earlier, since the well was located a few kilometers away from the seismic line, the final well-seismic tie location was affected due to differences in the geology between the well location and the seismic line.

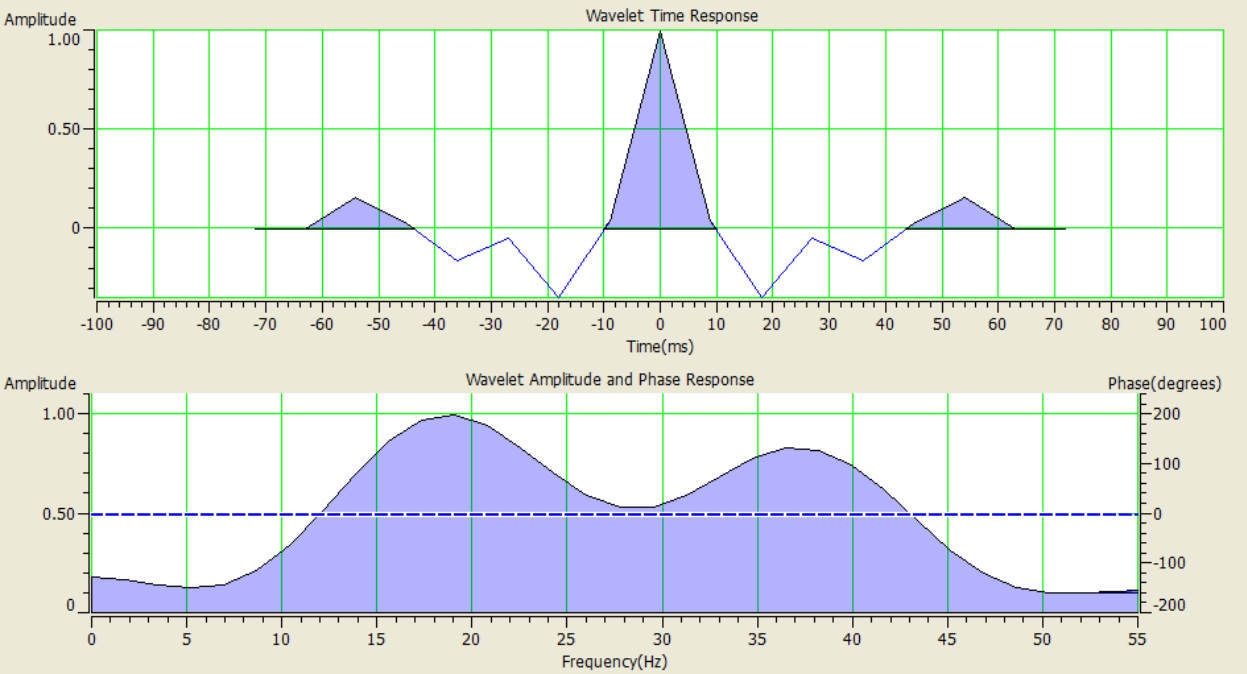

Figure 4-6: PP wavelet extracted from well 3-32-4-23 with its amplitude spectrum.

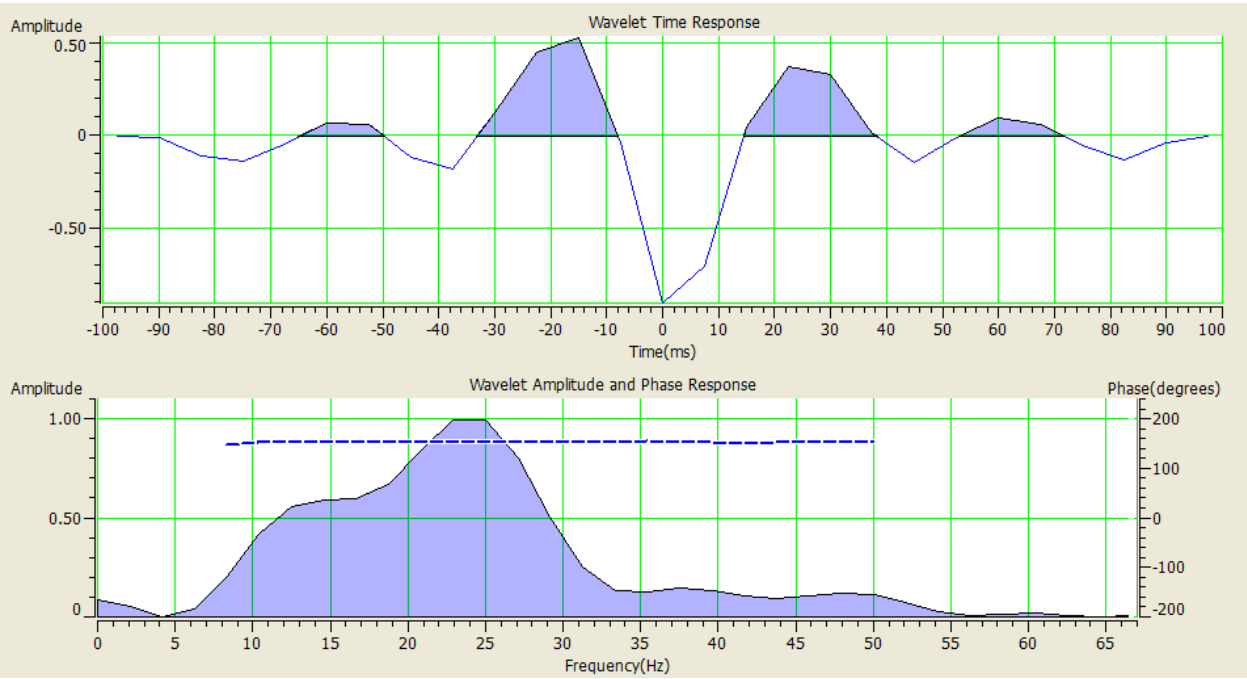

Figure 4-7: PS wavelet extracted from well 3-32-4-23 with its amplitude spectrum.

Seismic data was used to estimate the vertical resolution. This is a very important piece of information to know when interpreting data as it will help to estimate the minimum bed thickness that can be distinguishable on a dataset. To calculate the vertical resolution, the Rayleigh criterion was used, in which resolution = $\lambda/4$ where λ is the dominant wavelength, the wavelength was found to be 155 m, based on the dominant frequency of 22 Hz and a velocity of 3400 m/s. Thus, the vertical resolution of approximately 39 m was determined.

4.2.2 Well Tie Procedure

In the Spring Coulee experiment, only one well was used to perform the well ties. The exact well location was several kilometers away from the seismic line, thus affecting the final well correlation. The well provided bed top information that helped to identify the different horizons in the seismic section. Horizons extending from the Cretaceous to the Devonian periods were picked on each seismic section. Since this particular well did not have the check shot information, a manual check shot correction was performed by means of applying a bulk shift to the well seismogram to match an event on the seismic data. In addition, squeeze and stretch were performed on the logs to match the seismic data.

In Figure 4.8, the blue traces represent the synthetic seismograms that were calculated from convolving the reflectivity from the well with the extracted wavelet. The red traces beside the seismic represent the average of the 9 traces that are near the assumed well location (Hampson-Russell, 2014). The well 3-32-4-23 was projected on a location in the seismic line where the image of the events were clear of noise.

The correlation result is dependent on the correlation window; on the PP seismic section, the correlation window was from 500 ms to 1200 ms, the target of investigation for this study. On the PS seismic section, the correlation window was from 800 ms to 1800 ms.

The deepest horizon picked, called “H1”, was not included in the correlation window since log information at these depths was not available.

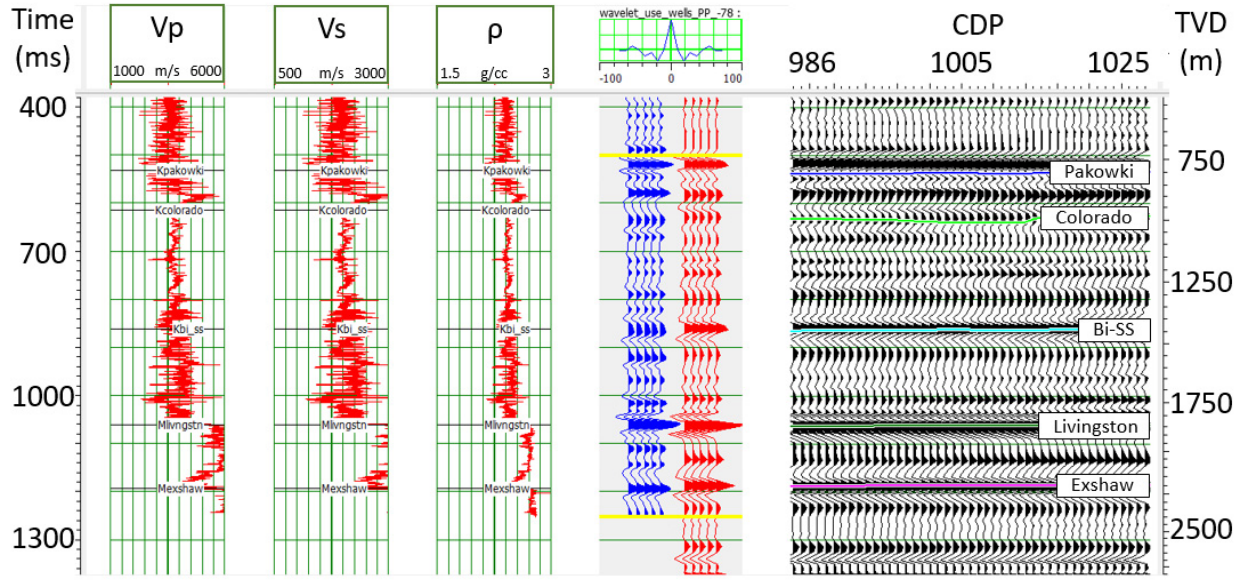

Figure 4-8: The final tie of well 3-32-4-23 on the PP section; the blue traces represent the synthetic seismogram and the red traces are the extracted trace from the seismic data near the well location.

Using both P and S-waves, a synthetic trace PS was created to help with the tie to the seismic (Figure 4.9). PS interpretations are often poorer in quality than P-wave seismic data due to the low-frequency content and customarily noisy data. The loss of high frequencies in the PS data may be related to Q attenuation, which is the loss of energy expressed in dB/cycle. Thus, PS seismic correlation to geology is significantly more difficult than for P-wave data.

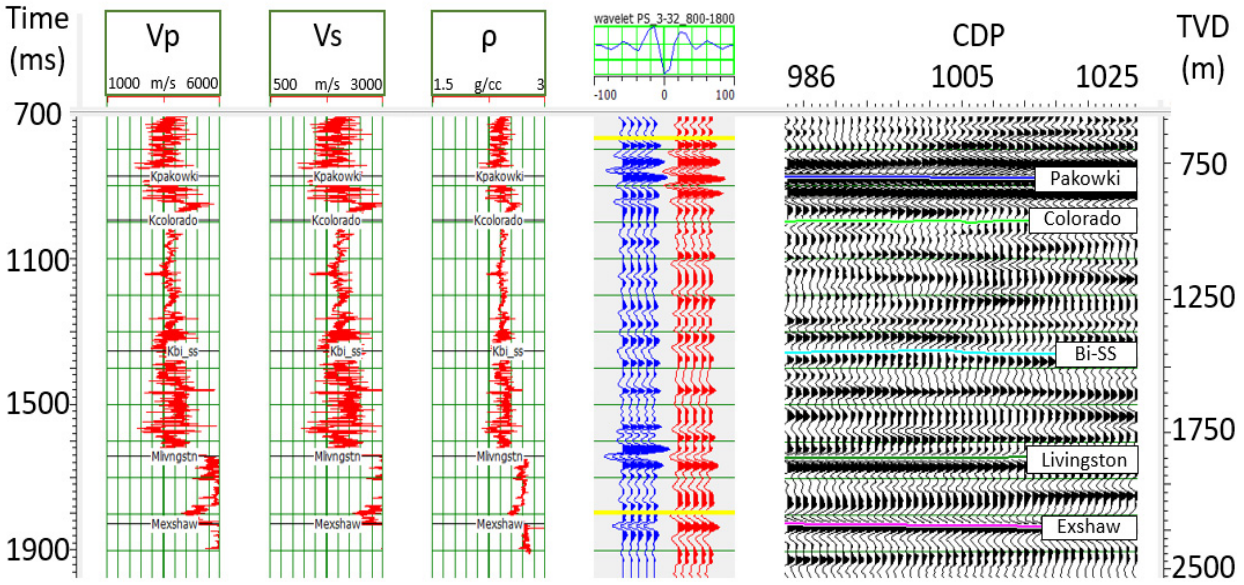

Figure 4-9: The final tie of well 3-32-4-23 on the PS section; the blue traces represent the synthetic seismogram and the red traces are the extracted trace from the seismic data near the well location.

4.2.3 Well Tie Quality Control

To verify the well tie consistencies on both the PP and PS sections, two logs were computed. The first log was a Vp/Vs ratio calculated from P and S-wave sonic logs and the second log was a Vp/Vs ratio calculated from the corrected depth-time curves. Both logs were overlaid to compare consistencies in values. As noticed in Figure 4.10, there were only small shifts of Vp/Vs values between both logs, indicating there was no excessive stretching or squeezing during the well tie process.

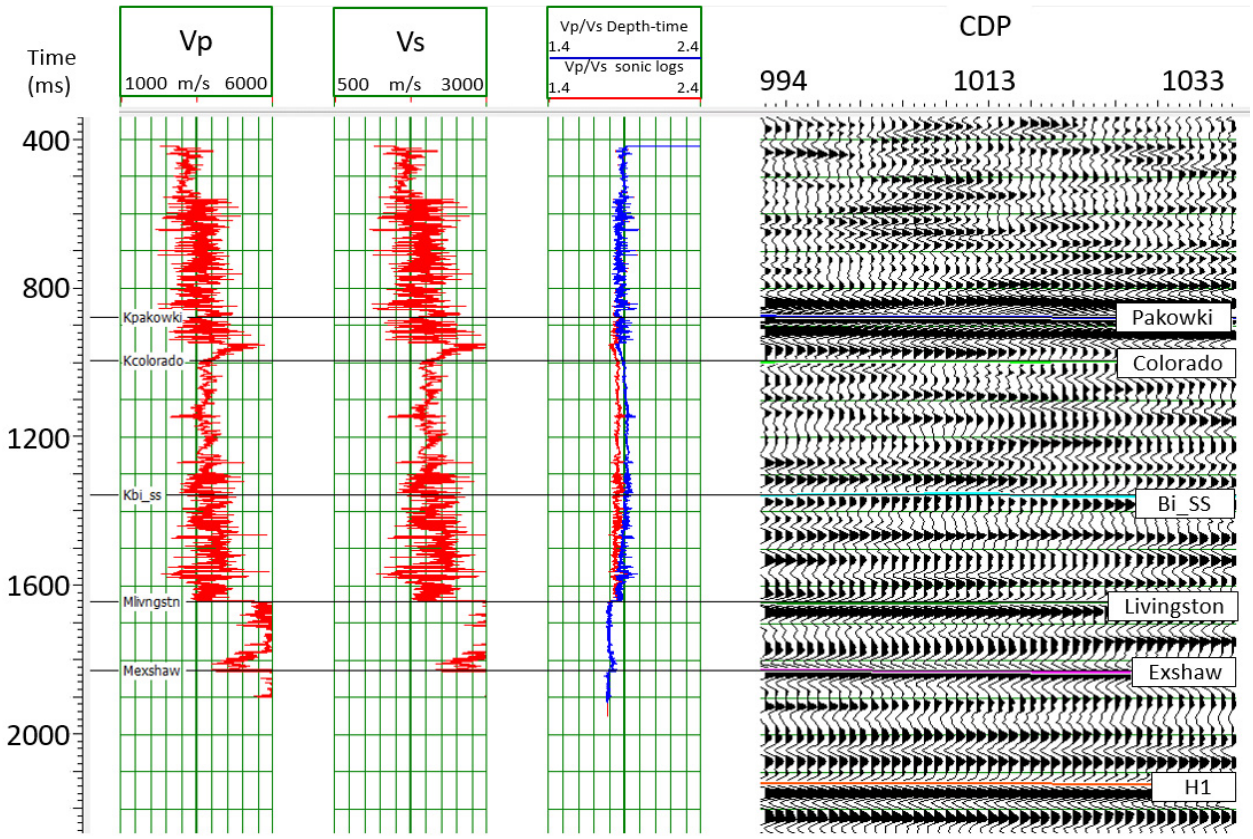

Figure 4-10: Quality control on well 3-32-4-23; the blue line represents the calculated Vp/Vs ratio from depth-time curves and the red line on the same track represents the ratio derived from the sonic logs; both lines showed consistency in the area of investigation.

4.2.4 Horizon Picking

After the well ties, the horizons of interest were picked on both the PP and PS datasets and intervals Vp/Vs values between these horizons were calculated using the Garotta relationship (Equation 1.12). The horizons interpreted in this experiment are shown in Figure 4.11 and 4.12. To verify that the horizons were correctly picked, Figure 4.13 shows the PP and PS sections side by side, where PS section is plotted at 2/3 the scale of the PP section; both sections were, generally aligned at the same depth.

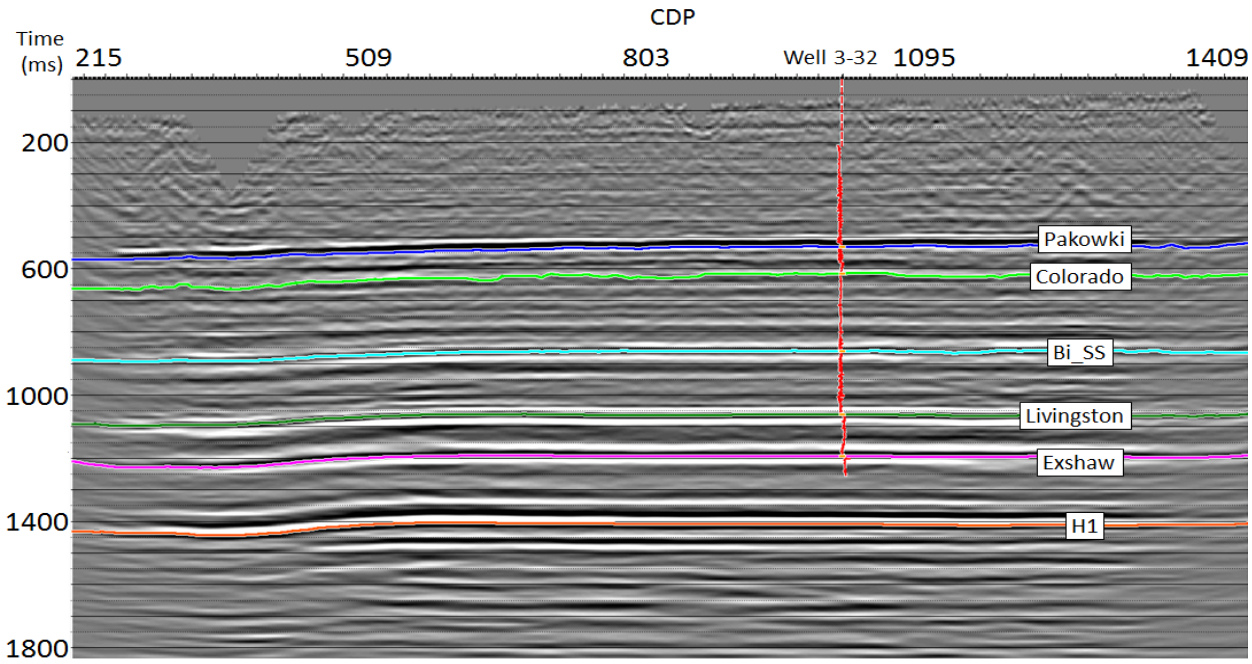

Figure 4-11: PP seismic section with all interpreted horizons and the well location. Well 3-32 included dipole sonic logs.

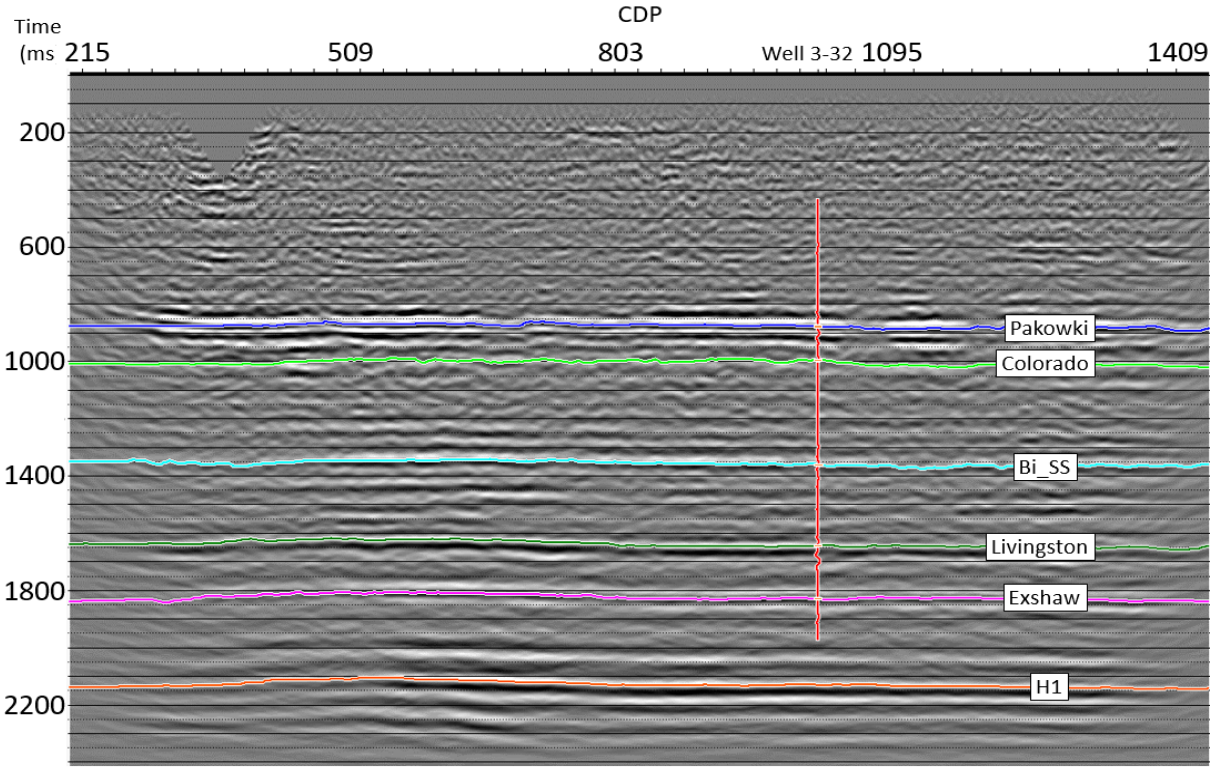

Figure 4-12: PS seismic section with all interpreted horizons and the well location. Well 3-32 included dipole sonic logs.

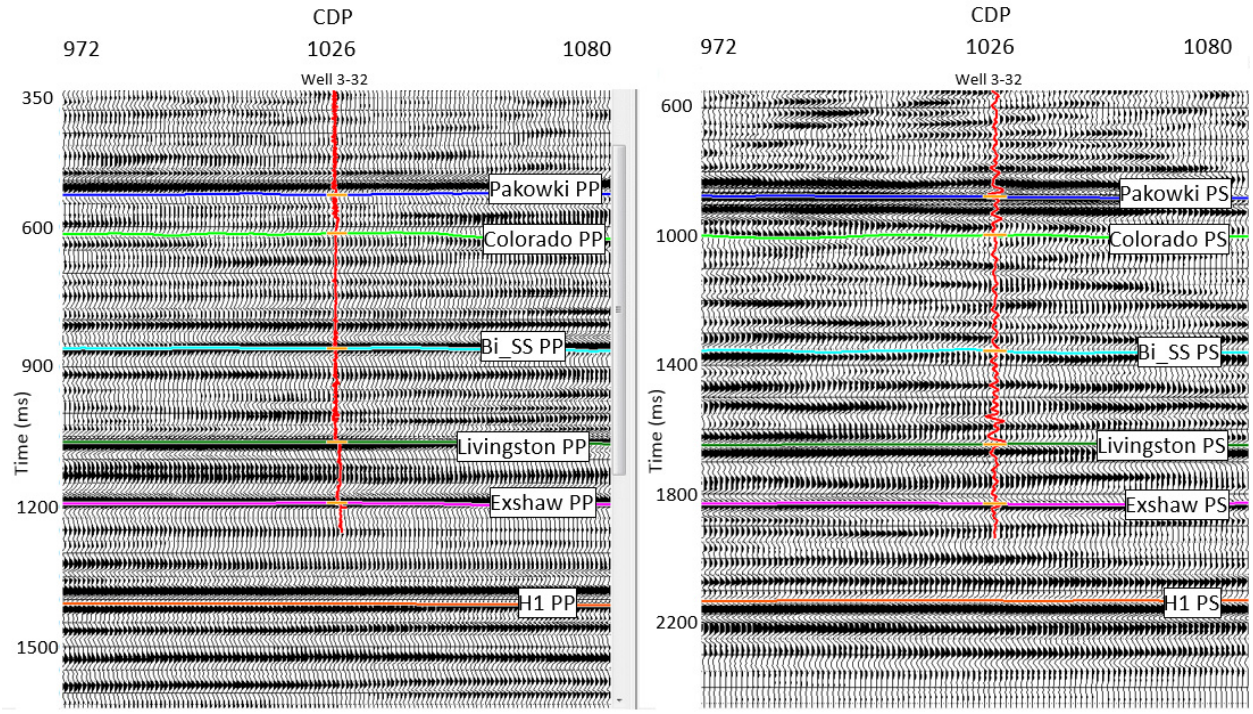

(a) **(b)**

Figure 4-13: Interpretation of (a) the PP section and (b) the PS section; the PS section is plotted at 2/3 the scale of the PP section.

To improve the interpretation of the horizons, a small time shift was applied. Horizons picks are generally made at peaks, troughs or zero crossings in the seismic data and may not necessarily fall exactly at the wells top locations. Thus making time shift adjustments in the picks can help increase the accuracy of the intense analysis over thin beds. Improvements on horizons, as shown in Figures 4-14 and 4-15, could be from a few milliseconds to several milliseconds, particularly for the PS section, due to the lower dominant frequency of the data. Since the Spring Coulee dataset had only one well, there was no ability to average the horizon and top time differences between the wells. After the time shift was applied, the horizons closely match the top location contributing to the reduction of the overall uncertainty of the Vp/Vs calculation.

	3-32-4-23 Log		
PP Seismic	Horizon Time	Top Time	Time Diff.
Exshaw	1192.70	1196.14	3.44
Exshaw Corr.	1196.14	1196.14	-

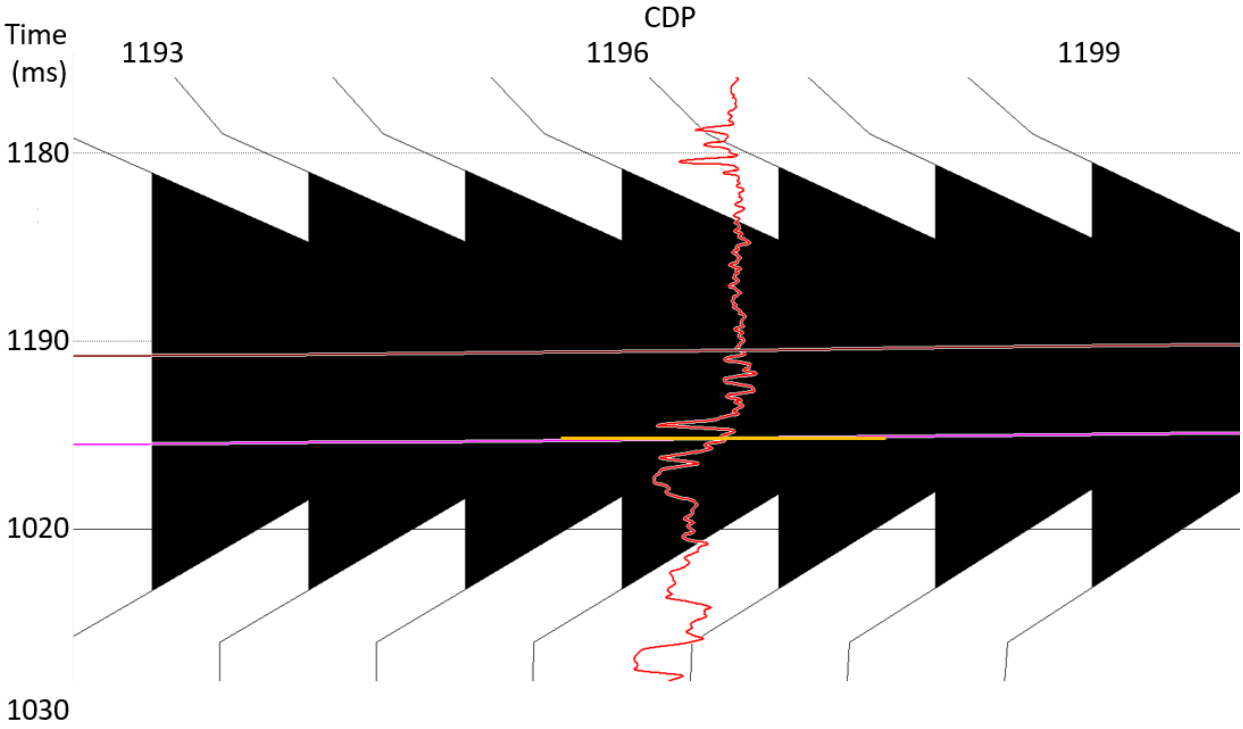

Figure 4-14: The table shows the time improvement in the red box after the corrections were applied on the PP section for the Exshaw horizon. The corrected horizon time is noted in the red box.

	3-32-4-23 Log		
PS Seismic	Horizon Time	Top Time	Time Diff.
Pakowki	873.24	877.38	4.14
Pakowki Corr.	877.38	877.38	-

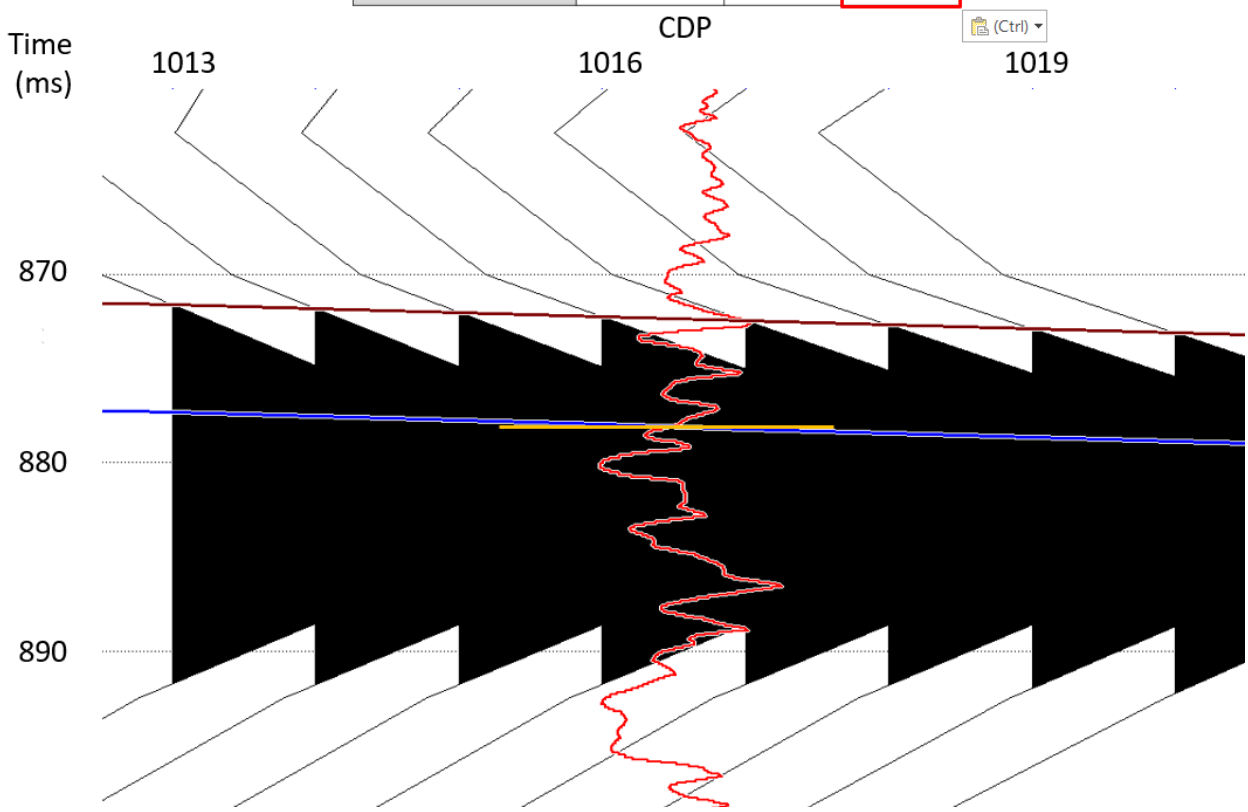

Figure 4-15: The table shows the time improvement in the red box after the corrections were applied on the PS section for the Pakowki horizon. The corrected horizon time is noted in the red box.

4.3 Vp/Vs Error Analysis

All possible isochrons were used for the analysis of the Vp/Vs ratio. The 6 horizon picked provided a total of 15-time intervals with ranges from about 80 ms to about 900 ms. Isochron intervals in the Spring Coulee dataset were larger than those found in the Hussar dataset. Hence, the error analysis in this chapter concentrated on finding how precise picking of the horizons interacts with errors for each specific interval. This was done by calculating errors for

uncorrected and corrected horizons. Table 4.1 shows both interval times for corrected and uncorrected horizons.

Table 4.1 Interval PP time averages for both corrected and uncorrected horizons.

	PP Time Interval (ms) Corrected Horizons	PP Time Interval (ms) Uncorrected Horizons
Pakowki-Colorado	82.9	90.9
Colorado-Bi-ss	246.7	243.0
Bi-ss-Livingston	199.7	201.5
Livingston-Exshaw	131.7	125.2
Exshaw-H1	216.3	220.4
Pakowki-H1	877.4	881.0
Pakowki-Exshaw	661.1	660.6
H1-Colorado	794.4	790.1
H1-Livingston	348.0	345.6
Exshaw-Bi-ss	331.4	326.7
Pakowki-bi-ss	329.7	333.9
Pakowki-Livingston	529.4	535.4
Colorado-Livingston	446.5	444.5
Colorado-Exshaw	578.1	569.7
Bi-ss-H1	547.7	547.1

Figure 4.16 shows the interval Vp/Vs values of time intervals at each specific CDP point along the seismic line. As expected, the deviation of Vp/Vs ratio for each isochron interval was large. Deviation in ratio calculations inversely correlates to the sampling size; thus, the larger the time interval, the smaller the deviation. For example, in Figure 4.16, the Pakowki-Colorado isochron was about 83 ms after horizon correction. The variation in Vp/Vs for this particular sample oscillates greatly compared to the Exshaw-Bi-SS isochron, which is about 332 ms.

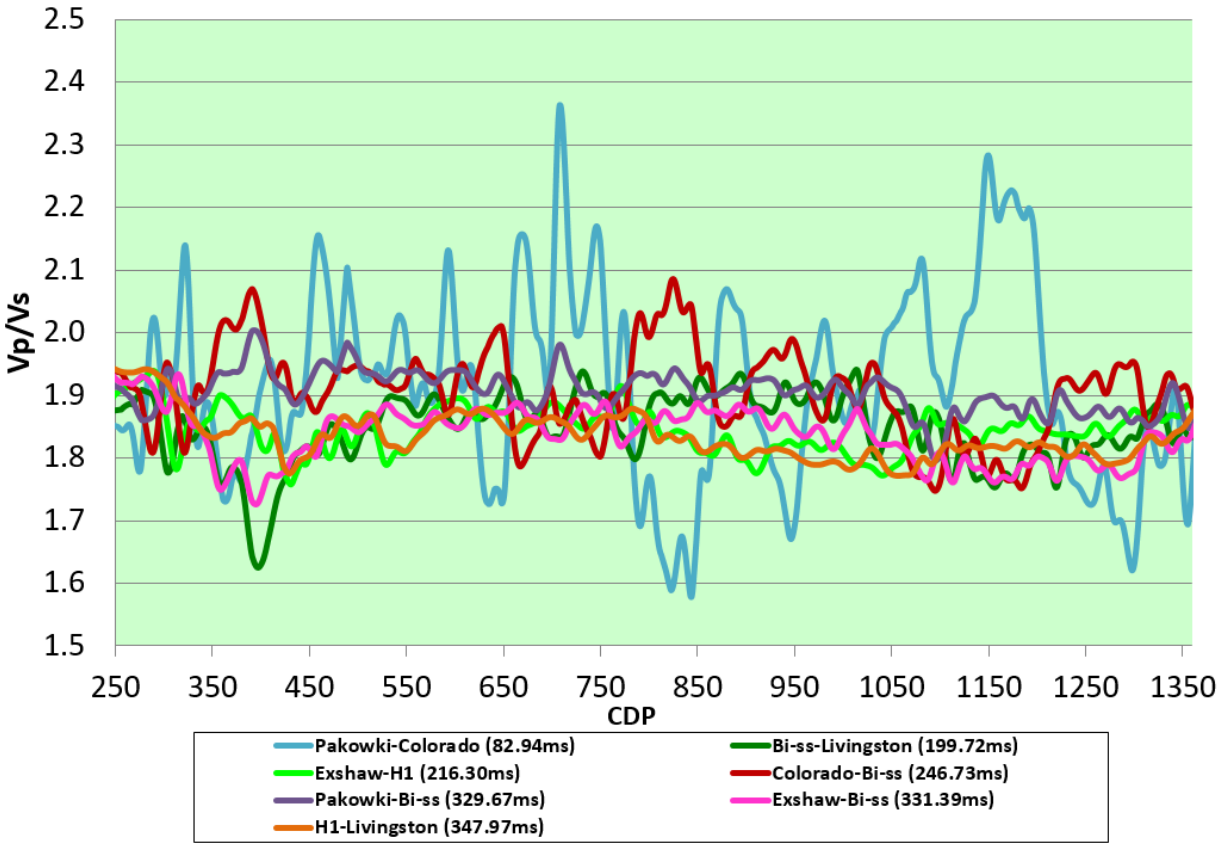

Figure 4-16: Interval Vp/Vs along the seismic line, for PP isochrons less than 400 ms.

Figure 4.17 shows the remaining isochrons, which have time intervals more than 400 ms for the Spring Coulee dataset. As seen in Figure 4.17, the deviations on this graph are smaller because the time intervals are large enough to offset the uncertainty errors. For this reason, larger isochrons are ideal for geological interpretation. The isochron ratios follow a similar trend throughout the line. The horizons picked in this project corresponded to shales, carbonates and sandstones formations. The lithology indicates the areas with low ratios correspond to higher sandstones concentrations and the areas with high ratio indicate a higher presence of shale.

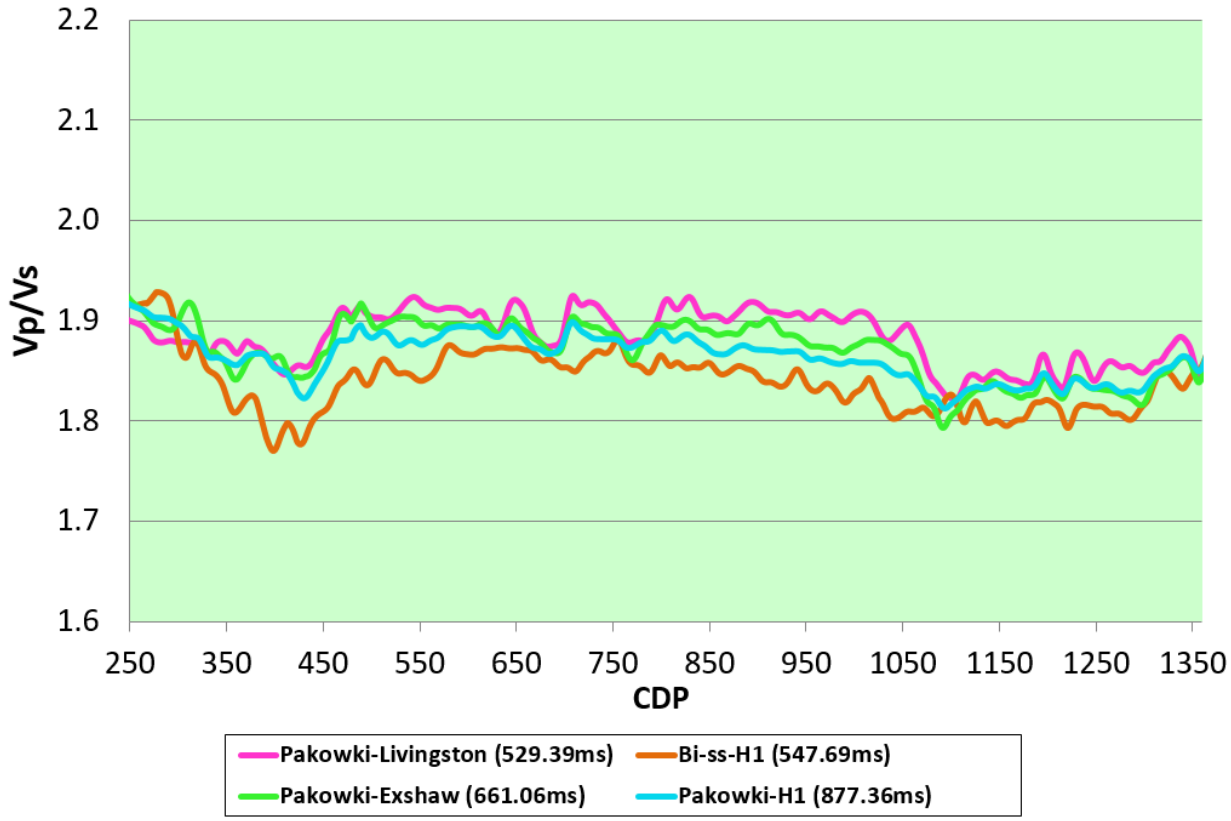

Figure 4-17: Interval Vp/Vs ratio of large isochrons along the seismic line, for isochrons of more than 400 ms in PP time.

4.4 Time Interval Error Analysis

Figure 4.18 shows all means and standard deviation values for large isochrons, which have time intervals greater than 400 ms. The black line with the triangle shows the mean values for all of the curves for every 20 CDP intervals. The vertical bars represent one standard deviation away from the mean at each interval. This figure shows a meaningful lateral change in Vp/Vs because most of the values throughout the line lie within one standard deviation of the mean.

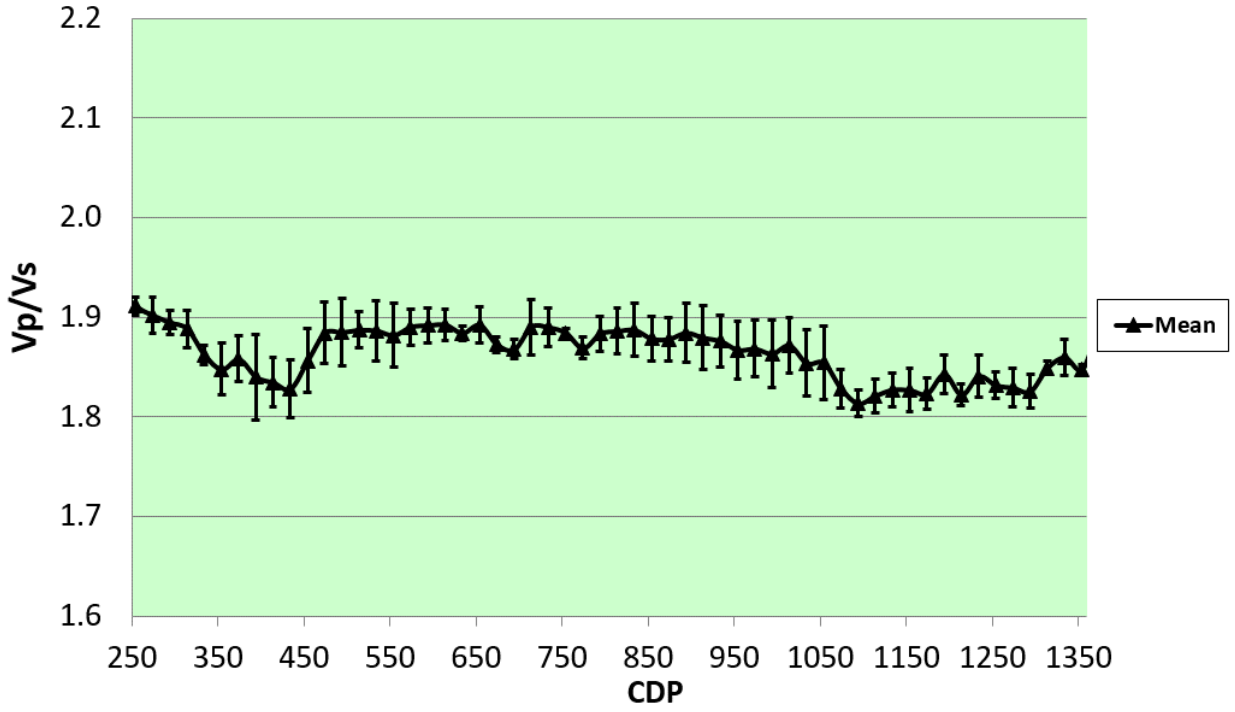

Figure 4-18: Interval Vp/Vs mean and standard deviation for large isochrons in PP time (>400 ms) along the seismic line. The black line with the triangle represents the mean Vp/Vs value at a specific CDP. Vertical bars represent one standard deviation away from the mean.

Figure 4.19 shows all interval Vp/Vs mean and standard for small isochrons, which have time intervals less than 400 ms. As seen in the previous chapter, smaller isochrons have greater standard deviation and curve values are very different from each other. Since the curves' values lie outside one standard deviation from the mean, these values should not be used to interpret the lateral variation of the Vp/Vs. It is better to use larger isochrons for geological interpretation.

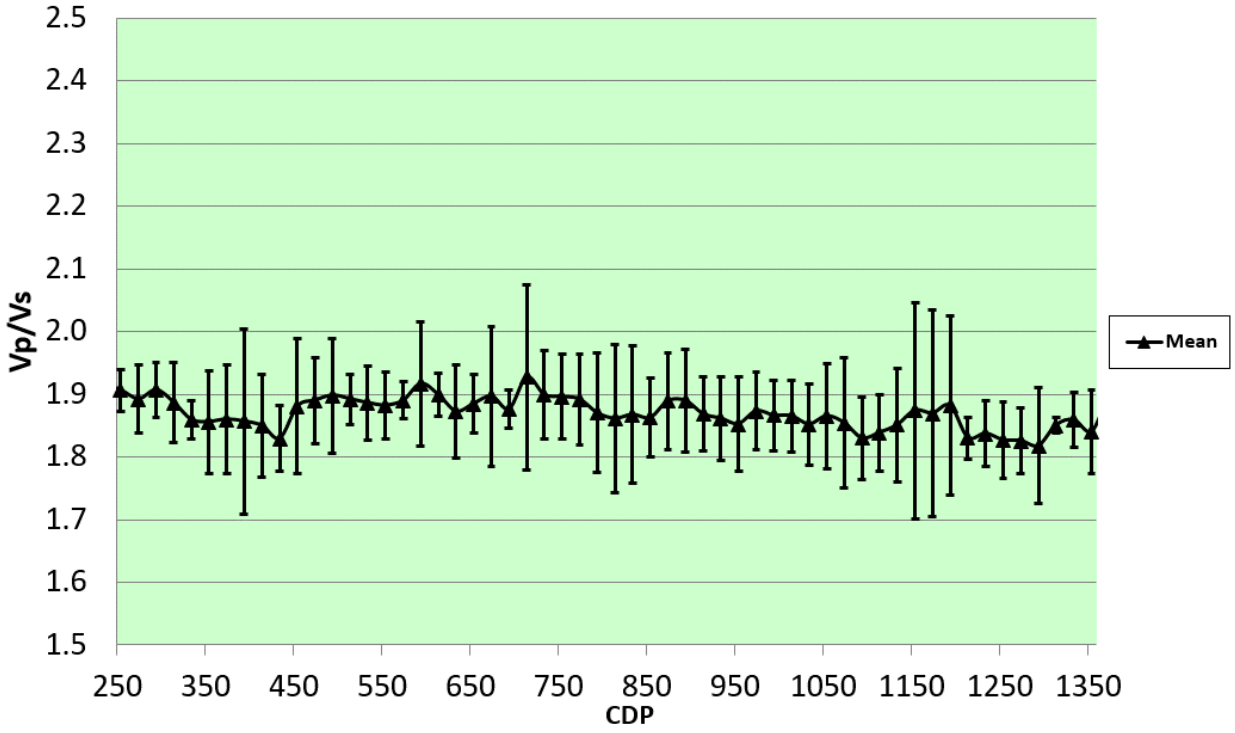

Figure 4-19: Interval Vp/Vs mean and standard deviation for small isochrons in PP time (<400 ms). The black line with the triangle represents the mean Vp/Vs value at a specific CDP. Vertical bars represent one standard deviation away from the mean.

The error for each time interval was calculated using the Vp/Vs error equation (Equation 2.4). A cross plot of percentage error versus time interval (Figure 4.20) for both corrected and uncorrected horizon shows that for larger time intervals the errors are similar, with error values ranging from 0.42 to 1.83 percent for isochrons larger than about 200 ms. In this cross plot, the red line represents the corrected horizon's best-fit line, which is a power function equation presented in the red outline box. The blue line represents the best-fit line for the uncorrected horizons, whose power function is presented with the blue outline box. Both of these lines are asymptotic. For small time intervals, less than 150 ms, there is a significant separation between

both lines. The blue presents a higher uncertainty error than the red line, especially as time intervals becomes smaller.

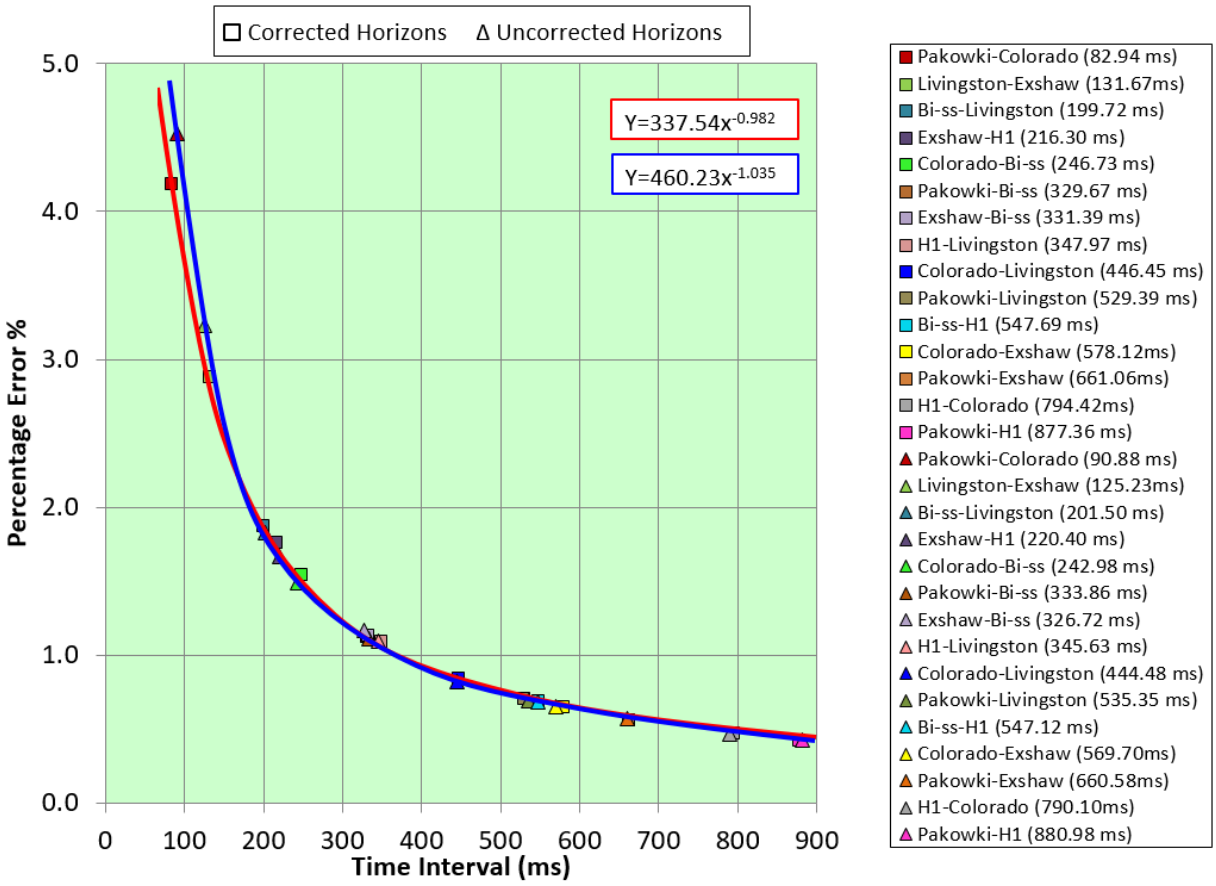

Figure 4-20: Cross-plot of percent relative error in Vp/Vs versus ΔTpp time interval; the error increases as the time interval becomes smaller. The red trendline represents horizons with time corrections and is represented by the power function in the red box. The blue line represents the uncorrected horizons and is represented by the power function in the blue box.

4.5 Vp/Vs Results

Results for the Vp/Vs analysis are shown in Figures 4.21 and 4.22 for uncorrected and corrected horizons, the seismic section from the Spring Coulee experiment had low reflection amplitudes around the Colorado formation pick, which affected the Vp/Vs calculations for the

Pakowki-Colorado time interval considerably. In the seismic section with uncorrected horizons, the Vp/Vs for the Pakowki-Colorado interval was 1.44. On the other hand, on the corrected Vp/Vs section this time interval had an average Vp/Vs of 1.91. In general, all Vp/Vs values were adjusted after the horizons were corrected; the adjustment in Vp/Vs became larger as the time interval became smaller.

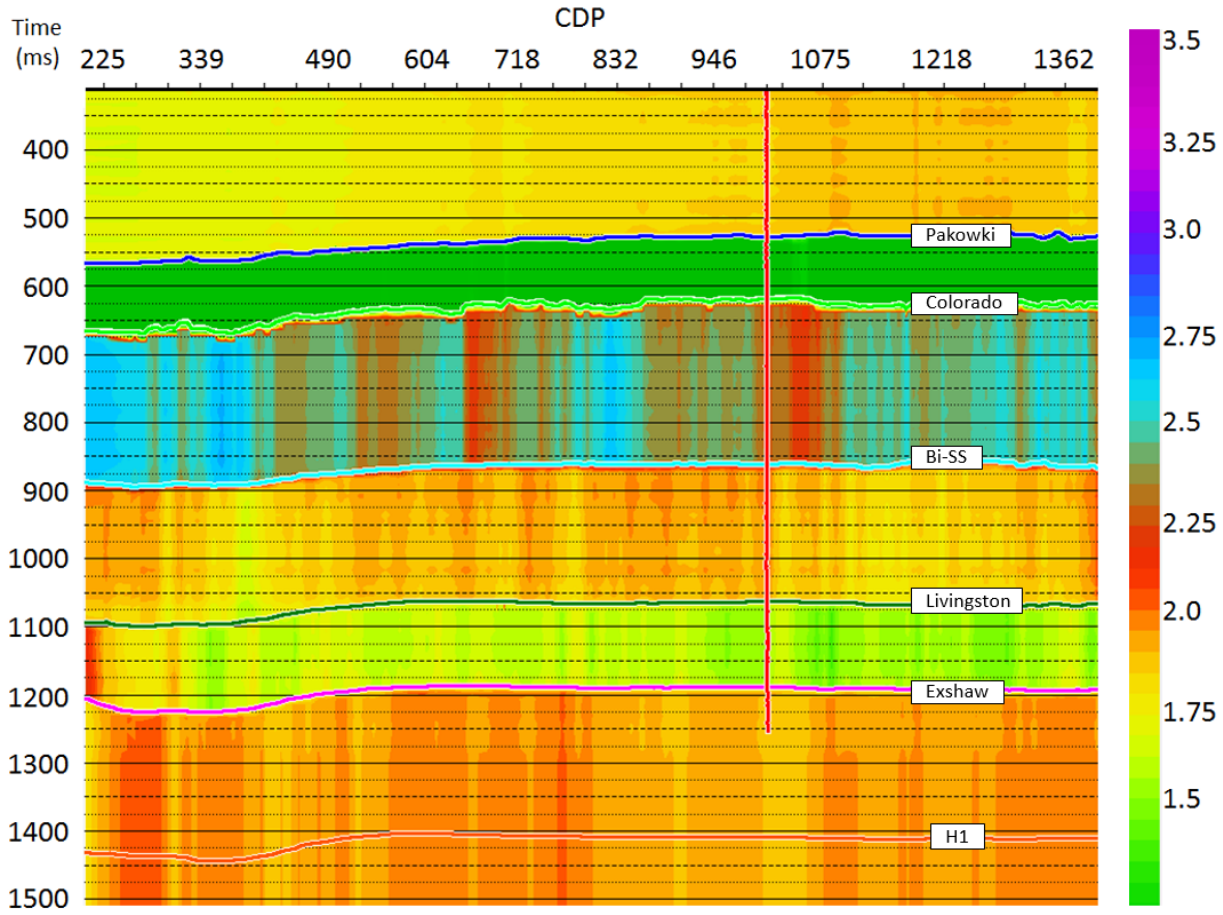

Figure 4-21: Seismic section with color bar for Vp/Vs for uncorrected horizons.

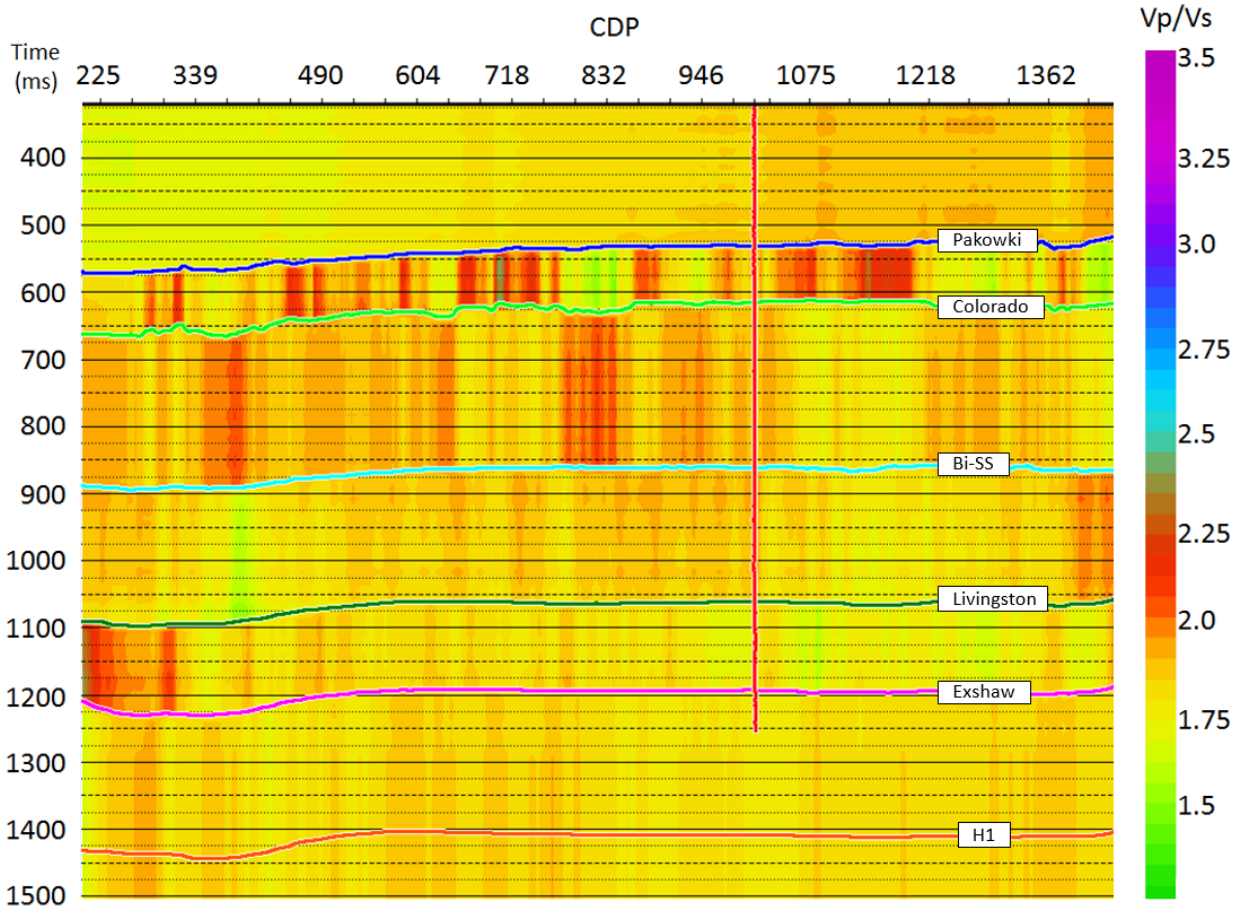

Figure 4-22: Seismic section with color bar for Vp/Vs for corrected horizons.

4.6 Summary

Based on the Spring Coulee study results, Vp/Vs ratios are affected by time interval size as well as by how well the horizons are picked. As found in the previous chapter, it is recommended not to use time intervals smaller than 150 ms for Vp/Vs interpretation. Horizons corrections only made slight improvements in the percentage of error of approximately .5 % on the smallest isochron.

This dataset showed a small lateral variation in Vp/Vs, which indicates that lithological changes along the seismic line are small.

Chapter Five: Conclusions and Recommendations

5.1 Conclusions

The main goal of this thesis was to evaluate the uncertainty in the Vp/Vs analysis and to provide a guideline for the smallest bed thickness to use when estimating this ratio, with confidence. The following conclusions have been reached based on the results of this study:

- The synthetic geological model analysis showed that the uncertainty played a factor in the estimation of Vp/Vs ratio error, especially when the beds were as thin as 10 m. Although the model presented isotropic properties, it did follow the trend line of the power function that was characteristic of the Hussar and Spring Coulee case studies.
- The Hussar seismic data showed that Vp/Vs uncertainty increases as the analysis time window decreases. The Vp/Vs error suggested that as the isochron becomes smaller, the calculated velocity ratio will become less reliable for lithology discrimination analysis.
- The Spring Coulee data also showed that Vp/Vs ratios are affected by time interval size as well as by how accurately the horizons are picked. Horizons corrections made slight improvements in the uncertainty of approximately 0.5% on the smallest isochron. This indicates that the time interval has greater influence on the reliability of Vp/Vs ratio.
- Changes in the Vp/Vs ratio is affected not only by the value of the isochron but also by the geology surrounding the study area. It is important to understand the geology of the area and identify the formations of the area of study.

5.2 Recommendation

This thesis focused on studying the sensitivity of the velocity ratio using two datasets and a geological model. The following are recommendations based on the results of this research:

- It is recommended not to use time intervals smaller than 150 ms for Vp/Vs interpretation. Isochron smaller than 150 ms in PP time have high uncertainty, making the ratio not reliable for lithologies studies.
- Accurate horizon picks help improve results in the estimation of the Vp/Vs ratio. It is important for the interpreter to perform precise picks on the seismic data, as this improves the Vp/Vs ratio accuracy.
- It is suggested to use isochron intervals in PP time greater than 150 ms for robust results. Interval Vp/Vs analysis for intervals greater than this isochron have low uncertainty. The studies showed that horizon pick adjustments can reduce uncertainty by a small factor. In all cases, it was confirmed that thin beds can play a significant role in Vp/Vs uncertainties that could lead to erroneous results. In addition, it was shown that interpreters should work with bed thicknesses greater than 150 ms to perform horizon adjustments for more precise results.
- Future work could include performing an inversion on both the PP and PS datasets to compare the Vp/Vs ratios from the inversion method to the Garotta approach.

References

Allan, J. A., & Rutherford, R. L. (1934). *Geology of Central Alberta: Alberta Geological. Survey, Report 30*.

Bertram, M. B., Hall, K. W., Stewart, R. R., Gallant, E. V., Margrave, G. F., & Maier, R. M. (2008). Overview of multicomponent seismic field work at Spring Coulee. *Alberta: CREWES Research Report*, *20*.

Domenico, S. N. (1984). Rock lithology and porosity determination from shear and compressional wave velocity. *Geophysics*, *49*(8), 1188–1195.

Douglas, R. J. W. (1953). Carboniferous stratigraphy in the southern Foothills of Alberta. *Third Annual Alberta Society of Petroleum Geologist Field Conference & Symposium*, 66–88.

Gardner, G. H. F. (1974). Formation Velocity and Density—The Diagnostic Basics for Stratigraphic Traps. *Geophysics*, *39*, 770. Retrieved from http://doi.org/10.1190/1.1440465.

Garotta, R., & Grange, P. (1987). Comparison of responses of compressional and converted waves on a gas sand. In *SEG Technical Program Expanded Abstracts 1987* (Vols. 1–0, pp. 627–630). Society of Exploration Geophysicists.

Gavotti, P. E. (2014). *Model-based inversion of broadband seismic data*. University of Calgary. Retrieved from http://theses.ucalgary.ca/handle/11023/1257.

Geis, W. T., Stewart, R. R., Jones, M. J., & Katopodis, P. E. (1990). Processing, correlating, and interpreting converted shear waves from borehole data in southern Alberta. *Geophysics*, *55*(6), 660–669. Retrieved from http://doi.org/10.1190/1.1442878.

Isaac, J. H., & Margrave, G. F. (2011). Hurrah for Hussar. *Comparisons of Stacked Data: CREWES Research Report*, *23*(55).

Kearey, P., Brooks, M., & Hill, I. (2013). *An introduction to geophysical exploration*. John Wiley & Sons.

Louro, A. A. (2014). An introduction to measurement uncertainties. University of Calgary PHYS 255 Course Notes.

Lu, H., & Hall, K. W. (2008). Preliminary processing results, Spring Coulee, Alberta. CREWES Research Report Vol. 20.

Margrave, G. F., Bertram, M. B., Lawton, D. C., Innanen, K., Hall, K. W., Mewhort, L., & Hall, M. (2011). The Hussar low-frequency experiment. CREWES Research Report Vol. 23.

Miller, S. L., & Stewart, R. R. (1990). Effects of lithology, porosity and shaliness on P-and S-wave velocities from sonic logs. *Canadian Journal of Exploration Geophysics*, *26*(1–2), 94–103.

Mossop, G. D., & Shetsen, I. (1994). *Geological atlas of the Western Canada sedimentary basin*. [Calgary]: Published jointly by the Canadian Society of Petroleum Geologists and the Alberta Research Council.

Pemberton, S. G., & MacEachern, J. A. (1995). The sequence stratigraphic significance of trace fossils: examples from the Cretaceous foreland basin of Alberta, Canada. Retrieved from http://archives.datapages.com/data/specpubs/memoir64/ch14/0429.htm.

Pengelly, K. J., Lines, L. R., & Lawton, D. C. (2005). Multicomponent processing of seismic data at the Jackfish Heavy Oil Project, Alberta. CREWES Research Report Vol. 17.

Pickett, G. R. (1960). The use of acoustic logs in the evaluation of sandstone reservoirs. *Geophysics*, *25*(1), 250–274.

Rider, M. H., & Kennedy, M. (2011). *The Geological Interpretation of Well Logs* (3rd Edition). Scotland: Rider-French Consulting Limited.

Simm, R., Bacon, M., & Bacon, M. (2014). *Seismic Amplitude: An Interpreter's Handbook*. Cambridge University Press.

Smith, G. G., Cameron, A. R., & Bustin, R. M. (1994). Coal resources of the Western Canada sedimentary basin. *Geological Atlas of the Western Canada Sedimentary Basin. Edited by G. Mossop and I. Shetson. Canadian Society of Petroleum Geologists and Alberta Research Council, Calgary, Alta*, 20.

Stewart, R. R., Gaiser, J. E., Brown, R. J., & Lawton, D. C. (2002). Converted-wave seismic exploration: Methods. *Geophysics*, *67*(5), 1348–1363.

Tatham, R. H., McCormack, M. D., & Neitzel, E. B. (1991). *Multicomponent seismology in petroleum exploration*. Society of Exploration Geophysicists.

Tatham, R. H. (2006). Successful Applications of P-and S-wave Seismic Data. In *2006 SEG Annual Meeting*. Society of Exploration Geophysicists. Retrieved from https://www.onepetro.org/conference-paper/SEG-2006-0586.

Widess, M. B. (1973). How thin is a thin bed? *Geophysics*, *38*(6), 1176–1180.

Williams, M. Y., & Dyer, W. S. (1930). *Geology of southern Alberta and southwestern Saskatchewan* (Vol. 163). FA Acland, Printer to the King's most excellent majesty.

Yilmaz, Ö. (2001). *Seismic Data Analysis: Processing, Inversion, and Interpretation of Seismic Data*. Society of Exploration Geophysicists. Retrieved from http://library.seg.org/doi/book/10.1190/1.9781560801580.

Appendices

A. Vp/Vs Relation to Poisson's Ratio.

A.1 Derivation of the formula.

$$V_s = \sqrt{\frac{\mu}{\rho}} \Longrightarrow \mu = \rho V_s^2$$

$$V_p = \sqrt{\frac{K + 4/3\mu}{\rho}} \Longrightarrow K = \rho V_p^2 - 4/3\mu$$

$$K = \rho(V_p^2 - 4/3{V_s}^2)$$

$$\lambda = \frac{3K - 2\mu}{3} = \frac{3\rho(V_p^2 - 4/3{V_s}^2) - (2\rho V_s^2)}{3} = \frac{3\rho{V_p}^2 - 4\rho{V_s}^2 - 2\rho{V_s}^2}{3} = \frac{3\rho{V_p}^2 - 6\rho{V_s}^2}{3}$$

$$\lambda = \rho(V_p^2 - 2{V_s}^2)$$

$$\upsilon = \frac{\lambda}{2(\lambda + \mu)} = \frac{\rho({V_p}^2 - 2{V_s}^2)}{2(\rho(V_p^2 - 2{V_s}^2) + \rho V_s^2)} = \frac{V_p^2 - 2{V_s}^2}{2{V_p}^2 - 4{V_s}^2 + 2{V_s}^2} = \frac{V_p^2 - 2{V_s}^2}{2{V_p}^2 - 2{V_s}^2}$$

$$= \left(\frac{1}{2}\frac{V_p^2 - 2{V_s}^2}{{V_p}^2 - {V_s}^2}\right)\left(\frac{1/{V_s}^2}{1/{V_s}^2}\right) = \frac{1}{2}\frac{\left(\frac{V_p^2 - 2{V_s}^2}{{V_s}^2}\right)}{\left(\frac{V_p^2 - {V_s}^2}{{V_s}^2}\right)} = \frac{1}{2}\frac{\left(\frac{V_p^2}{{V_s}^2} - \frac{2\cancel{V_s^2}}{\cancel{V_s^2}}\right)}{\left(\frac{V_p^2}{{V_s}^2} - \frac{\cancel{V_s^2}}{\cancel{V_s^2}}\right)}$$

$$\upsilon = \frac{1}{2}\frac{(V_p/V_s)^2 - 2}{(V_p/V_s)^2 - 1}$$